



ERASMUS MUNDUS MSc PROGRAMME

COASTAL AND MARINE ENGINEERING AND MANAGEMENT
CoMEM

FINITE ELEMENT MODELLING OF A SHEAR BOX EXPERIMENT ON ICE RUBBLE

Norwegian University of Science and Technology
June, 2011

Weizhi Ji
712763



The Erasmus Mundus MSc Coastal and Marine Engineering and Management is an integrated programme organized by five European partner institutions, coordinated by Delft University of Technology (TU Delft). The joint study programme of 120 ECTS credits (two years full-time) has been obtained at three of the five CoMEM partner institutions:

- Norges Teknisk- Naturvitenskapelige Universitet (NTNU) Trondheim, Norway
- Technische Universiteit (TU) Delft, The Netherlands
- City University London, Great Britain
- Universitat Politècnica de Catalunya (UPC), Barcelona, Spain
- University of Southampton, Southampton, Great Britain

The first year consists of the first and second semesters of 30 ECTS each, spent at NTNU, Trondheim and Delft University of Technology respectively. The second year allows for specialization in three subjects and during the third semester courses are taken with a focus on advanced topics in the selected area of specialization:

- Engineering
- Management
- Environment

In the fourth and final semester an MSc project and thesis have to be completed. The two year CoMEM programme leads to three officially recognized MSc diploma certificates. These will be issued by the three universities which have been attended by the student. The transcripts issued with the MSc Diploma Certificate of each university include grades/marks for each subject. A complete overview of subjects and ECTS credits is included in the Diploma Supplement, as received from the CoMEM coordinating university, Delft University of Technology (TU Delft).

Information regarding the CoMEM programme can be obtained from the programme coordinator and director

Prof. Dr. Ir. Marcel J.F. Stive
Delft University of Technology
Faculty of Civil Engineering and geosciences
P.O. Box 5048
2600 GA Delft
The Netherlands

Weizhi Ji

Finite Element Modelling of a Shear Box Experiment on Ice Rubble

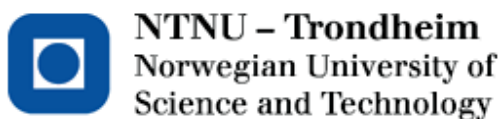
A thesis presented in partial fulfillment of the requirements for the degree of MSc
in Civil Engineering Coastal and Marine Engineering and Management (CoMEM)

Master's thesis

Trondheim, June 2011

Norwegian University of Science and Technology
Faculty of Engineering Science and Technology
Department of Civil and Transport Engineering

Academic supervisor: Knut V. Høyland



Master's thesis

Weizhi Ji

Finite Element Modelling of a Shear Box Experiment on Ice Rubble

Trondheim, June 2011

NTNU
Norwegian University of
Science and Technology
Faculty of Engineering Science and Technology
Department of Civil and Transport Engineering



Report Title: Finite Element Modelling of a Shear Box Experiment on Ice Rubble	Date: 21st, June 2011		
	Number of pages (incl. appendices): 114		
	Master Thesis	X	Project Work
Name: Weizhi Ji			
Professor in charge/supervisor: Prof. Knut V. Høyland			
Other external professional contacts/supervisors: None			

<p>Abstract:</p> <p>Analytical and numerical analysis of laboratory-scale shear box experiments on ice rubble have been performed. The experiments were done at NTNU in 2010 (Serré et al., 2011 and Repetto and Høyland, 2011). Three phases in the force-time history of the tests were identified (similar to what Serré et al., 2011 did). The first phase lasted about 2 seconds (compared to 6 seconds in Serré et al., 2011) and ended with a shift in the force-time gradient corresponding to plastic behaviour. Phase one was studied numerically while phase two and three were analysed conceptually.</p> <p>The experiments were done with different vertical confinement and different submersion times, altogether 14 individual tests were carried out. Each combination of parameters (initial and boundary conditions) was repeated three times. There was a large difference within the three tests with the same initial and boundary conditions. Mostly 2 tests were similar, while one test was different. The use of Hellmann's (1984) definition of 3 phases in shear box testing cannot directly be used to analysis these tests, as the boundary conditions were different. Hellmann had zero displacement perpendicular to the moving piston, while Serré et al. (2011) had constant pressure.</p> <p>The friction angle was derived from phase three assuming that all freeze-bonds were broken and that the rubble was essentially without cohesion. The test with 20 hours (long) submersion times had lower friction angle (9° to 31°) than the ones with 10 minutes (short) submersion times (33° to 74°). This derivation is only indicative, but suggests that the submersion time govern the material properties.</p> <p>Phase 1 was studied numerically with the use of a continuum finite element model with Lagrange method (ABAQUS/Standard 6.10-2). An elastic-perfect plastic model with Drucker-Prager material model was applied, and the three most important material parameters, namely Young modulus, cohesion and friction angle were the main focus. These three were retrieved by trial and error method so as to match the experimental results. Young modulus give the initial slope of the force-time curve, while DP model cohesion and friction angle determine when the yielding points occurred and the force at that moment. So by carrying out numerical simulation, the values of Young modulus for different situations were given and a series pairs of cohesion and friction angle in DP model were given as well so as to match the experiment results. The long submersion times had lower Young modulus (0.9 MPa) than the short submersion times gave (2-4.5 MPa). But which pair of cohesion and friction angle that was the most suitable for the ice rubble material in nature could not be derived from the present study. The numerical simulation showed that the crack patterns predicted by numerical simulation were more or less the same as the ones observed. The question on whether or not a cap hardening model should be used to simulate the primary phase was also discussed and only in the Extra_High_Short test, a cap model is needed. Scaling problems were discussed by assuming that Froude scaling law could be used and it is found that the cohesion after scaling up to full-scale was larger than two recent studies: one is model-scale punch tests done by Serré (2010), another is full-scale punch tests done by Heinonen (2004). The results of this thesis could provide a better understanding for the material properties of freeze-bonds and be beneficial for future study in this field.</p> <p>The conceptual analysis of phase two and three showed that there were some shortcomings in the experiment setup and based on this, some improvement of the experiment equipment and suggestions were given.</p>

Keywords:

1. Ice rubble
2. Finite element modelling
3. Drucker-Prager model
4. Shear box experiment

(signature)

ACKNOWLEDGEMENTS

I would like to express my sincere gratitude to my supervisor, Prof. Knut V. Høyland, who has provided valuable guidance to the shaping of the thesis and has offered me a lot of constructive suggestions from time to time during my thesis writing and I am also thankful for his critical reading of the drafts for the improvement of this thesis.

I would also like to thank PhD student Nicolas Serré and Ada Repetto-Llamazares for their experiment, great help and useful suggestions for numerical modelling.

Special thanks to Prof. Thomas Benz and PhD student Wenjun Lu for their suggestion on ABAQUS work; Prof. Øivind A. Arntsen and Prof. Sveinung Løset for their contribution to CoMEM program; Marion Beentjes for her outstanding administration work and Kenneth Sundli for his IT support.

I would also like to thank all the professors and teachers who have taught me during my master study. Their wonderful lectures enlighten me on study and provide me with essential knowledge used in this thesis.

MASTER THESIS
(TBA4920 MARIN BYGGTEKNIKK, master thesis)

Spring 2011
for
Student: Weizhi Ji

Finite Element Modelling of a Shear Box Experiment on Ice Rubble

BACKGROUND

First-year ice ridges play an important role in ice-structure interaction process, especially in the Arctic circle region. And the rubble above the water line (the sail) has a volume of about one tenth of the rubble below the water line (the keel), so the potential threat from the keel is quite large and it will be the major contributor to the load during ice-structure interaction process. An important feature of ice rubble in keel is the freeze-bonding between ice blocks. It has been acknowledged as one of the physical mechanisms giving the rubble ice its peculiar aspects in comparison with other geotechnical materials such as sand and gravel (Serré et al., 2011). This feature is vital since it will always result in peak force during ice-structure interaction. But not so much research has been done in this aspect. Serré et al. (2011) has done a 2D shear box experiment in lab in NUNU in order to study the properties of freeze-bonds. 14 individual tests were carried out with different confining pressure and submerging time of ice rubble, which tried to relate qualitatively the freeze-bond properties to the rubble deformation behaviour through shear box and freeze bond testing. But that work just gave a description of the results and how it is affected by the level of freeze-bonding, so a more detailed and quantitatively study is needed to in order to research on the material properties of freeze-bonds.

TASK DESCRIPTION

The task of the work is to study quantitatively the material properties of freeze-bonds, focusing mainly on the interpretation of the shear box experiment results derived by Serré et al. (2011). A continuum finite element model using Lagrange method is developed by using commercial finite element software ABAQUS/Standard 6.10-2 in order to simulate this shear box experiment. The scaling problem is also important that needs to be discussed, since we can compare the results from experimental and numerical modelling with the properties of ice rubble in nature by scaling. Besides, a further conceptual analysis of the shear box experiment is also needed to provide basic information and assumptions for numerical simulation.

GENERAL ABOUT CONTENT, WORK AND PRESENTATION

The task description for the master thesis is meant as a framework for the work of the candidate. Adjustments might be done as the work progresses. Tentative changes must be done in cooperation and agreement with the supervisor and professor in charge at the Department. (Also including external cooperative partners where this is applicable).

In the evaluation thoroughness in the work will be emphasized, as will be documentation of independence in assessments and conclusions. Furthermore the presentation (report) should be well organized and edited; providing clear, precise and orderly descriptions without being unnecessary voluminous.

The report shall include: (templates are found on <http://www.ntnu.no/bat/skjemabank>)

- Standard report front page.
- Title page with abstract and keywords (signed by the student).
- Summary and acknowledgement. Table of content including list of symbols, figures, tables and enclosures. If useful and applicable a list of important terms and abbreviations should be included.
- The main text.
- Clear and complete references to material used, both in text and figures/tables. This also applies for personal and/or oral communication and information.
- Text of the Thesis (these pages) signed by the professor in charge.
- The report must have a complete page numbering.
- The thesis may possibly be written as a scientific article. The report must come with report front and title pages and, if necessary, with appendices that document the work performed in the process of writing of the article.

Submission procedure

- The complete, original report (un-bounded).
- Two copies (bounded).
- If applicable: X additional copies if agreed upon for instance with external partner (to be paid for by the Department or the external partner)
- CD with the complete report (pdf-format) and all assisting or underlying material.
- A brief (one to two A4 pages including possible illustrations) popular science summary of the work, aiming at publication on the Department's web-site. Include a copy of this html document on the CD. Template is found on: <http://www.ntnu.no/bat/skjemabank>

The summary shall include the objectives of the work, explain how the work has been conducted, present the main results achieved and give the main conclusions of the work.

Advice and guidelines for writing of the report is given in: "Writing Reports" by Øivind Arntsen. Additional information on report writing is found in "Råd og retningslinjer for rapportskrivning ved prosjekt og masteroppgave ved Institutt for bygg, anlegg og transport" (In Norwegian). Both are posted on <http://www.ntnu.no/bat/skjemabank>

Documentation collected during the work, with support from the Department, shall be handed in to the Department together with the report.

According to the current laws and regulations at NTNU, the report is the property of NTNU. The report and associated results can only be used following approval from NTNU (and external cooperation partner if applicable). The Department has the right to make use of the results from the work as if conducted by a Department employee, as long as other arrangements are not agreed upon beforehand.

Tentative agreement on external supervision, work outside NTNU, economic support etc
Separate description to be developed, if and when applicable.

Health, safety and environment (HSE)

The health, safety and environmental (HSE) work at NTNU shall constitute continuous and systematic efforts that are integrated into the primary activities. NTNU emphasizes the safety for the individual employee and student. The individual safety shall be in the forefront and no one shall take unnecessary chances in carrying out the work. Information in English on HSE is given on: <http://www.ntnu.no/hse>. In particular, if the student is to participate in field work, visits, field courses, excursions etc. during the Master Thesis work, he/she shall make himself/herself familiar with the *Fieldwork HSE Guidelines* <http://www.ntnu.no/hms/retningslinjer/HMSR07E.doc>. General HSE provisions that apply in all laboratories and workshops are given on: <http://www.ntnu.no/hse/labhandbook>.

The students do not have a full insurance coverage as a student at NTNU. If a student wants the same insurance coverage as the employees at the university, he/she must establish an individual travel and personal injury insurance. More information about students and insurance is found on the faculty HSE page on: <http://www.ntnu.no/ivt/adm/hms/>. (Documents are in Norwegian only, ask the supervisor to explain).

Start and submission deadlines

The work on the Master Thesis starts on **January 31, 2011**

The thesis report original (not bounded) and 2 bounded copies and the CD as described above shall be submitted at the latest on **June 21, 2011 at 1500 hrs.**

Professor in charge: Prof. Knut V. Høyland

Other supervisors: none

Signature

Prof. Knut V. Høyland

Department of Civil and Transport Engineering, NTNU

Date

CONTENTS

ABSTRACT.....	i
ACKNOWLEDGEMENTS.....	vii
CONTENTS.....	ix
LIST OF FIGURES	xiii
LIST OF TABLES	xvii
LIST OF ABBREVIATIONS AND SYMBOLS	xix
1. INTRODUCTION	1
1.1 General	1
1.2 Problem description.....	2
1.3 Objectives and scope of the thesis.....	2
1.4 Limitation of the thesis.....	3
2. THEORY AND BACKGROUND	5
2.1 Overview of ice ridge properties	5
2.1.1 General.....	5
2.1.2 Formation process and internal structure of ice ridge.....	5
2.1.3 Porosity and consolidation.....	7
2.2 Experimental testing and numerical analysis	8
2.3 Material model	9
2.3.1 General.....	9
2.3.2 Continuum and discrete mathematic model.....	10
2.3.3 Mohr-Coulomb model	11
2.3.4 Drucker-Prager model.....	13
2.3.5 Relation between Drucker-Prager and Mohr-Coulomb material parameters and the setup of parameters in this thesis.....	15
2.4 Literature review of shear box test and freeze-bonds mechanical properties	17

3. ANALYSIS OF SHEAR BOX EXPERIMENT	21
3.1 General	21
3.2 Ice rubble and equipment setup.....	21
3.3 Test procedure	23
3.4 Analysis of the three different phases in shear box experiment.....	25
3.4.1 General.....	25
3.4.2 Results and analysis of phase 1.....	26
3.4.3 Results and analysis of phase 2.....	29
3.4.4 Results and analysis of phase 3.....	38
4. RESULTS OF NUMERICAL MODELLING	41
4.1 General	41
4.2 Brief introduction to the numerical model	42
4.3 Setup and influence of input data	44
4.3.1 Simulation time.....	44
4.3.2 Rubble height and rubble density	44
4.3.3 Normal pressure	45
4.3.4 Friction.....	46
4.3.5 Mesh density	47
4.3.6 Dilatation angle.....	48
4.3.7 Summary	50
4.4 Results of the crack growth in numerical modelling.....	51
4.5 Results of the effect of the material parameters	52
4.5.1 General.....	52
4.5.2 A brief study of the influence of material parameters.....	52
4.5.3 A detailed study of material parameters and comparison between numerical and experiment results	55
4.6 Summary	67
5. ANALYSIS AND DISCUSSION	69
5.1 General	69

5.2 Analysis of material parameters	69
5.2.1 Young modulus	69
5.2.2 Friction angle and cohesion	70
5.3 Analysis of the application of cap hardening model	75
5.4 Scaling and comparison with recent studies.....	78
5.5 Analysis of uncertainties	79
5.5.1 Experimental uncertainties.....	79
5.5.2 Numerical modelling uncertainties	80
5.6 Summary	81
6. CONCLUSION AND RECOMMENDATION FOR FUTURE WORK.....	83
6.1 Conclusions	83
6.1.1 Testing.....	83
6.1.2 Numerical simulations	84
6.2 Recommendation for future work	85
6.2.1 Recommendation for experiment modelling	85
6.2.2 Recommendation for numerical modelling	86
REFERENCE.....	87
Appendix 1: The force-time series of the 14 tests	90
Appendix 2: Results of numerical simulation.....	93

LIST OF FIGURES

Figure 2.1 - Long and curvilinear ice ridge	6
Figure 2.2 - Principal cross-section sketch of an ice ridge	6
Figure 2.3 - The dimension of ice ridge.....	7
Figure 2.4 - The relation between experimental testing and numerical analysis.....	9
Figure 2.5 - Mohr-Coulomb yield surface in the meridional plane and the deviatoric plane.....	12
Figure 2.6 - Expression for deviatoric stress t and linear DP model	14
Figure 2.7 - Drucker-Prager stress criterion in the meridian plane.....	15
Figure 2.8 - Relationship between Drucker-Prager and Mohr-Coulomb material parameters as a function of the friction angle in the MC model.....	17
Figure 3.1 - Schematic drawing of the shear box experiment equipment.....	22
Figure 3.2 - Dimension and structure of the shear box.....	23
Figure 3.3 - Equipment setup for shear box experiment just before testing	24
Figure 3.4 - Time vs. displacement for High_Long tests.....	26
Figure 3.5 - Force time series from the shear box of High_Long_1/2/3 of phase 1	27
Figure 3.6 - Force time series from the shear box of High_Short_1/2/3 of phase 1	27
Figure 3.7 - Force time series from the shear box of Low_Long_1/2/3 of phase 1.....	28
Figure 3.8 - Force time series from the shear box of Low_Short_1/2/3 of phase 1	28
Figure 3.9 - Force time series from the shear box of Dry_Low of phase 1	28
Figure 3.10 - Force time series from the shear box of Extra_High_Short of phase 1 .	29
Figure 3.11 - Results of Hellmann's experiment	30
Figure 3.12 - Typical figure of the shear box experiment done in 2010.....	31
Figure 3.13 - Equipment of Hellmann's test in 1984.....	32
Figure 3.14 - Time force series of Low_Short_1	33
Figure 3.15 - The three individual experiment in the Low_Long situation.....	34
Figure 3.16 - Model tests and numerical modelling results in Serré's punch test	35

Figure 3.17 - The pre-described shear plane in the shear box experiment.	37
Figure 3.18 - The equipment after improvement	37
Figure 3.19 - A typical trend for phase 3	38
Figure 4.1 - Illustration of numerical model with coordinates.....	43
Figure 4.2 - The force under the condition of low and high confinement	46
Figure 4.3 - The force under the condition of different friction coefficient	47
Figure 4.4 - The force by using different grain size.....	48
Figure 4.5 – The force under the condition of different dilatation angle in the High_Short test	49
Figure 4.6 - The force under the condition of different dilatation angle in the Extra_High_Short test.....	49
Figure 4.7 - The Mises stress in the ice rubble (t=1 s).....	51
Figure 4.8 - The cracks in shear box experiment.....	51
Figure 4.9 - The figure of force vs. time by choosing different friction angle	53
Figure 4.10 - The figure of force vs. time by choosing different cohesion	54
Figure 4.11 - The figure of force vs. time by choosing different Young modulus.....	54
Figure 4.12 - Low_Long experiment results and numerical modelling with different Young Modulus.....	56
Figure 4.13 - High_Long experiment results and numerical modelling with different Young Modulus.....	56
Figure 4.14 - Low_Short experiment results and numerical modelling with different Young Modulus.....	57
Figure 4.15 - High_Short experiment results and numerical modelling with different Young Modulus.....	58
Figure 4.16 - Dry_Low experiment results and numerical modelling with different Young Modulus.....	59
Figure 4.17 - Extra_High_Short experiment results and numerical modelling with different Young Modulus	59
Figure 4.18 - Load-time curves in Test Low_Long with different cohesion when	

$\beta = 45^\circ$	60
Figure 4.19 - Load-time curves in Test Low_Long with different cohesion when $\beta = 25^\circ$	61
Figure 4.20 - Load-time curves in Test High_Long with different cohesion when $\beta = 45^\circ$	62
Figure 4.21 - Load-time curves in Test High_Long with different cohesion when $\beta = 25^\circ$	62
Figure 4.22 - Load-time curves in Test Low_Short with different cohesion when $\beta = 45^\circ$	63
Figure 4.23 - Load-time curves in Test Low_Short with different cohesion when $\beta = 25^\circ$	63
Figure 4.24 - Load-time curves in Test High_Short with different cohesion when $\beta = 45^\circ$	64
Figure 4.25 - Load-time curves in Test High_Short with different cohesion when $\beta = 25^\circ$	64
Figure 4.26 - Load-time curves in Test Dry_Low with different cohesion when $\beta = 35^\circ$	65
Figure 4.27 - Load-time curves in Test Dry_Low with different cohesion when $\beta = 15^\circ$	65
Figure 4.28 - Load-time curves in Test Extra_High_Short with different cohesion when $\beta = 45^\circ$	66
Figure 4.29 - Load-time curves in Test Extra_High_Short with different cohesion when $\beta = 25^\circ$	66
Figure 5.1 - Force at yielding point in Low_Long test versus corresponding initial cohesion with different values for the internal friction angle.....	70
Figure 5.2 - Force at yielding point in High_Long test versus corresponding initial cohesion with different values for the internal friction angle	71
Figure 5.3 - Force at yielding point in Low_Short test versus corresponding initial cohesion with different values for the internal friction angle	72

Figure 5.4 - Force at yielding point in High_Short test versus corresponding initial cohesion with different values for the internal friction angle	72
Figure 5.5 - Force at yielding point in Dry_Low test versus corresponding initial cohesion with different values for the internal friction angle	73
Figure 5.6 - Force at yielding point in Extra_High_Short test versus corresponding initial cohesion with different values for the internal friction angle.....	73
Figure 5.7 - Curve describing possible combination of the corresponding cohesion and friction angle.....	74
Figure 5.8 – Failure plane and stress state for High_Long test	76
Figure 5.9 - Failure plane and stress state for Extra_High_Short test.....	76
Figure 5.10 - Failure plane and stress state for Dry_Low test.....	77

LIST OF TABLES

Table 2.1 - Parameter differences between associated and non-associated flow.....	16
Table 3.1 - Test matrix of the shear box experiment specifying the normal confinement σ , the submersion time Δt , the rubble height h_r , the number of blocks N_b and the porosity η	25
Table 3.2 - Average loading velocity of each test	26
Table 3.3 - Chosen calculation time domain and friction angle of phase 3	39
Table 4.1 – Numerical simulation results by applying different rubble height.....	45
Table 4.2 - Numerical simulation results by applying different porosity	45
Table 4.3 – Numerical simulation results by applying different dilatation angle	50
Table 4.4 - Modelling parameters	50
Table 4.5 - The Young modulus for numerical modelling	60
Table 4.6 – Summary of the results	67
Table 5.1 - Possible combinations of cohesion and friction angle of numerical model for different test in order to fit with experiment data.....	74
Table 5.2 – Cap hardening	77
Table 5.3 - Comparison between present study and recent study of Drucker-Prager cohesion, for variable scaling parameters. (Full scale (FS) and model scale (MS)) ...	79

Note: Tables and Figures in appendixes are not included in the Lists above.

LIST OF ABBREVIATIONS AND SYMBOLS

Abbreviations

DP	Drucker-Prager
FB	Freeboard
FE	Finite Element
FEM	Finite Element Method
ISO	International Organization for Standardization
MC	Mohr-Coulomb
NASA	National Aeronautics and Space Administration
NTNU	Norwegian University of Science and Technology
PPT	Parts Per Thousand
RVE	Representative Volume Element
2D	Two-dimensional
3D	Three-dimensional

Symbols

c	Cohesion for MC model/Friction coefficient
d	Cohesion for DP model
d_{FS}	Cohesion for full scale
d_{MS}	Cohesion for model scale
e	Void ration
f	Mohr-Coulomb yield function
h_b	Block thickness
h_{cl}	Consolidated layer thickness
h_i	Level ice thickness
h_k	Keel thickness
h_r	Rubble height
h_s	Sail thickness
h_{kFS}	Keel thickness for full scale
h_{kMS}	Keel thickness for model scale
t	Time
A	Shear plane area
E	Young modulus
G	Linear plastic potential
K	Flow stress ratio

L_b	Block length
L_B	Shear box length
N_b	Number of ice blocks
R_{mc}	A measure of the shape of the yield surface in the deviatoric plane
V	Rubble volume
V_C	Cavities volume
V_S	Solid material volume
β	Friction angle for DP model
η	Porosity ratio
θ	Deviatoric polar angle
ρ	Rubble density
σ	Normal pressure
σ_C	Uniaxial compression pressure
σ_t	Uniaxial tension pressure
τ	Shear stress
φ	Friction angle for MC model
ν	Poisson's ratio
ψ	Dilatation angle
∇t	Submersion time

1. INTRODUCTION

1.1 General

First-year ice ridges play an important role in ice-structure interaction process in both arctic and sub-arctic marine areas. They are bulky ice features that can pose a major threat to offshore structures (Serré et al., 2011). Ice ridges are formed when sea ice is compressed or sheared under the action of wind and currents, and they are constantly shifting due to wind and sea current against offshore structures during interaction, which can cause remarkable loads (Heinonen, 2004).

Ice ridges are composed of a sail and a keel. The keel consists of a consolidated layer and an unconsolidated layer. The consolidated layer is a refrozen solid ice zone on top of the keel. The unconsolidated zone is made up of ice rubble and both the sail and the keel are porous. The voids in the sail comprise air and slush, while the voids in the keel consist of water and slush. Because of the equilibrium of ice rubble density and water buoyancy, the rubble above the water line (the sail) has a volume of about one tenth of the rubble below the water line (the keel) (Heinonen, 2004). So the potential threat from the keel is quite large and it will be a major contributor to the load during ice-structure interaction process. Because of this, the mechanical behaviour of the rubble in the keel is being researched in recent years.

According to the ISO standards (2010), ice rubble is defined as a granular material whose behaviour can be approximated by a hydrostatic pressure dependent model such as the Mohr-Coulomb model. Based on this definition, many ways to analysis ice rubble are introduced, namely field test, model test, analytical method and finite element method. Each of them has their own advantages and disadvantages. Field test is the most suitable situation for comparison with reality, but the boundary conditions are hard to define and error could happen during equipment setup process. Model tests are easier to set up and control, the boundary condition can be well defined, but the biggest problem of model test is scaling (Serré, 2011). The level ice strength can be weakened according to the scaling ratio by heating, but this is not possible for the mechanical properties of the rubble, as it is already at the freezing point in the full scale problem (Serré, 2011). Analytical methods are much simpler and more suitable for numerous simulations, such as probabilistic modelling with the Monte Carlo method. However, these methods imply the use of numerous assumptions, which often make them suitable and validated for only one type of boundary value problem (Serré, 2011). But numerical modelling, like finite element method could be helpful in this aspect. It can model more complex situations and it can combine a series of boundary conditions, model dimensions and material properties together in one simulation and repeat different assumptions in a shorter and easier way. But how to

verify the results of finite element method remains a problem and some other difficulties still remain unsolved, like not enough material definition in FE method, localized strain zone, how to model crack propagation and so on.

Punch test and shear box test are the two major tests which can be used to investigate the mechanical properties of ice rubble. Punch test is a kind of field test, which can be used to study rubble property in field, but boundary conditions are hard to predefine. As for shear box test, it is a model test and little has been done in this aspect. It uses man-made ice rubble produced in ice tank or rubble from field in a smaller scale, although the scaling is a major difficulty, the boundary conditions can be controlled by people. A brief literature review of both punch test and shear box test will be given in chapter 2.

1.2 Problem description

An important feature of ice rubble in keel is the freeze-bonds between ice blocks. It has been acknowledged as one of the physical mechanisms giving the rubble ice its peculiar aspects in comparison with other geotechnical materials such as sand and gravel (Serré et al., 2011). This feature is vital since it will always result in relative large force during ice-structure interaction. But not so much research has been done in this aspect. Serré (2011) shows the implement of cohesion softening could better simulate the post peak stress during punch test. Repetto et al. (2011 a, b and c) measured the freeze-bonds of individual ice blocks and related the strength of freeze-bonds to the ice rubble strength. The rubble strength and failure mechanism were investigated through 2D shear box testing of the rubble (Serré et al., 2011).

14 individual tests were done in the ice laboratory in NTNU (Norwegian University of Science and Technology). This study is the first one that relate the freeze-bonds properties to the shear strength and cohesive properties of the ice rubble. This work uses the assumption made by Liferove and Bonnemaire (2005) about a 3-phase description of the rubble deformation in the shear box tests of Hellman (1984). And the most important phase during shear box experiment is the primary phase controlled by the breakage of skeleton of ice rubble which is freeze-bonds. However, only model tests were preformed at that time and conclusions are made qualitatively and conceptually instead of being quantitatively.

1.3 Objectives and scope of the thesis

The objective of this thesis is to build up a finite element model of the shear box experiment mentioned above and analyse the tests numerically. Since the post-peak stress of ice rubble may not be that important, the main body of the thesis focuses on how to model the primary phase of the rubble deformation in the shear box experiment, which is governed by freeze-bonds of ice rubble. In order to achieve this

goal, the commercial finite element software ABAQUS 6.10-2 has been used to model the primary phase of the shear box experiment. The shear box tests were analysed with the finite element method using a Lagrange formulation that puts limitation on the size of the displacements, but can solve the initial short steps accurately. The thesis will study quantitatively the influence of cohesion and friction angle, Young modulus and other parameters for the primary phase of the experiments. Besides this, some conceptual analysis towards the second and third phases will be given, some shortcomings of the shear box experiment will be analysed and some advice and suggestions for further experiment improvement will be discussed at a later stage.

The organizations of the thesis are as follows. In the first chapter, a brief introduction of ice ridges and rubble, the shear box experiment, and objectives of the master thesis will be given. The second chapter gives the basic theory of ice rubble and the material model and provides a brief literature review of punch test, shear box test and mechanical properties of freeze-bonds. In the third chapter, the setup of the experiment done by Serré et al. (2011) will be presented, some results of their shear box experiment will be briefly introduced and a further analysis towards the three phases of the experiment together with some experimental limitations of the shear box test will be given. In the fourth chapter, the setup of the model, the assumptions during the modelling process and results of the finite element of primary phase will be given, some detailed analysis, like the crack pattern, the stress in the rubble, the failure mode, the parameter analysis for the shear box experiment will also be presented in this chapter. In the fifth chapter, discussion and further analysis of the physical experiment and modelling will be discussed. And conclusion and recommendation for further work will be given in the last chapter.

1.4 Limitation of the thesis

The thesis uses Lagrange method in finite element modelling process and this restricts large element distortion from happening during modelling, so only the primary stage of shear box test is analysed in this paper. Another limitation is how the results could be used when it comes to rubble-structure interaction happening in reality, for example, the question is to what extent the cohesion and friction angle that we get from this experiment could be applied when it comes to real world ice-structure interaction remains unsolved.

2. THEORY AND BACKGROUND

2.1 Overview of ice ridge properties

2.1.1 General

First-year ice ridges are common in Northern seas and can be a major threat to offshore structures. In this section, a brief introduction of ice ridge will be given. Information in this section is based on chapter 2 of Heinonen's (2004) doctor thesis.

2.1.2 Formation process and internal structure of ice ridge

Ridges are formed when level ice areas are compressed and sheared against each other due to environmental driving forces such as sea currents and wind. A compression ridge is formed when two large ice floes or ice fields collide with each other. The ice field might split into two parts before or during the compression process. Rubble is a result of crushing and flexural failure during the ridge formation process. A compression ridge is often irregular, both in the horizontal plane and in the vertical direction. A shear ridge is normally straight, because separate ice fields move laterally in opposite directions. Rubble formed this way contains smaller ice blocks than in the compression ridge. Rafting is a process during which an ice plate overrides or underides another ice plate. Finger-rafting with alternating upthrust and downthrust is also commonly observed (Sanderson, 1988).

Usually the first-year ice ridge is formed by a combination of these modes. In the Gulf of Bothnia, the ice ridge usually contains some layers of rafted ice with rubble. Ice ridge formation is, however, quite poorly known. The ice sheet thickness and the thickness inhomogeneity are important factors controlling which process is predominating, whether ridging or rafting. Increasing the thickness inhomogeneity raises the probability of ridging, while homogenous sheets have a high probability of rafting. Ridges are often found in the zone between land fast ice and drift ice. Ridges or rubble piles are also found in front of large structures like lighthouses or bridge piers. Generally, ridges can clearly be observed in an ice field, because they are usually long and curvilinear. However, large partially grounded ridge fields near the shore can also exist. In that case the field can be several hundred meters or several kilometres wide and it is impossible to say where the ridge line goes. Figure 2.1 shows a long and curvilinear ridge (NASA Earth Observatory, 2009).



Figure 2.1 - Long and curvilinear ice ridge (NASA Earth Observatory, 2009)
<http://earthobservatory.nasa.gov/Features/SeaIce/>

The internal structure of ice ridge can be referred in Figure 2-2 below:

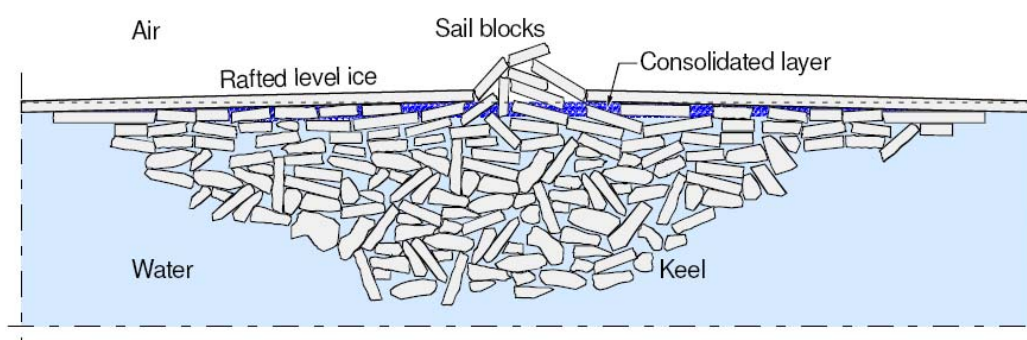


Figure 2.2 - Principal cross-section sketch of an ice ridge (Jensen et al., 2001)

The ice ridge contains a large number of ice pieces of varying sizes and shapes that are piled arbitrarily. Due to the hydrostatic equilibrium, the rubble above the sail has a volume of about one tenth of the rubble below the water line.

The dimensions, shapes and size distribution of the ice blocks determine the texture of the rubble. The initial ice condition, before the ridge was formed, is an important indicator. The ice block thickness is about the same as the level ice thickness when ridge was formed. The snow thickness above the ice indicates how much slush is present in the pores. Environmental conditions around the ridge such as the ambient temperature and the wind, as well as the snow cover, play a major role in heat transfer and consolidation. In the underwater part, the presence of currents causes shape modification of the ice block, deteriorating the rubble through thermal and mechanical erosion.

The main dimensions of a ridge are defined in Figure 2.3, in which h_k is the thickness of the keel and h_s is the thickness of the sail. Both of them are measured

from the water level. h_i is the level ice thickness and h_{cl} is the consolidated layer thickness. FB is the freeboard.

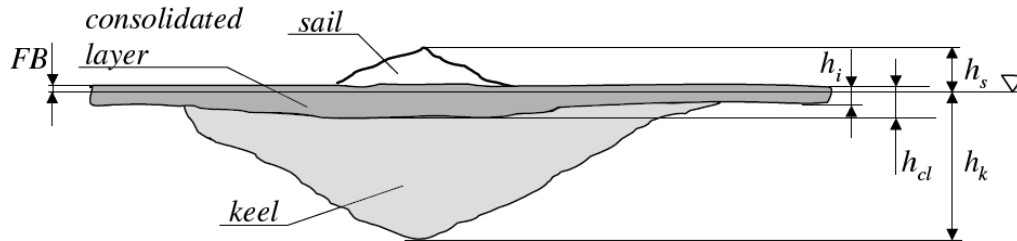


Figure 2.3 - The dimension of ice ridge (Heinonen, 2004)

The dimension of h_s , h_k , h_i , h_{cl} and FB is not arbitrary, there is a certain ratio between each other according to experience and field data. These ratios are discussed in the paper of Timco and Burden (1997), Kankaanpää (1998), Høyland (2002) and these results will not be present in this thesis.

2.1.3 Porosity and consolidation

Cavities in the rubble of the keel are filled with water and slush, but in the sail they contain snow and air. Hence the ridge is a porous feature. Once a ridge is formed it starts to freeze, because the average air temperature in winter is below the freezing point of water. The freezing zone expands downwards and ice blocks freeze together with the level ice layer or rafted layers, creating the consolidated layer which also is porous. Beneath the fully consolidated layer in the freezing zone the rubble is partially consolidated. Due to incomplete freezing, voids in the partially consolidated region contain water.

As it is stated above, the pores in ice ridges contain non-solid materials, like water, slush, snow and air. So there are two ratios that can be used to define ridge porosity. The porosity ratio η , which is defined as a volume of cavities V_c between the solid ice blocks compared with the total volume of rubble V . Another ratio is called void ratio e , which is defined as the ratio between the volume of voids and the volume of solid material V_s . The equations of these two ratios are given below:

$$\eta = \frac{V_c}{V} \quad e = \frac{V_c}{V_s} \quad (2.1)$$

$$\eta = \frac{e}{1 + e} \quad e = \frac{\eta}{1 - \eta} \quad (2.2)$$

The porosity depends on the internal stress state. The weight of the sail is balanced by hydrostatic forces in the consolidated layer with the keel underneath. The buoyancy in the keel causes hydrostatic pressure, compressing the rubble and resulting in denser

packing. Theoretically the rubble porosity is not constant in the vertical direction, because the total force distribution due to gravitation in the sail and buoyancy in the keel are not constant.

According to the values from the Baltic Sea by Kankaanpää (1998), the average porosity is usually around 30-35% in the keel, while the sail porosity is a bit less, around 20-27%. Similar values for keel porosity are also presented by Høyland et al. (2000) with the average of 38%.

The consolidated layer is the strongest part of an ice ridge. Once the ridge has been formed, the consolidation of rubble proceeds. Ice blocks freeze together with the level ice or with rafted ice layers. The internal structure of the ice is usually different than before the ridge was formed, because broken ice blocks have been reoriented during the ridge building process. The voids contain mainly water and slush in the partially refrozen zone. When the freezing continues, the water in the voids freezes, reducing the porosity. As the voids freeze solid, volume expansion causes cracking and further increases the inhomogeneity. Voids in the fully refrozen part contain mainly air. Due to the variation of environmental conditions during winter, the consolidated layer thickness, as well as the internal structure, has a strong seasonal dependency. Yasunaga et al. (2001) has performed uniaxial compression tests for a consolidated layer prepared in an ice tank from saline water. And they came to the conclusion that the constitutive models for sea ice could be applied also for refrozen ice to get an approximate ice load against a structure.

2.2 Experimental testing and numerical analysis

Model basin and laboratory-scale testing and numerical analysis are the two main methods we can use when we lack field test data or it is impossible or difficult to use analytical method. These two methods are correlated with each other. The experiments can provide basic data and confirm some assumptions for the numerical analysis, and the numerical could in return calibrate the results of experiments, improve the method of experiment testing and repeat some steps and operation which can take long time to do during experiment testing. By applying both of them, the final conclusion could be trustful and the design could be improved all the time. Figure 2.4 is taken from ABAQUS company's training course in 2003 and illustrates the relation between experimental testing and numerical analysis well.

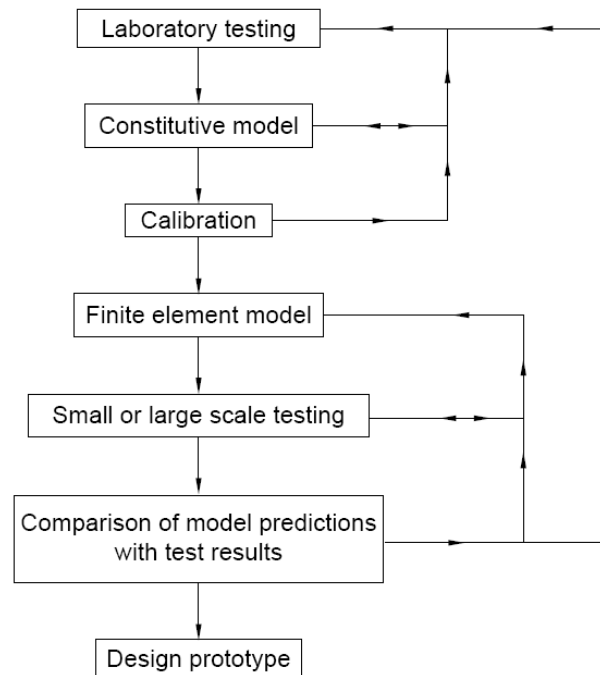


Figure 2.4 - The relation between experimental testing and numerical analysis

Figure 2.4 can be explained like this according to the company's training materials: *The measurements required in the simple laboratory tests depend on the proposed constitutive model. The constitutive model must be proposed based on simple experimental observations. Laboratory testing and constitutive model development are closely tied. The constitutive model must first be chosen qualitatively: it is important to capture the major features of material behaviour while minor features may be ignored in the model. Calibration (or quantitative choice) of the model parameters follows. Calibration should not be attempted beyond available (and repeatable) experimental results. The finite element model must capture important features of the physical situation, without irrelevant detail. Use of an adequate constitutive model is critical although simplifications are often justifiable. Small or large scale testing usually requires some knowledge of the physical behaviour being modelled. Details of the physical tests and finite element models must be compatible for meaningful comparisons. (ABAQUS, Inc, 2003)*

In this thesis, the previous work of the shear box experiment is done by carrying out physical experimental testing in lab and this thesis will focus on the numerical analysis using ABAQUS.

2.3 Material model

2.3.1 General

Continuum and discrete model are the two main mathematic approaches that can be used to describe the mechanical behaviour of ice rubble in the keel. And they have

their own disadvantages and advantages respectively, which will be discussed in section 2.3.2.

According to ISO standards (2010), the rubble in ice ridge keels can be considered as a granular material whose behaviour is approximated by a hydrostatic pressure dependent model. Two hydrostatic pressure dependent models are used frequently in ice rubble simulation, they are Mohr-Coulomb and Drucker-Prager model, section 2.3.3 will introduce these two models briefly. Section 2.3.3 is based on the ABAQUS company's training lessons-Analysis of Geotechnical problems with ABAQUS in 2003.

2.3.2 Continuum and discrete mathematic model

Continuum model is widely used in analysis and finite element modelling. They are easy to analysis since they consider the global behaviour of the whole rubble instead of the individual ice block. The continuum model requires less computational time and memory and also this model can fit in a wide range of physical model, since little specific requirement is needed for continuum model. Therefore deriving the mechanical property suitable for such type of models requires the study of a volume of rubble which is sufficiently large to avoid that the behaviour of one particular ice block introduces large variations in the global behaviour of the whole rubble, i.e. representative volume element (RVE) (Serré et al, 2011). But the question is that how to select the dimension of RVE? Since lacking in field test data, the RVE is difficult to choose thus preventing the continuum model from being accurate. The continuum approach is not ideal because the size of the particles (ice blocks) is large in comparison with the dimensions of the ridge and the structure. (Serré, 2011). Model scale investigations can provide insights into understanding of the concepts governing the rubble behaviour, but the scaling of its properties is still a matter of research (Høyland, 2010).

As for the discrete method, it can overcome the difficulty of choosing the proper dimension of RVE, since by applying the discrete method, the individual block can move by themselves and can avoid the behaviour of one particular ice block introducing large variations to the global behaviour of the whole rubble. But this method requires particular setup to each situation, which can not be always applied to every condition and it also requires large computational time and memory. Besides this, it also requires a custom description of the particle shapes and their contact properties, which has not been yet extensively studies for ice ridge problems (Serré, 2011).

In this thesis, we focus on the global behaviour of ice rubble instead of the individual performances of ice block and also the equipment setup and boundary condition is complex, so we choose continuum method to model the shear box experiment in our case.

2.3.3 Mohr-Coulomb model

ABAQUS has many constitutive models, they can be classified in the following categories:

Elasticity models:

- Linear, isotropic
- Porous, isotropic (nonlinear)
- Damaged, orthotropic (nonlinear; used in concrete, jointed material)

Plasticity models:

- Open surface, pressure independent (Mises)
- Open surface, pressure dependent (Drucker-Prager, Mohr-Coulomb)
- Closed surface (Cam-clay, Drucker-Prager with Cap)
- Multisurface (jointed material)
- Nested surfaces (bounding surface)

Other inelastic models:

- Continuum damage theories
- Endochronic theories

In this section, the open surface pressure dependent model-Mohr-Coulomb will be introduced.

The Mohr-Coulomb plasticity model is intended for modelling granular materials such as soils under monotonic loading conditions and does not consider rate dependence.

The ABAQUS Mohr-Coulomb plasticity model has the following characteristics:

- There is a regime of purely linear elastic response, after which some of the material deformation is not recoverable and can, thus, be idealized as being plastic.
- The material is initially isotropic.
- The yield behaviour depends on the hydrostatic pressure. One of the consequences of this is that the material becomes stronger as the confining pressure increases.
- The yield behaviour may be influenced by the magnitude of the intermediate principal stress.
- The material may harden or soften isotropically.
- The inelastic behaviour will generally be accompanied by some volume change: the flow rule may include inelastic dilatation as well as inelastic shearing.
- The plastic flow potential is smooth and non-associated.
- Temperature may affect the material properties.
- It does not consider rate-dependent material behaviour.

The most common expression for the Mohr-Coulomb failure criteria is written like this:

$$\tau = c + \sigma \tan \varphi \quad (2.3)$$

Where c is the cohesion, φ is the angle of internal friction and τ is the shear stress.

However, in ABAQUS implement, the Mohr-Coulomb model is written in terms of three stress invariants as below:

$$f = R_{mc}q - p \tan \varphi - c = 0 \quad (2.4)$$

Where $R_{mc}(\theta, \varphi)$ is a measure of the shape of the yield surface in the deviatoric plane (Figure 2.5),

$$R_{mc}(\theta, \varphi) = \frac{1}{\sqrt{3} \cos \varphi} \sin \left(\theta + \frac{\pi}{3} \right) + \frac{1}{3} \cos \left(\theta + \frac{\pi}{3} \right) \tan \varphi \quad (2.5)$$

φ is the slope of the Mohr-Coulomb yield surface in the $R_{mc}q$ - p stress plane, which is commonly referred to as the friction angle of the material, $0 \leq \varphi < 90^\circ$;

c is the cohesion of the material;

θ is the deviatoric polar angle defined as:

$$\cos 3\theta = \left(\frac{r}{q} \right)^3 \quad (2.6)$$

The Mohr-Coulomb model assumes that the hardening is defined in terms of the material's cohesion, . The cohesion can be defined as a function of plastic strain, temperature, or field variables.

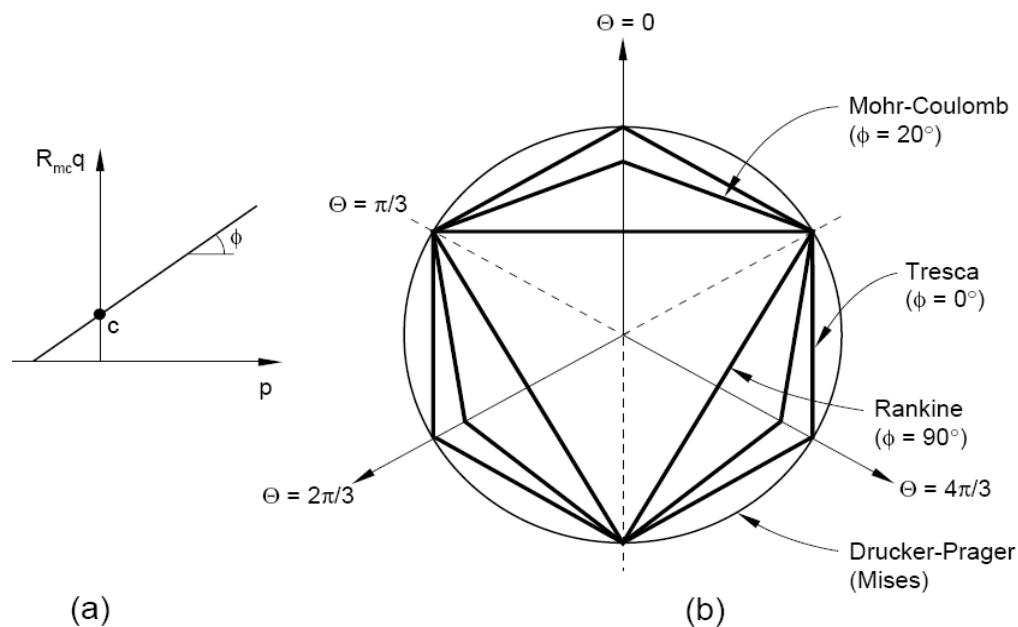


Figure 2.5 - Mohr-Coulomb yield surface in the meridional plane (a) and the deviatoric plane (b)

2.3.4 Drucker-Prager model

The DP model is a smooth approximation of the MC model. The parameters are matched by adjusting the cone size in the DP model. The reason is that the MC yield envelope contains corners in the stress space, so the MC model is not robust in numerical FE analysis without any modification.

The DP model is also intended to simulate material response under essentially monotonic loading, such as the limit load analysis of a soil foundation. These models are the simplest available for simulating frictional materials.

The basic characteristics of this set of models in ABAQUS implement are:

- There is a regime of purely elastic response, after which some of the material deformation is not recoverable and can, thus, be idealized as being plastic.
- The material is initially isotropic.
- The yield behaviour depends on the hydrostatic pressure. One of the consequences of this is that the material becomes stronger as the confining pressure increases. The material may harden or soften isotropically. The models differ in the manner in which the hydrostatic pressure dependence is introduced.
- The inelastic behaviour will generally be accompanied by some volume change: the flow rule may include inelastic dilatation as well as inelastic shearing. Two different flow rules are offered.
- The yield behaviour may be influenced by the magnitude of the intermediate principal stress.
- The material may be sensitive to the rate of straining.
- Temperature may affect the material properties.

A choice of three different yield criteria is provided in ABAQUS within DP model. The differences are based on the shape of the yield surface in the meridional plane: a linear form, a hyperbolic form, or a general exponent form.

The yield surface of the linear model is what we use in our modelling, it can be written as:

$$F = t - p \tan \beta - d = 0 \quad (2.7)$$

The cohesion, d , is related to the hardening input data as

$$d = (1 - \frac{1}{3} \tan \beta) \sigma_c \text{ if hardening is defined by uniaxial compression, } \sigma_c;$$

$$d = (\frac{1}{K} + \frac{1}{3} \tan \beta) \sigma_t \text{ if hardening is defined by uniaxial tension, } \sigma_t$$

$$d = d \text{ if hardening is defined by shear (cohesion)}$$

β (the friction angle) and K are material parameters. d, σ_c or σ_t is used as the

isotropic hardening parameter, which is assumed to depend on the equivalent plastic strain.

β is the cohesion angle which depends on the cohesion angle c in MC model. The K is flow stress ratio, which reflects the influence of intermediate principal stress to the plane and K must be within this range $0.778 \leq K \leq 1.0$. K is shown in Figure 2.6.

The measure of deviatoric stress, t , allows matching of different stress values in tension and compression in the deviatoric plane, thus providing flexibility in fitting experimental results. The t is shown in Figure 2.6. When $K=1$, we have $t=q$, which is curve a (Mises) in Figure 2.6.

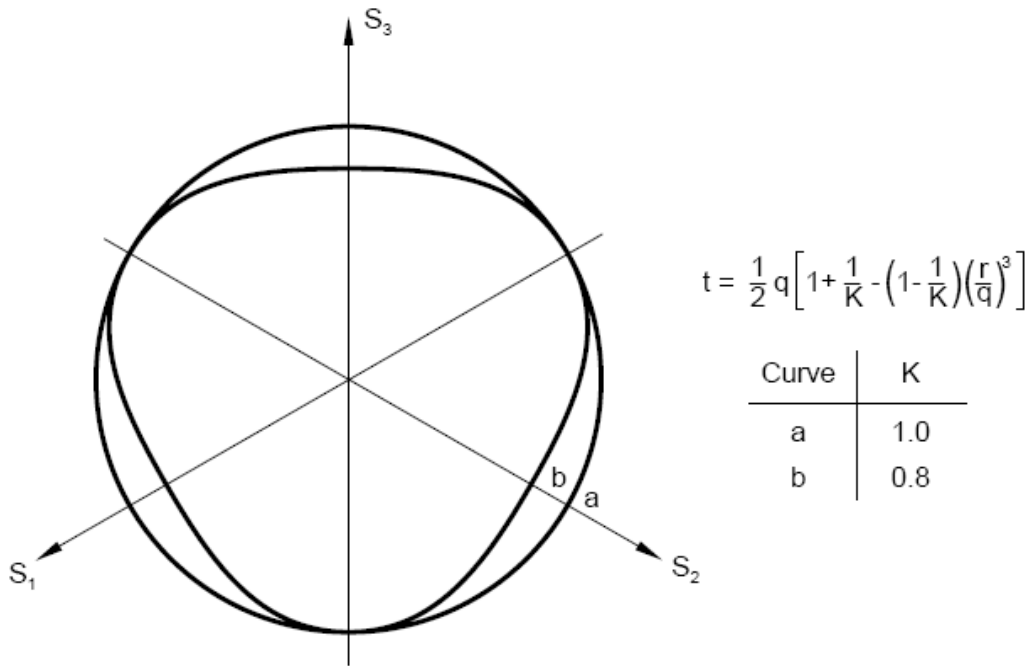


Figure 2.6 - Expression for deviatoric stress t and linear DP model

We assume a (possibly) non-associated flow rule, where the direction of the inelastic deformation vector is normal to a linear plastic potential, G :

$$d\epsilon^{pl} = \frac{d\bar{\epsilon}^{pl}}{c} \frac{\partial G}{\partial \sigma} \quad (2.8)$$

Where $G = t - p \tan \psi$, c is a constant that depends on the type of the hardening data,

$d\bar{\epsilon}^{pl} = |d\epsilon_{11}^{pl}|$ in uniaxial compression,

$d\bar{\epsilon}^{pl} = d\epsilon_{11}^{pl}$ in uniaxial tension, and

$d\bar{\epsilon}^{pl} = \frac{d\gamma^{pl}}{\sqrt{3}}$ in pure shear.

ψ is the dilatation angle in the p-t plane. This flow rule definition precludes dilatation angles $\psi > 71.5^\circ$ ($\tan\psi > 3$), which is not likely to be a limitation for real materials.

Flow is associated in the deviatoric plane but non-associated in the p-t plane if $\psi \neq \beta$. For $\psi = 0$, the material is non-dilatational and if $\psi = \beta$, then $K=1$ and the model is fully associated, which is classic Drucker-Prager model in ABAQUS that we use in our simulation.

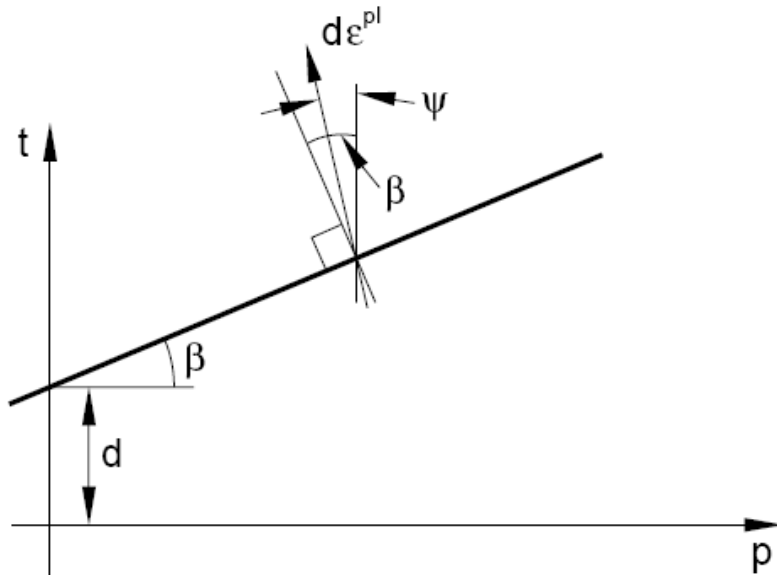


Figure 2.7 - Drucker-Prager stress criterion in the meridian plane

So in summary, as for MC model, there are two parameters that need to be decided as the input to the model, they are cohesion c and friction angle φ . As for DP model, there are four parameters that need to be defined. In order to make differences between MC and DP parameters, cohesion in the MC model is c and the friction angle φ , while in the DP model the corresponding parameters are d and β . The other two input parameters in DP model are dilatation angle ψ and flow stress ratio K . The setup of these parameters will be discussed in the following chapter.

2.3.5 Relation between Drucker-Prager and Mohr-Coulomb material parameters and the setup of parameters in this thesis

As for the plane strain condition and shear condition, we can assume $K=1$ and the relation between parameters of Drucker-Prager and Mohr-Coulomb is shown below:

$$\sin\varphi = \frac{\tan\beta\sqrt{3(9 - \sin^2\psi)}}{9 - \tan\beta\tan\psi} \quad (2.9)$$

$$\cos\varphi = \frac{\sqrt{3(9 - \sin^2\psi)}}{9 - \tan\beta\tan\psi} \quad (2.10)$$

For associated flow model, we have $\psi = \beta$, so that

$$\tan\beta = \frac{\sqrt{3}\sin\varphi}{\sqrt{1 + \frac{1}{3}\sin^2\varphi}} \quad (2.11)$$

$$\frac{d}{c} = \frac{\sqrt{3}\cos\varphi}{\sqrt{1 + \frac{1}{3}\sin^2\varphi}} \quad (2.12)$$

For non-associated flow, we have $\psi = 0$, so that

$$\tan\beta = \sqrt{3}\sin\varphi \quad (2.13)$$

$$\frac{d}{c} = \sqrt{3}\cos\varphi \quad (2.14)$$

The differences between parameters of DP model and MC model are decreasing along with the increase of MC model friction angle φ . For normal friction angle in reality, the differences between the parameters of associated and non-associated flow is not very large, which can be illustrated in Table 2.1.

Table 2.1 - Parameter differences between associated and non-associated flow

Friction angle of MC model φ	Associated flow		Non-associated flow	
	Friction angle of DP model β	d/c	Friction angle of DP model β	d/c
10°	16.7°	1.70	16.7°	1.70
20°	30.2°	1.60	30.6°	1.63
30°	39.8°	1.44	40.8°	1.50
40°	46.2°	1.24	48.1°	1.33
50°	50.5°	1.02	53.0°	1.11

Above is the relation between the parameters of DP and MC model in shear and plane strain situation. Another two relations are given when it comes to compressive and tension situation:

$$\text{Compressive:} \quad \tan\beta = \frac{6\sin\varphi}{3 - \sin\varphi}; \quad d = \frac{6c \cos\varphi}{3 - \sin\varphi} \quad (2.15)$$

$$\text{Tension:} \quad \tan\beta = \frac{6\sin\varphi}{3 + \sin\varphi}; \quad d = \frac{6c \cos\varphi}{3 + \sin\varphi} \quad (2.16)$$

In Heinonen's (2004) paper, he gives a more detailed description for the relation between DP and MC material parameters in compression, tension and shear

situation. It is shown in Figure 2.8:

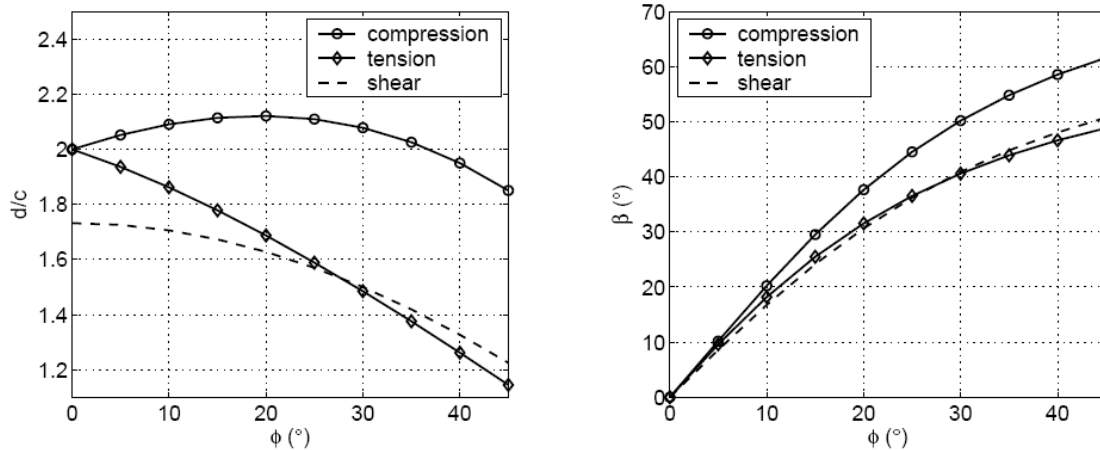


Figure 2.8 - Relationship between Drucker-Prager and Mohr-Coulomb material parameters as a function of the friction angle in the MC model (Heinonen, 2004)

In this case in our thesis, the situation is plane strain and the rubble will go through shear failure, meanwhile we assume that there is no dilatation happening during the primary phase, so $\psi = 0$ and $\psi \neq \beta$, so it is non-associated flow, the plain stress ratio K equals to 1 and the relation of the parameters between DP and MC model is:

$$\text{Shear:} \quad \tan\beta = \sqrt{3}\sin\phi; \quad d = \sqrt{3}c \cos\phi \quad (2.17)$$

2.4 Literature review of shear box test and freeze-bonds mechanical properties

Many shear box experiments were done, like the direct shear box experiment done by Prodanovic (1979), Weiss et al. (1981), Hellmann (1984), a simple shear box done by Urroz and Ettema (1987) and so on, they have come into various of different conclusions towards ice rubble properties and freeze-bonds mechanics. This section will review some of the articles and highlight the properties of freeze-bonds of ice rubble.

Prodanovic (1979) conducted a series of direct shear tests using unconsolidated ice rubble and he gave the value of 0.25 and 0.56 kPa for cohesion as well as 47° and 53° for the friction angle corresponding to ice rubble piece thickness of 19 mm and 38 mm. The larger confinement pressure indicated an increase of the effective shear modulus due to densely packed ice rubble. And Prodanovic attributes the resistance of the rubble to different mechanisms: friction at ice blocks contact point, interlocking between ice pieces and cohesion or shear strength of the bonding between the ice pieces. The friction and interlocking govern the frictional part of the shear strength,

whereas the freeze-bonds is responsible for the cohesive part.

Weiss et al. (1981) measured saline unconsolidated rubble on a scale of 1:10 with a direct shear box and they reported cohesion from 1.7 to 4.1 kPa and friction angle from 11° to 34°. They also found that the cohesion strength was proportional to the ice rubble piece thickness, a parameter that can be called relative cohesion, which is the cohesion divided by the ice rubble thickness. The value for relative cohesion is 16 ± 8 kPa/m.

Hellmann (1984) has conducted an interesting and profound experiment, which has given a clear description of the process in the shear box experiment. The experiment equipment he used is a square shear cylinder and two square side chambers of about 0.5m² cross section orthogonally arranged. Two mechanically coupled pistons displace the ice material within the main chamber inducing a shear process. The experiment equipment will completely enclosed and confined the ice rubble and was able to discern three distinct phases or shear modes. Three significant phases were presented in his paper:

Phase 1: At the beginning of the tests, a steep increase in the shear force can be identified while the normal force remains at the original value. This process can be interpreted as a denser packing of ice particles before the real shearing starts. The highest value of this phase is reached after less than 2 mm displacement. This is the primary shear box of the test.

Phase 2: While in phase 1, the normal force remains nearly constant, in phase 2 this normal force starts to increase due to dilatation of ice fragments. Simultaneously the shear force increases further but at a slower rate than phase 1. The absolute maximum value of the shear force happens at the end of this phase. It occurs within a displacement range of about 50 to 150 mm. It is called secondary shear mode.

Phase 3: After exceeding the maximum value, the shear force drops off more or less abruptly and remains at a lower level until the end of the shear process, while the normal force further increases until it remains at a nearly constant value. The phase can be defined as a continuous friction process after the initial failure of the ice.

Urroz and Ettema (1987) has conducted a simple shear box experiment in order to study the shear strength characteristics of floating layers of vertically unconstrained ice rubble comprised of parallelepiped ice blocks. And a comparative set of experiments was conducted using polyethylene blocks in order to elucidate the shear strength characteristics unique to a layer of floating ice rubble. They came to the conclusion that the shear strength of a layer of floating ice rubble is a function of normal stress, time, layer thickness and porosity, fragment size, shape and roughness, as well as temperature of air, water and ice fragments. And after the comparison between ice rubble and polyethylene blocks, they came to the conclusion that freeze-bonds has played an important role in ice rubble. While the ice rubble

undergoes continuous shear, a floating layer of ice rubble behaves as a cohesionless material and the shear strength can be expressed as $\tau = K\gamma_e H \tan\phi$, where $\gamma_e H$ is the average vertical stress acting through a layer of thickness H and porosity; K is a parameter that is usually taken to be the coefficient for passive stress for the layer of ice rubble; $\gamma_e = 0.5(1 - \eta)(1 - \rho_i/\rho)\rho_i g$, which is an equivalent specific weight of the ice rubble. ρ_i and ρ are densities of ice and water respectively.

Urroz and Ettema (1989) described the significance of internal friction between ice blocks and interlocking phenomena under rubble deformation. They came to the conclusion that the previous work, like Prodanovic (1979) has resulted in a higher friction angle due to the confinement resulting from buoyancy load. And they also reported that the cohesion of ice rubble depends on the stress state resulting in an effective angle, which is less than the friction angle associated with an apparent Mohr-Coulomb criterion.

Urroz and Ettema (1991) argued that accumulations of ice rubble undergoing continuous shear deformation are essentially cohesionless. In terms of the Mohr-Coulomb failure criterion, therefore, they do not exhibit a cohesive intercept at zero confining pressure. The argument leads to the conclusion that a linear Mohr-Coulomb relationship may not be fully appropriate for describing the shear deformation of ice rubble in continuous shear. The term usually described as ice-rubble cohesiveness should be replaced with terms which more accurately account for freeze bonding between contacting ice pieces and ice-piece deformation (crushing and/or flexure).

Sayed et al. (1992) observed in shear box tests with plain strain conditions that deformations in rubble are non-recoverable. Rubble didn't have time to consolidate between sample preparation and testing. They also reported that the porosity of rubble decreases due to an increase of hydrostatic pressure since they measured the relation between the hydrostatic pressure and volumetric strain describing the compressibility of rubble.

Timco and Cornett (1999) had done tests where two principal strains continuously increased at constant rates and the two strain rates were of opposite sign. By doing this, they had created a plane strain condition and they found that the angle of internal friction decreased with increasing degree of compression. And they found that the previous direct shear box tests had the advantage of simplicity but the rubble has to fail along a specified failure plane, preventing from getting reliable quantitative results.

Liferov (2005) and Shafrova (2007) have conducted a series numerical simulation using 2D discrete ice rubble and they concluded that the freeze-bonds properties are important for the strength evaluation and deformation behaviour of ice rubble. They are responsible for the cohesive strength of the rubble. After that, Liferov and

Bennemaire (2005) further analysis the phase of shear box experiment based on the work of Hellmann (1984) and they concluded that during the initial failure of shear box experiment, the ice rubble skeleton, which is freeze-bonds network joining the ice rubble has failed. Cohesion resistance and interlocking between ice rubble have dominated the primary stage, while friction doesn't function at all or play a minor role in this stage. Along with the propagation of rubble failure, the freeze-bonds has totally been destroyed, which can mobilize the entire frictional resistance, but no freeze-bonds is left to contribute to the cohesive resistance. When the freeze-bonds breaks, the ice rubble became totally cohesionless, which draws the same conclusion of Ettema and Urroz's work in 1991.

Heinonen (2004) has carried out a series of punch tests and numerical simulations in his paper. He came to the conclusion that cohesive-frictional material models like Drucker-Prager and Mohr-Coulomb describe only the shearing failure with volumetric expansion. If rubble undergoes loading which causes confinement, the presence of hydrostatic pressure increases the material strength without any limit, although the material fails by shearing. He also found that all tested material models resulted in high values for initial cohesion compared with earlier published small-scale data. The reason is that in the experiments he carried out the global failure is not simultaneous, so the initial cohesion is larger than the average cohesion in the global shear failure surface at the peak force, whereas cohesion is smaller due to the softening behaviour.

Serré (2011) has modelled the action of the model rubble ice on the punch tests with a Mohr–Coulomb friction angle of 45° and a 0.5 kPa homogeneous or 1.2 kPa linearly distributed cohesion, respectively for the warm and cold ridges. The cohesion was assumed to soften linearly over a 0.02 plastic strain range in order to represent the freeze-bonds failure in the rubble. And he came to the conclusion that the cohesive softening model better reproduced the experiment post peak behaviour than the constant cohesion (in time) model. Also the ridge history and previous disturbances play a significant role on the value of the cohesion. The maximum cohesive and frictional force cannot be present together in any particular location in the rubble ice.

3. ANALYSIS OF SHEAR BOX EXPERIMENT

3.1 General

In this chapter, a brief introduction of the shear box experiment performed by Nicolas Serré and Ada Repetto in 2010 (Serré et al., 2011 and Repetto and Høyland, 2011) will be given and the numerical simulation results in chapter 4 will be based on this experiment. Section 3.2 and 3.3 will explain the setup of the equipment and the test procedures.

The ice rubble dimension was 60mm×40mm×22mm (depth) and the shear box dimension was 600mm×40mm×600mm (depth), so the width of the rubble and shear box was the same, which will result in 2D plane strain conditions. The upper part of the Plexiglas shear box could move while the lower part is fixed, which created the shear conditions. Freeze-bonds were created by submerging the newly made ice rubble into water for different time period. Different vertical confinements were applied at the top of the ice rubble during shearing process.

Section 3.4 is the initial analysis towards the results of the data in the shear box experiment and it is not done in the previous paper. The conclusion of section 3.4 will provide further information and assumptions for the numerical modelling process in the next chapter.

3.2 Ice rubble and equipment setup

The ice rubble was created in the ice tank in NTNU. The ice tank is called FRYSIS II, which is 0.8m×1.2m×1.3m (depth) with heated walls and bottom. During the ice grow process, the air temperature was set to be -20°C and the salinity of the water was 8 ppt. According to experience, the ratio between water salinity and ice block salinity is 5:1, so the average ice sample salinity is around 3 ppt in this case. At last, a 20 cm layer of columnar saline ice was grown.

The scaling ratio in this experiment was set to be 1:20. And the dimension of the ice rubble is chosen according to the observations of Høyland (2007): he observed that the full scale average sail block dimension in the Barents Sea was 1.2m×0.8m×0.44m. So finally the ice rubble was cut to 60mm×40mm×2 mm (depth) with a band saw. All the rubble ice in this experiment is composed of ice blocks presenting all the same dimension.

The ice rubble was piled randomly into the shear box and it is worthwhile to mention that the blocks are not necessarily oriented randomly as it is expected to be, because

the block thickness is much less than the block width and length (Heinonen, 2004), so they will present a certain trend of orientation instead of being packed randomly. But this assumption of randomly packing is good enough for this experiment. After the blocks were produced, they were stored in plastic boxes at -7°C .

A schematic drawing of the shear box is shown in Figure 3.1. There are three parts in this system. The upper part is supported by wheels rolling along a lubricated rail with the friction to be 11 N during all the tests and this force will be subtracted from all the force time series in this experiment. The lower part is fixed to a stiff metal frame, which can not move during the tests. Another part is the sliding roof supported wholly by the ice rubble, which will supply the normal confinement during the tests.

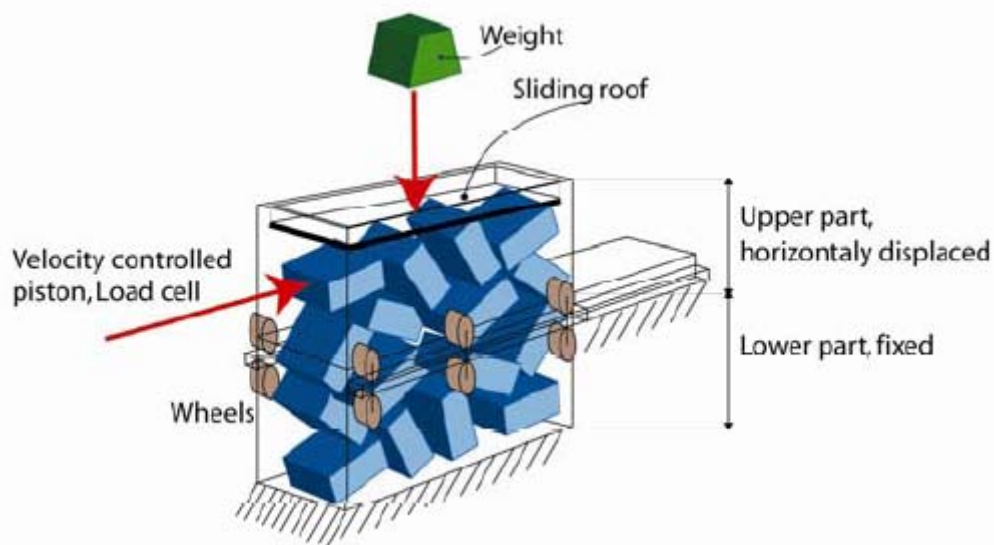


Figure 3.1 - Schematic drawing of the shear box experiment equipment (Serré et al., 2011)

The upper part is moved by a velocity controlled hydraulic piston. The force exerted by the piston is recorded with a sampling rate of 1 Hz by a load cell with maximum capacity of 5 kN. The velocity during the test is constant, but in between tests it varies from 0.0012 m/s to 0.0020 m/s (average value of 0.0016 m/s). The velocity in each test will be presented in details in section 3.4. The box had holes in the bottom of the lower part to allow water to drain out after submersion.

The size of the shear box is illustrated below in Figure 3.2. A 100 mm high wooden board was placed in the bottom of the shear box in order to avoid the ice rubble from sticking to the Plexiglas box. The size of the shear box should in principal contain at least one RVE (representative volume element). Although there is no agreement on how large the RVE should be for ice rubble, for continuum behaviour it is often given as 10 times the size of the heterogeneities (Lemaitre and Chaboche, 1990), so the shear box length (600 mm) is selected to be 10 times larger than the rubble length (60

mm). As it is stated before, the width of the ice rubble (40 mm) is selected to be the same of the width of the shear box (40 mm) in order to study the behaviour of the rubble in two dimensions only and remove the complications linked to 3D effects.

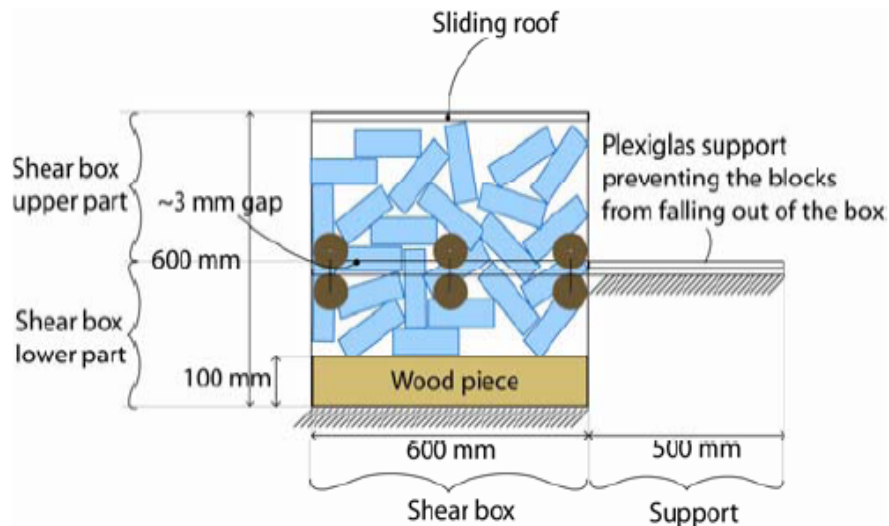


Figure 3.2 - Dimension and structure of the shear box
(Serré, Repetto and Høyland, 2011)

In summary, a 2D ice rubble shear box experiment was created. The rubble will slide along a pre-defined path and fail the ice for different normal pressures. Now the only difficult is how to build up freeze-bonds in the experiment, which will be introduced in the next section.

3.3 Test procedure

The rubble will be put in the shear box until the rubble height is approximately 400 mm. The number of blocks in each test was recorded in order to calculate the initial porosity of the ice rubble in the shear box experiment:

$$\eta = 1 - \frac{N_b h_b L_b}{h_r L_B} \quad (3.1)$$

Where N_b is the number of ice blocks, h_b is the block thickness, L_b is the block length, h_r is rubble height and L_B is the shear box length. The porosity is within the range of 20% to 40%, a summary of the ice rubble porosity is summarised in Table 3.1.

As it is stated above, the shear box will be kept in temperature -7°C situation once the filling is completed. After that, the ice rubble together with the sliding roof will be submerged into another ice basin with a salinity equal to the salinity from the ice tank

(8 ppt). The air temperature is set to be -1°C and the water in another basin is set to be at its freezing point, which is -0.3°C . During submersion, the normal confinement over the rubble is the same in all the tests, and equal to the weight of the roof-665 Pa.

Two kinds of submersion time are employed in the experiment, one is 20 hours, referred as Long tests, another is 10 minutes, referred as Short test. The longer the ice rubble submerges in the water, the more deterioration it will go through. After submersion, the shear box is removed from the water, left for a couple of minutes to drain and placed in the stiff metal frame for mechanical testing. Figure 3.3 shows the equipment just before testing.

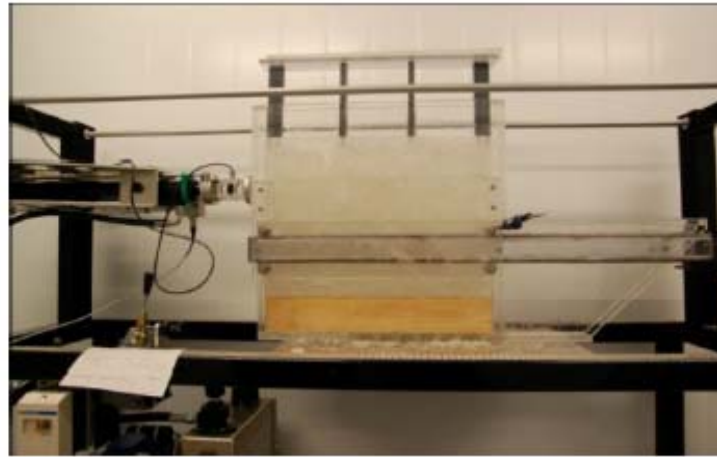


Figure 3.3 - Equipment setup for shear box experiment just before testing
(Serré et al., 2011)

The air temperature during the mechanical tests was -7°C . Two kinds of confinement pressure are used: one is 3020 Pa, referred as High test, another is 860 Pa, referred as Low test. Each combination of the two submersion times and the two normal confinement, which ran 3 times, see Table 3.1 for a test matrix. Another two extra tests were also carried out during the experiment, one dry situation where the ice rubble was not submerged with low confinement, referred as Dry_low test, another with short submerging time under the confinement pressure to be 20500 Pa, which is the weight of a standard person, referred as Extra_High_Short test. So there are 14 experiments in total.

Table 3.1 - Test matrix of the shear box experiment specifying the normal confinement σ , the submersion time Δt , the rubble height h_r , the number of blocks N_b and the porosity η . (Serré et al., 2011)

σ [Pa]	Δt [hr]	h_r [m]	N_b	η	Test Name
3020	20	0.450	132	35.5	High_Long_1
		0.471	123	42.6	High_Long_2
		0.364	131	20.8	High_Long_3
	0.17	0.405	123	33.2	High_Short_1
		0.425	131	32.1	High_Short_2
		0.425	126	34.7	High_Short_3
860	20	0.491	158	29.3	Low_Long_1
		0.456	142	31.5	Low_Long_2
		0.386	132	24.8	Low_Long_3
	0.17	0.406	127	31.2	Low_Short_1
		0.439	133	33.3	Low_Short_2
		0.399	129	28.9	Low_Short_3
	0	0.446	127	37.4	Dry_Low
20500	0.17	0.446	127	37.4	Extra_High_Short

3.4 Analysis of the three different phases in shear box experiment

3.4.1 General

Serré et al. (2011) came to the conclusion that a primary and a secondary failure mode were observed and the rubble failure was initiated by freeze-bonds failures. And based on the experiment data, they concluded that the three phases of the shear box tests can be described by Hellmann (1984), which has been discussed in section 2.4.

In the following three sections, 3.4.2 will analysis and present the data for phase one and put forward a method on how to define the simulation time properly for phase 1 in the numerical modelling in order to compare the results between experimental and numerical modelling accurately. Section 3.4.3 will analysis phase two and will reach the conclusion that the description and conclusion towards phase 2 in Serré et al. (2011) paper is not that accurate and the experiment setup has some flaws that it is impossible to model the post-peak phase accurately. Section 3.4.4 will analysis phase three. Since most of the rubble has been sheared to failure, so it is possible to calculate the friction coefficient of the ice rubble during the last phase. But the question whether this friction coefficient can be related to friction angle of ice rubble and freeze-bonds still need discussion and further work.

3.4.2 Results and analysis of phase 1

3.4.2.1 Loading velocity

As it is stated above, the loading speed in this experiment varied from 0.0013 m/s to 0.0024 m/s, with an average speed of 0.0016 m/s. The loading speed was critical to the determination of different phases, especially to the primary phase, because the primary phase will only have a few centimetres. Any speed variation will result in large displacement variation, so this part will calculate the loading speed in each individual tests.

Figure 3.4 shows the loading velocity of the 3 reparative High_Long tests.

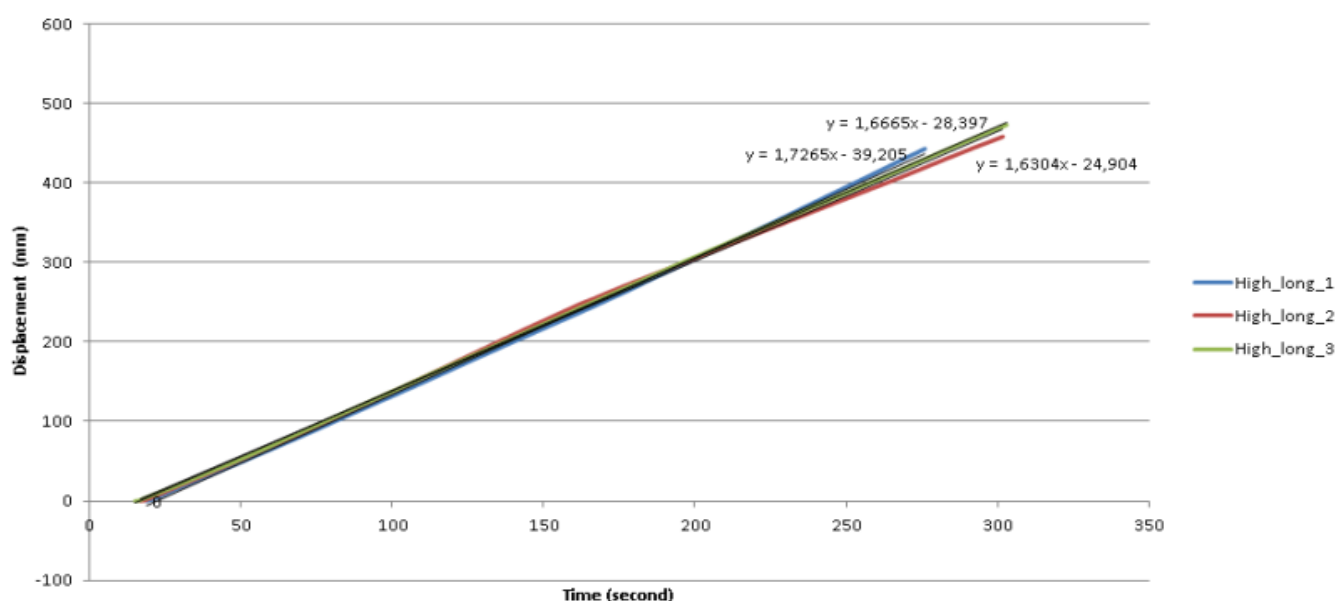


Figure 3.4 - Time vs. displacement for High_Long tests

It shows that the loading velocity is constant through the experiment, but varies a bit between each test. The speed for High_long_1, 2 and 3 is 1.7265 mm/s, 1.6304 mm/s and 1.6665 mm/s respectively. Table 3.2 summarizes the loading speed in all the 14 rounds of tests.

Table 3.2 - Average loading velocity of each test

Test Name	Loading Velocity [mm/s]
High_long_1/2/3	1.7265/1.6304/1.6665
High_short_1/2/3	1.552/ 1.355/1.717
Low_long_1/2/3	1.417/1.629/1.776
Low_Short_1/2/3	1.344/1.449/1.450
Dry_Low	1.409
Extra_High_Short	2.368

3.4.2.2 Force time series from the shear box test for phase 1

At this stage, the force time series diagrams will be drawn until the initial 6 seconds according to the assumption made in the previous paper. The friction force of the lubricated rail, which is 11 N has been subtracted from all of the diagrams.

Below there are 6 figures, showing the curve of force vs. time for the first phase in the 14 cases.

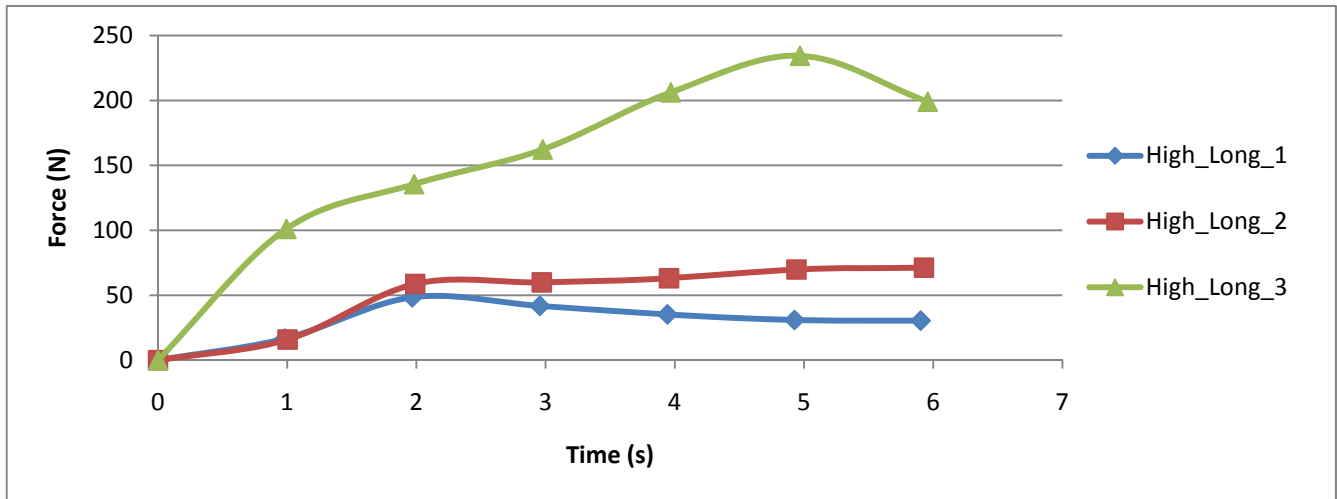


Figure 3.5 - Force time series from the shear box of High_Long_1/2/3 of phase 1

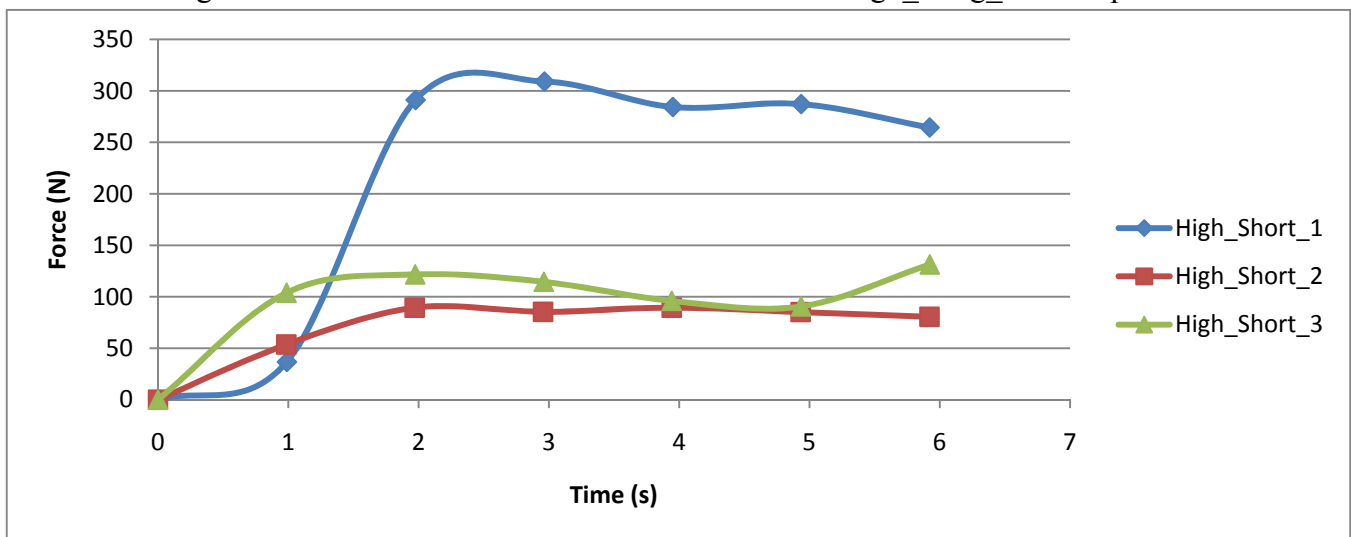


Figure 3.6 - Force time series from the shear box of High_Short_1/2/3 of phase 1

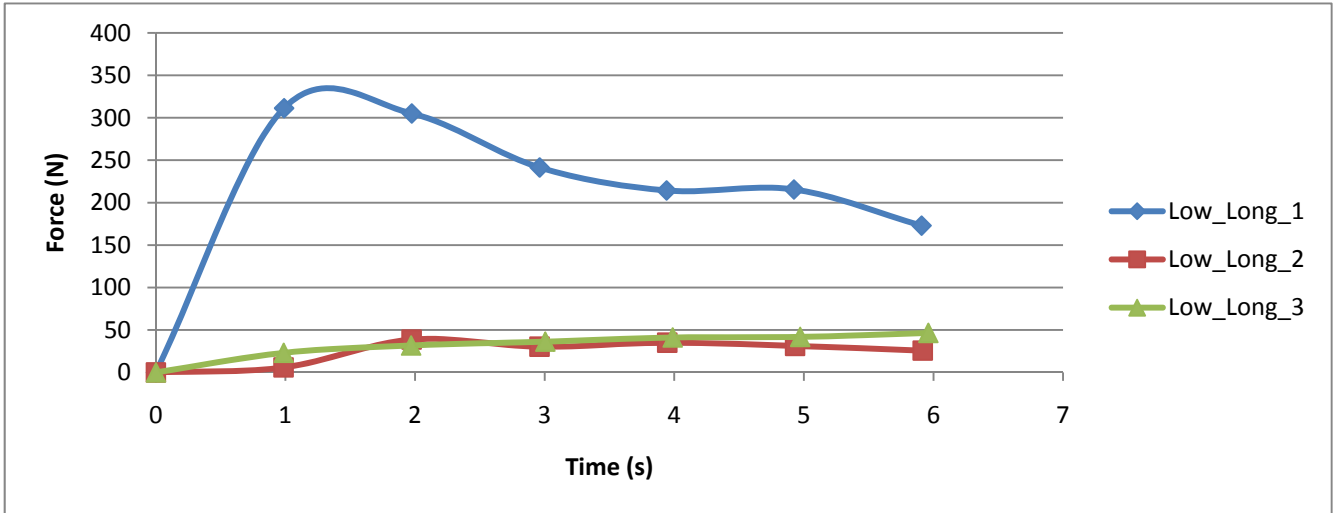


Figure 3.7 - Force time series from the shear box of Low_Long_1/2/3 of phase 1

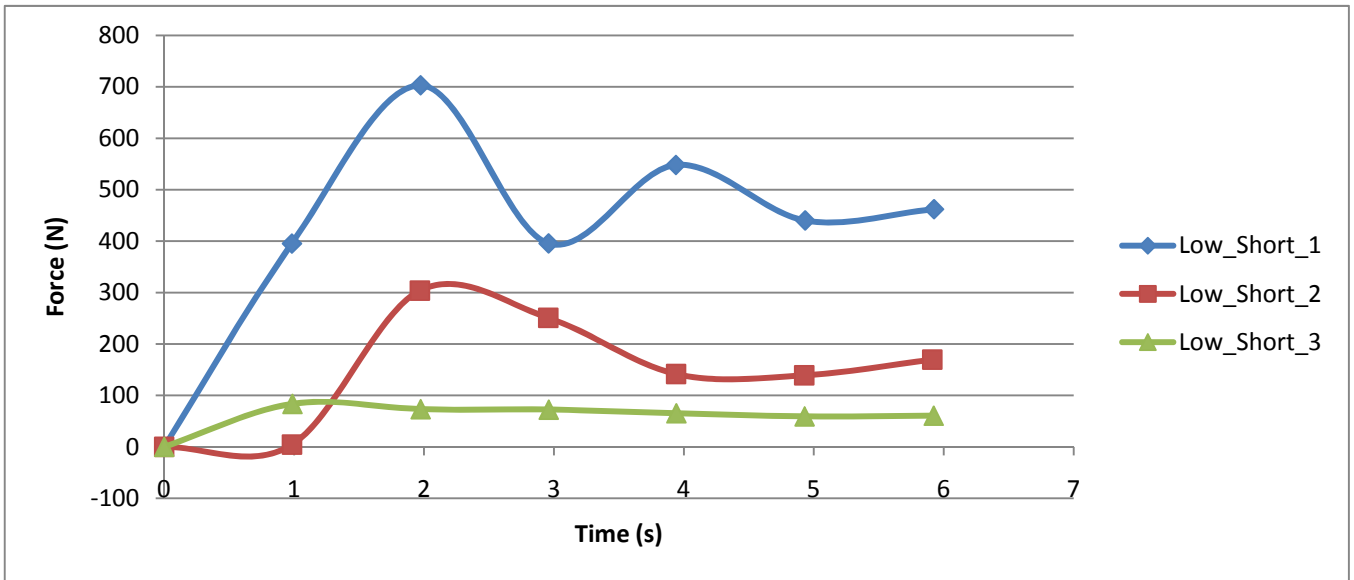


Figure 3.8 - Force time series from the shear box of Low_Short_1/2/3 of phase 1

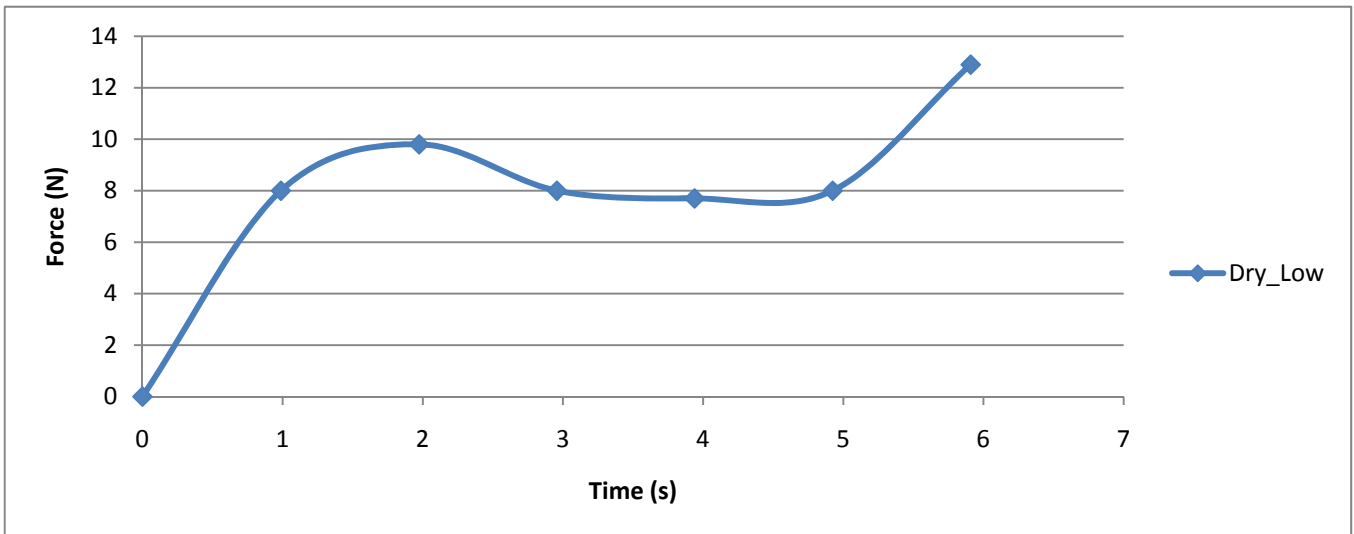


Figure 3.9 - Force time series from the shear box of Dry_Low of phase 1

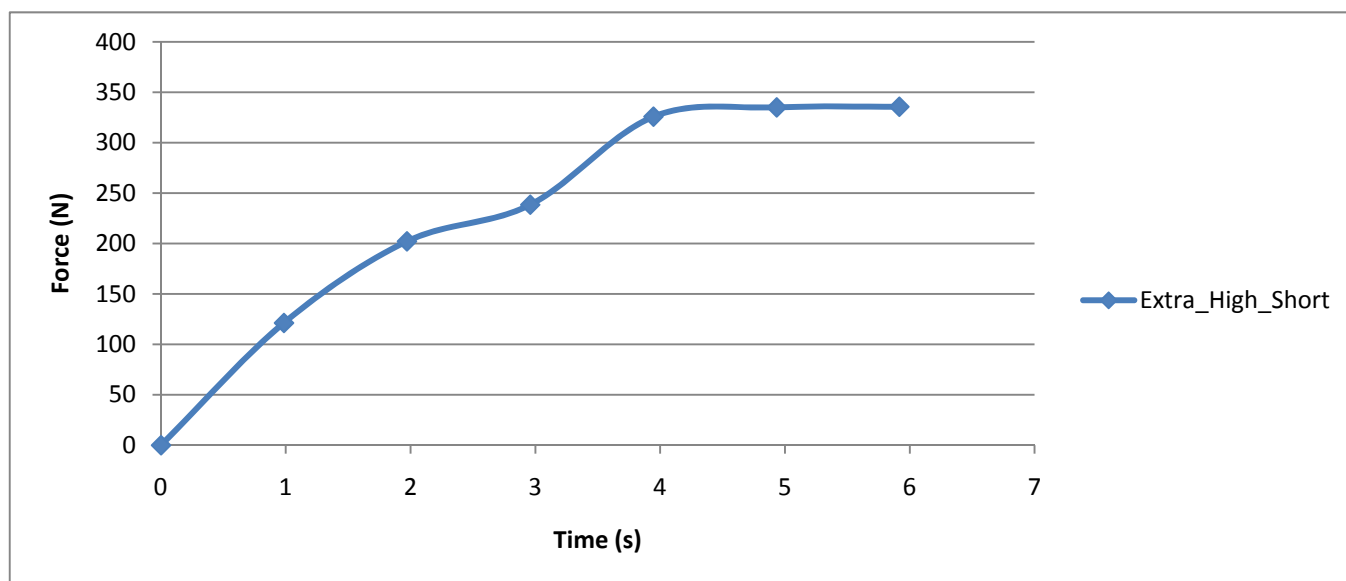


Figure 3.10 - Force time series from the shear box of Extra_High_Short of phase 1

3.4.2.3 Analysis of phase 1 and assumptions for modelling time

We can see from the above 6 figures that the force increases sharply until 2 seconds and then remains constant or even drops quickly in all of these 14 tests. This can be explained in Mohr-Coulomb model that the shear stress has met the criteria for shear failure, or more explicitly the freeze-bonds can not withstand such a large shear stress and come to failure at that moment. Serré et al. (2011) defined phase 1 as the first 6 seconds after the load started to increase, but after carefully reading the data, it is more accurately to define 2 second as the time breaking point to distinguish phase 1 and phase 2. There are also some other evidence that can support this point of view.

Hellmann (1984) wrote that the highest value of this phase is reached after less than 2 mm displacement (the entire displacement in the entire test is 480 mm) and in our case, we define 2 seconds as phase 1, which is approximately 3.2 mm on average in the entire 600 mm shear box. The ratio between displacement of phase 1 and entire box length is more or less the same in these two tests.

So based on the analysis above, the total numerical modelling time in our case of phase 1 is chosen to be 6 seconds, but we will compare the results between numerical modelling and experimental results within the initial 2 seconds instead of the results at the end of 6 seconds.

3.4.3 Results and analysis of phase 2

3.4.3.1 General

This section will analysis phase 2 of the entire shear box experiment. In section 3.4.3.2, a representative force vs. time figure will be given to show the common character of all the 14 individual plots of phase 2.

In section 3.4.3.3, analysis of phase 2 will be given and the thesis will come to the conclusion that the experiment done by Serré et al. (2011) is not accurate in phase 2 and the experiment can't successfully demonstrate the properties of ice rubble during phase 2, either. Apart from this disadvantage, the paper in order to present the results of this shear box experiment done by Serré et al. (2011) has used inappropriate theory to illustrate the results of phase 2. So in conclusion, if numerical simulation is done to compare with the experiment results of phase 2, one might not get satisfied results in this part. And Heinonen (2004) also concluded that in his experiment, the comparison between experimental and numerical data is not accurate in the post peak region.

3.4.3.2 Representative force time series of phase 2 and analysis of phase 2

Serré et al. (2011) chose the initial 120 seconds from the primary mode to be the time domain of the second phase. And that paper describes the second phase exactly as it is described by Hellmann (1984):

After the initial sharp increase the load continued to increase but at a slower rate, with numerous peaks randomly mounted on the base line. The load reached maximum value after approximately 20 to 30 seconds of shearing.

Figure 3.11 shows the force vs. time in Hellmann's work (1984), together with the change of normal confinement in Hellmann's experiment.

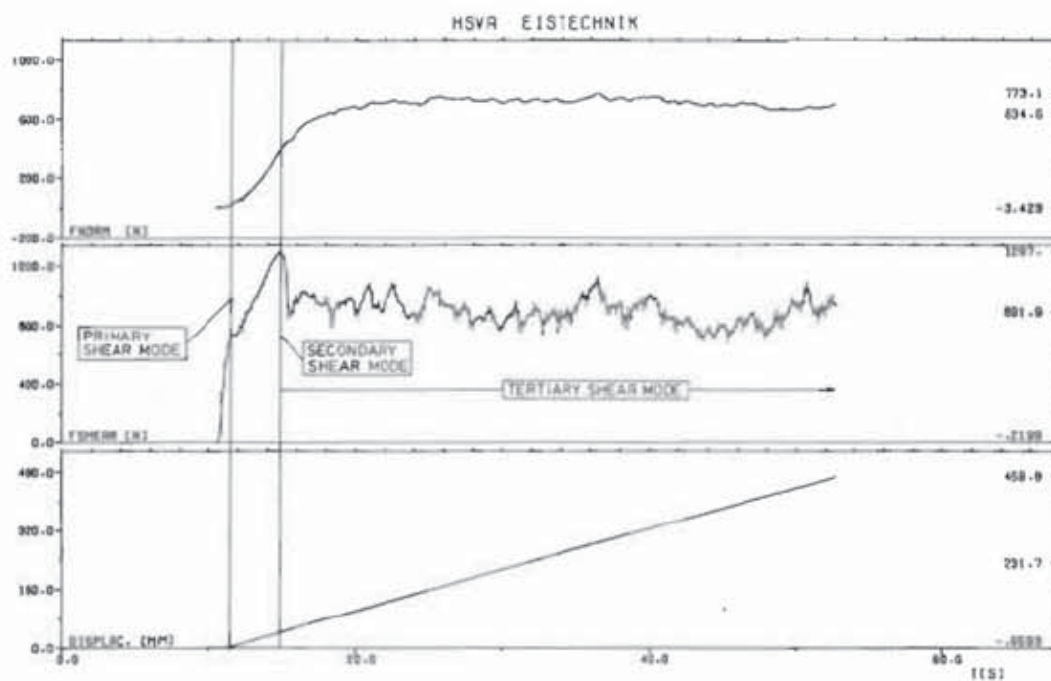


Figure 3.11 - Results of Hellmann's experiment (1984)
 Top: Normal stress vs. time. Middle: Shearing force vs. time.
 Bottom: Displacement vs. time.

And a typical figure of our shear box experiment results is also given in order to compare with the work done by Hellmann (1984).

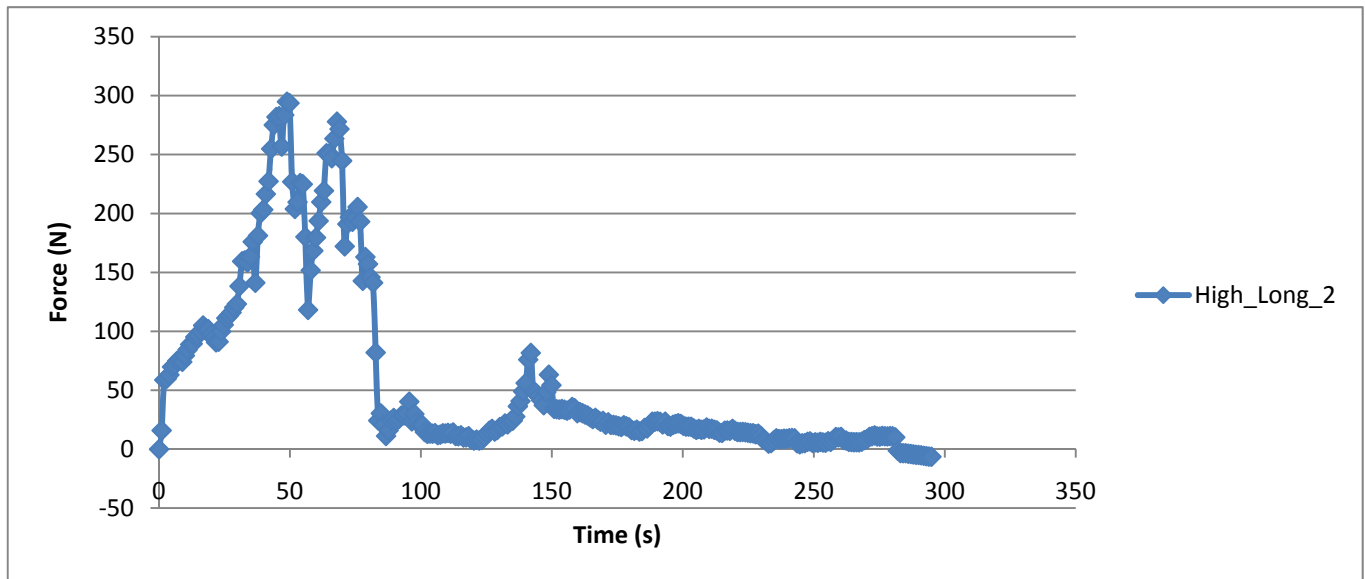


Figure 3.12 - Typical figure of the shear box experiment done in 2010
The High_Long_2 tests with phase 1, 2 and 3 together in one figure.

10 out of 14 tests showed a similar trend as Figure 3.12 shows. The other force-time plots from the experiments of Serré and Repetto are shown in the appendix. At first glance, the theory used in Hellmann's paper can be applied to describe the results of Serré and Repetto's experiment of phase 2. But after careful study of the experiment setup and results of Hellmann, it seems as if his theory can not explain the experiments of Serré and Repetto. The reasons are listed below:

1) The equipment setup is quite different in the two experiments, especially the control of normal stress.

In Hellmann's experiment, the equipment is illustrated below in Figure 3.13:

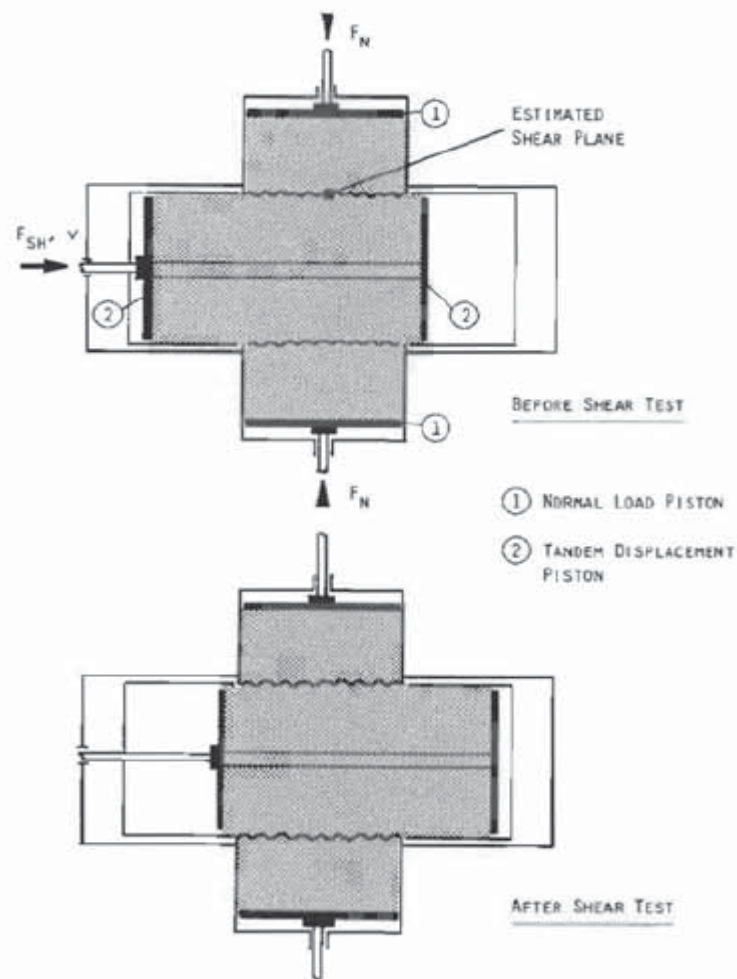


Figure 3.13 - Equipment of Hellmann's test in 1984
Top: Equipment before test. Bottom: Equipment after test

The equipment consists of a square shear cylinder and two square side chamber of about 0.5 m^2 cross section orthogonally arranged. Two numerical coupled piston displace the ice material within the main chamber including a shear process. The most important thing is that in this experiment the piston giving the normal load was fixed in space, in other words Hellmann created completely enclosed and confined the ice rubble (Urroz and Ettema, 1987), which means the dilatation was suppressed and the normal force (the confinement) increased. And increasing confinement explains the increasing shear force in the top of Figure 3.13. But Serré et al. used constant confinement, so that a continued increase in pushing force was not caused by increasing confinement. This is the biggest difference between these experiments.

It is understandable for Hellmann's experiment, that in phase 2, the friction has played an important role, and the normal pressure increases during phase 2, if applying Mohr-Coulomb equation, the shear stress will be linearly increase together with linear increase of normal pressure. But in Serré and Repetto's experiment, the question why the shear stress continues to increase with constant normal pressure needs some other

reasons to explain.

2) The magnitude of maximum force during phase 2 between Hellmann and Serré, Repetto's experiment varies a lot.

In Hellmann's experiment, the force has reached its maximum value at the end of the second phase and the magnitude of the maximum force in phase 2 is around 1.5 times than that of the maximum force in phase 1. But in the experiment done by Serré and Repetto, the maximum force appears quite randomly, sometimes the maximum force in phase 2 has reached at the beginning and sometimes the maximum force has reached at the middle or end of phase 2. There is no way to predict when the peaks happen during the shear box experiment. Apart from this, the ratio between maximum force in phase 2 and phase 1 in the experiment done by Serré and Repetto sometimes can be as large as 4 times. The reason why this has happened will be discussed in the next section.

Apart from the 10 out of 14 series of experiment which shows a typical profile of force time series, the other 4 profiles has showed extremely different patterns. Some has had large force drop after phase 1 (like Figure 3.14), some remain more or less the same force in both phase 1 and 2.

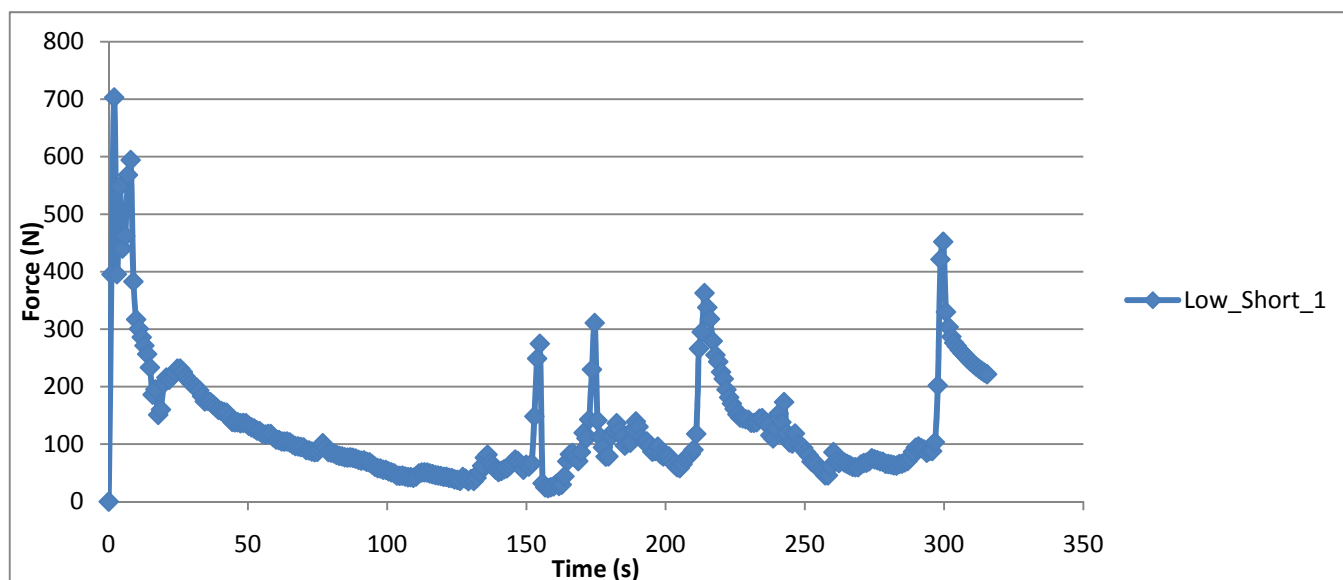


Figure 3.14 - Time force series of Low_Short_1, which decreases right after phase 1

Apart from this, the results of the three experiment in the same situation also vary a lot, not only the trend, but also the magnitude has shown dramatically different pattern. Here is one figure plotting the three experiment in the same situation of Low_Long test showing the differences.

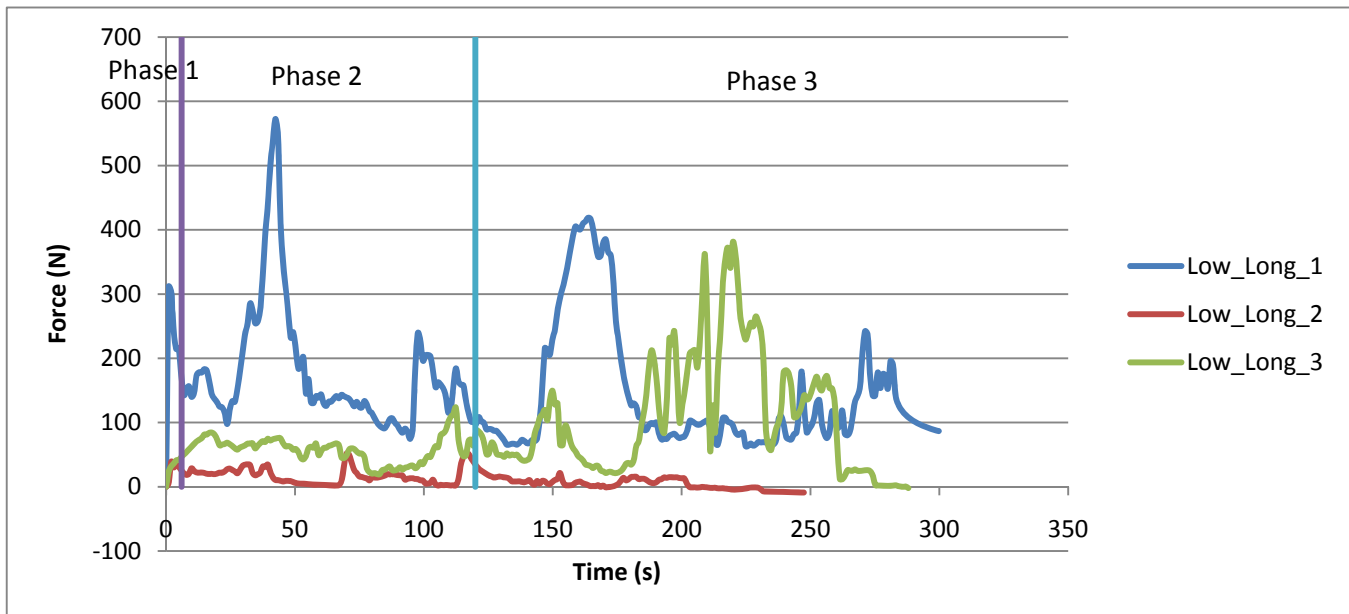


Figure 3.15 - The three individual experiment in the Low_Long situation

Figure 3.15 shows that although the three experiments are carried out in the same situation, they can have different results. In summary, there are a lot of random things happening during the experiment in phase 2, which shows that the design or setup of the experiment might have some deficits.

3) The random peaks between Hellmann and Serré et al.'s experiment varies a lot

Although there are random peaks happening in Hellmann (1984) experiment, their magnitude is small, which is more or less like noise during the whole profile, while in Serré and Repetto's experiment (2010), the random peaks have taken control of the shape of the profile, which also represent some deficits in experiment design or setup in their shear box experiment.

There are two reasons that can explain why the above three inaccuracies have happened and where the problems of the experiment design and setup are.

The first reason is that the RVE (representative volume element) in this experiment is not large enough to avoid the behaviour of one particular ice block, which will introduce large variations in the global behaviour of the whole rubble.

Serré has carried out model tests and numerical modelling of punch test in 2011 and the numerical and physical results are shown in Figure 3.16:

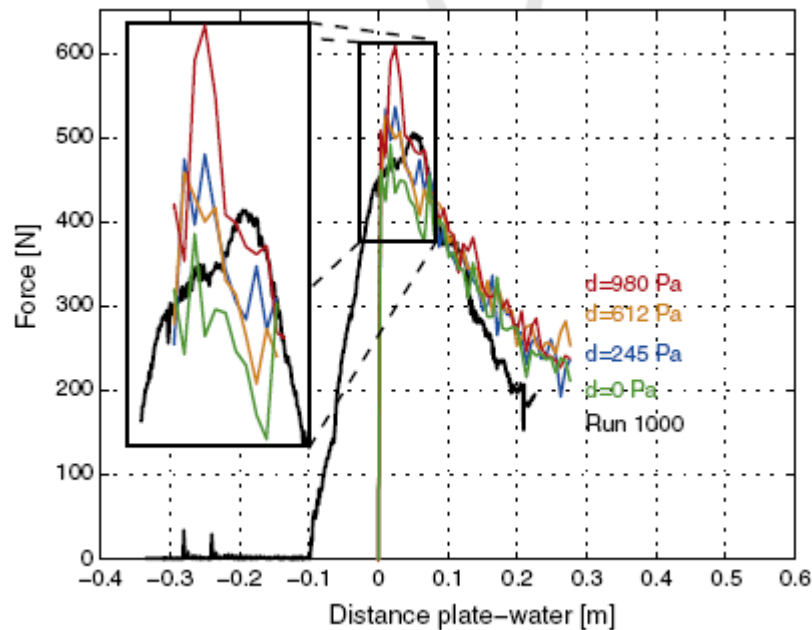


Figure 3.16 - Model tests and numerical modelling results in Serré's punch test
The black line is the result of model test, the other lines with different colours are the results of numerical modelling.

Figure 3.16 shows that the force has increased sharply at first and then decreases almost linearly until the end of the test. This was explained in Serré's punch test that the freeze-bonds were destroyed and the post-peak was modelling using cohesion softening materials. And there are also random peaks happening at the post peak stage, but the magnitude of these random peaks were not large enough to influence the general trend of this plot and the amplitude of these random peaks is around 50 N. It is interesting to find that the amplitude of the random peak in our shear box tests is also around 50 N, but in our case, the general trend is controlled by these random peaks.

It can be shown from the analysis above that the RVE in Serré (2011) punch test is large enough and individual block failure couldn't influence the overall trend of the forces. But in our shear box tests, the force of individual ice block has dominated the force of phase 2, by which the mechanical properties of rubble friction and cohesion can hardly be represented at all.

Some other evidences are also provided in the paper of Serré et al. (2011) to show that the RVE is smaller than the size it should be. For example, in 10 out of 14 tests, individual ice blocks were broken at the shear interface. And during the deformation, the confinement inside the rubble was pressing some blocks against each other, thus creating 'force chains' in the material. During the tests the rubble was extruded vertically by sliding against the side of the shear box in contact with the piston. Some of the tests also revealed that individual ice blocks or small block assemblies were rotating at the interface between the two parts of the shear box (Serré et al., 2011). In

the tests with the two lower levels of confinement, some of the ‘chain forces’ even extended all across the rubble. It might indicate that in the test configuration, the shear box size was well below the RVE size (Serré et al., 2011).

The second possible reason is that the shear-bonds don’t fail entirely in phase 1, and there still remains some freeze-bonds left which controls the behaviour of phase 2. In another word, the freeze-bonds don’t break instantaneously, but progressively.

This reason is possible because if freeze-bonds break progressively, there will be random peaks controlling the force-time profile and the force will also continue to increase in phase 2, which is almost the same trend as the experiment data, but the problem of analysing this possibility is that it is difficult to judge how far and how fast does the failure of freeze-bonds progress and also difficult to carry out numerical modelling, since the crack is impossible to model using the present finite element modelling tools. Another difficulty is, by far no evidence has shown the freeze-bonds could break progressively, so the possibility of this reason is quite low in our shear box experiment at this time.

3) The rubble has to fail along a specified failure plane which is pre-defined in the experiment design and setup process, thus will result in inevitable individual ice block failure during the experiment.

This reason is highly possible, since the shear plane is the horizontal plane parallel with the rolling rail, so the rubble is highly possible to fail individually. Failure of individual ice block is no problem as long as the shear box size is far beyond the RVE, but in our case, the RVE might not be enough large as it is explained in reason 1). So the main reason still lies in the choosing process of RVE.

Based on the reasons why there exists inaccuracies during phase 2 of the shear box experiment, three possible solutions are given in order to solve the problems.

1) Increasing the shear box size in order to meet the requirement of RVE.

This is the most practical and efficient improvement towards our shear box experiment, but how large the shear box should be and the size of the RVE for ice rubble remain unsolved and still needs a lot of work to be done in the future.

2) An experiment can be designed to judge whether the freeze-bonds break instantaneously or progressively.

This experiment is constant-load experiment. A certain load can be applied to the shear box and the displacement will be recorded. If a sudden displacement drop happens and after that the displacement remain the same, it shows that the freeze-bonds fail instantaneously. If the displacement continues to increase and no sudden drop happens, it can show that the freeze-bonds fail progressively. A similar experiment is presented in the paper of Hellmann (1984).

3) Another experiment can be designed to revise the experiment equipment a bit in order to avoid the situation where the rubble has to fail along a specified failure plane from happening, thus can get reliable quantitative results.

Figure 3.17 shows the experiment setup in our shear box experiment, together with the possible shear plane.

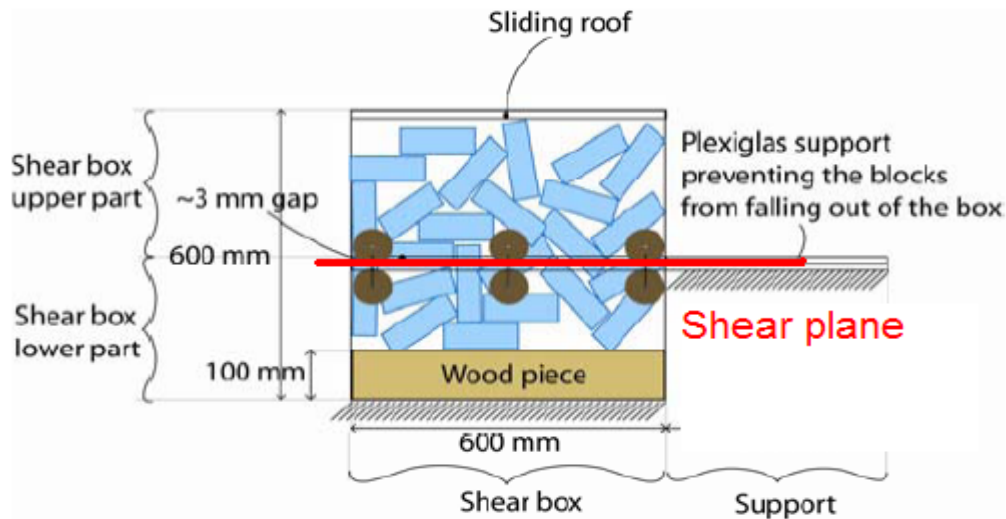


Figure 3.17 - The pre-described shear plane in the shear box experiment.

In this situation, the rubble has to fail along this specified failure plane, which will get involved of the breakage of individual rubble. We can improve the equipment a bit by removing the left part a bit slower, Figure 3.18 is the experiment equipment after improvement, the rubble can fail along many possible planes, which will avoid the influence of individual rubble failure. The figure is drawn based on one of the pictures in the doctor thesis of Shafrova in 2007.

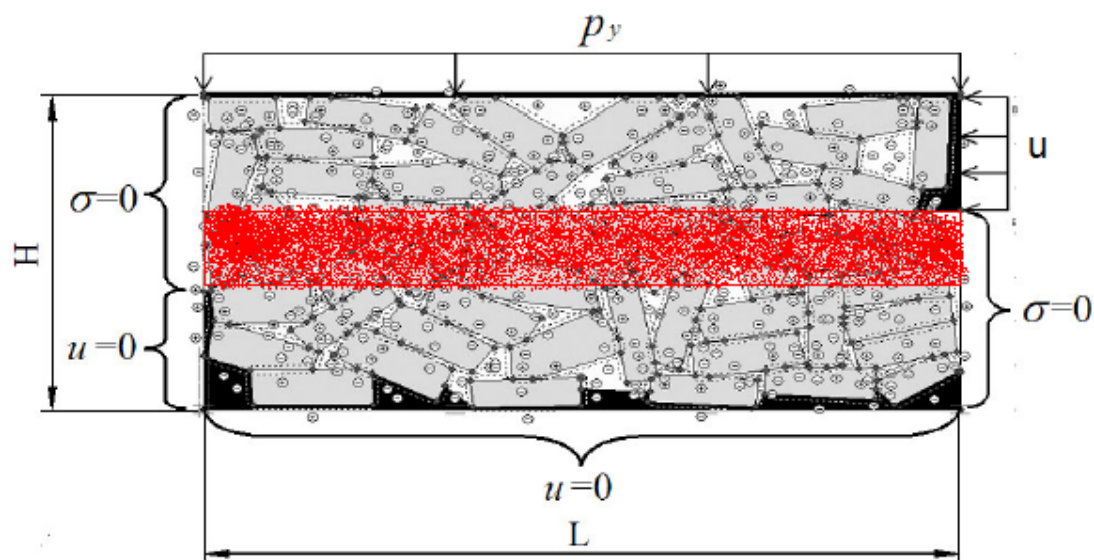


Figure 3.18 - The equipment after improvement

We can see from Figure 3.18 that any plane within the red shadow areas could become the shear plane, the rubble will find the easiest plane to fail which is more likely to avoid the breakage of individual ice rubble, since the mechanical property of individual ice rubble is stronger than the cohesion and friction between ice blocks. So this new equipment might work, but further studies need to be done to analysis this kind of improved model tank.

3.4.4 Results and analysis of phase 3

A typical plot of phase 3 is given below, taking High_Long_2 for example:

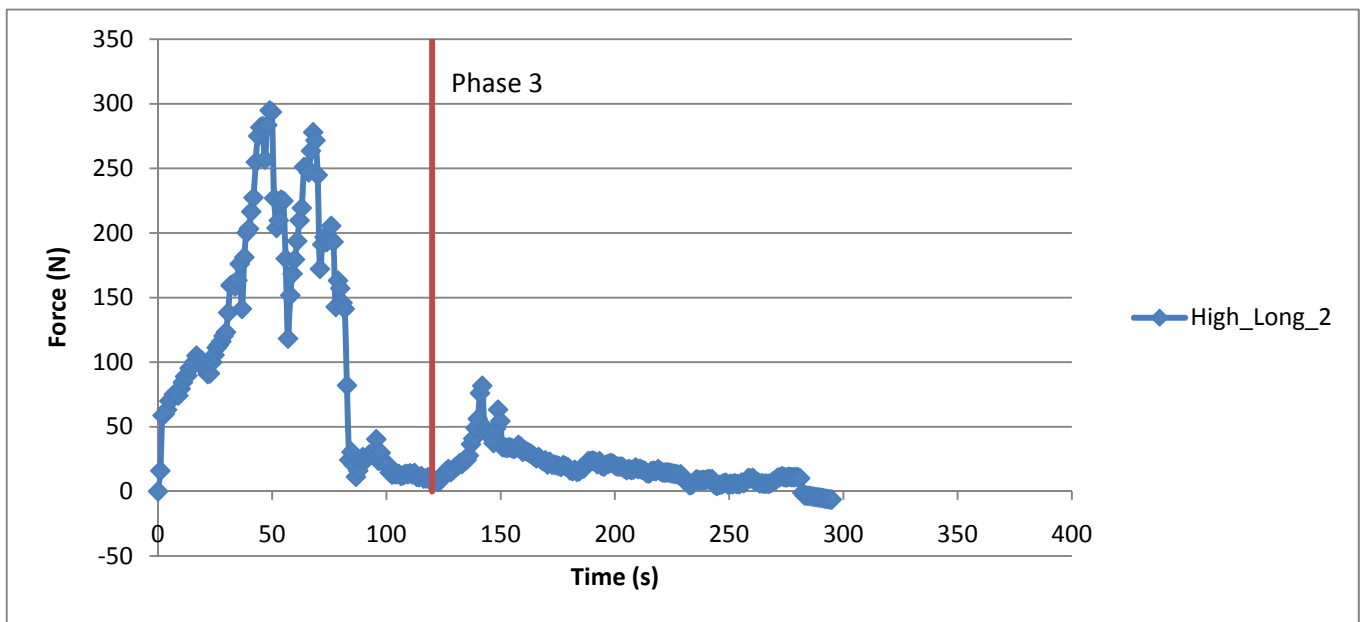


Figure 3.19 - A typical trend for phase 3

We can see that the typical trend of phase 3 can be described as the linear decreasing of the force, it can be explained that the contact area is decreasing linearly. Although random peaks still exist, it never dominates, since the shear box has gone through 120 seconds' displacement (with speed of 1.6 mm/s on average) and individual ice rubble has been sheared to failure, so at this time, it is the friction between ice rubble and slush dominate instead of the cohesion and individual ice rubble.

Based on the assumption that friction between ice rubble will dominate in phase 3, we can find a method to calculate the friction angle at this stage and the basic equation used in this calculation is also simple:

$$\frac{F}{A} = \sigma \cdot c = \sigma \cdot \tan\alpha \quad (3.2)$$

Where F is the shear force or friction at this time, A is the shear area, σ is the normal pressure and c is friction coefficient. $c = \tan\alpha$ shows the relation between friction

coefficient and friction angle. α is the final answer that is particularly interesting to this thesis. As for the experiment which doesn't show a typical linear decreasing profile, the friction will not be calculated.

Now test High_Long_2 in Figure 3.19 will be taken as an example to calculate the friction angle during the tests.

We can see from Figure 3.19 that the force between 150 s and 250 s shows a clear linear decreasing plot and the loading velocity in this situation is 1.63 mm/s with 3020 Pa as the normal pressure, so we will calculate the force in this time domain and use average force and average contact area.

The average force is 18.46 N and the average contact area is

$$\left[600 - \frac{(150 + 250)}{2} \times 1.63 \right] \times 40 = 10960 \text{mm}^2 \quad (3.3)$$

So we can have

$$\frac{F}{A} = \frac{18.64 \text{N}}{0.01096 \text{m}^2} = \sigma \cdot c = 3020 \cdot c \Rightarrow c = \tan \alpha = 0.563 \Rightarrow \alpha = 29.4^\circ \quad (3.4)$$

The table below shows the friction angle and time domain in which the average value is chosen in each test.

Table 3.3 - Chosen calculation time domain and friction angle of phase 3
(N/A means this profile doesn't show a typical linear decreasing trend of force)

σ [Pa]	Δt [hr]	Time domain	Friction angle $^\circ$	Test Name
3020	20	150-250 s	8.6 $^\circ$	High_Long_1
		150-250 s	29.4 $^\circ$	High_Long_2
		N/A	N/A	High_Long_3
	0.17	150-275 s	55.6 $^\circ$	High_Short_2
		150-200 s	33.4 $^\circ$	High_Short_4
860	20	N/A	N/A	Low_Long_1
		125-175 s	30.8 $^\circ$	Low_Long_2
		N/A	N/A	Low_Long_3
	0.17	N/A	N/A	Low_Short_1
		230-280 s	73.8 $^\circ$	Low_Short_2
	0	N/A	N/A	Low_Short_3
		125-225 s	51.5 $^\circ$	Dry_Low
20500	0.17	N/A	N/A	Extra_High_Short

We can see from Table 3.3 that the friction angle varies from 8° to 74° , while most of them lies between 30° to 55° . According to the assumption, the cohesion of the freeze-bonds and the influence of individual rubble breakage is small in phase 3, so it is appropriate to believe that the friction angle in phase 3 in every test out of the 14 tests should be more or less the same, but the result does not satisfy the assumption very well. The reason might still be the size of RVE which will bring great uncertainty to the test results.

It is worthwhile to mention that here we can get the friction angle of ice rubble, but the friction angle of the freeze-bonds material is not necessary the same as the rubble friction angle (Serré. 2011). But we will not discuss the differences between this parameter, since specific testing of freeze-bonds will be carried to determine it. So another assumption is that the friction angle of the freeze bond material is considered equal to the rubble friction angle.

4. RESULTS OF NUMERICAL MODELLING

4.1 General

Numerical simulations of the shear box tests were carried out by a commercial finite element program-ABAQUS/Standard 6-10.2. The Drucker-Prager model was used to model the material property of ice rubble. Only the primary phase of shear box tests was modelled and compared with the experiment results. ABAQUS/Standard uses implicit integration instead of the explicit integration as the solution method, which means it can only solve small displacement otherwise the structure could be distorted and become inaccurate.

Some basic assumptions in numerical modelling are made and summarised below:

1. The material is homogeneous in the shear box.

The temperature of the ice blocks in the shear box is constant from top to bottom. The cohesion and friction angle are constant everywhere and in every direction and this assumption agrees well with definition of ice rubble in ISO standard.

2. Time dependent deformation, like creep, is ignored.

The loading velocity in our case is neither slow enough to cause creep nor quick enough to cause pore water pressure build-up.

3. Only quasi-static analysis is carried out to simulate the shear box tests.

4. Cohesion softening doesn't happen during modelling.

In previous study, the cohesion remains the same, but in some cases, one can assume a cohesive softening behaviour for material, which allows the cohesion to decrease when the plastic strain increases. Normally this behaviour happens in order to suppress the cohesive forces after initial deformation has occurred, usually after the post-peak phase. In our case, we are not interested in the post-peak situation, so we will still choose a constant cohesion material whatever the strain is.

5. Cap model will not be used in the modelling.

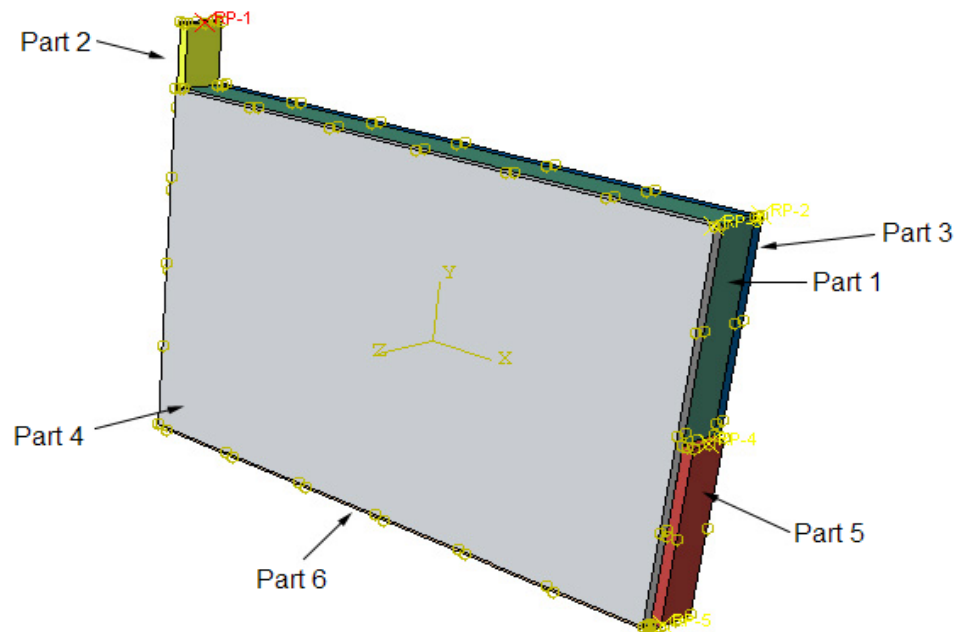
When the hydrostatic stress increase, the hydrostatic compressive yielding of the rubble is likely to occur during experiment, so at this time, we will add a cap to the yield surface. This is the definition of cap model. In the present modelling, we will not use cap modelling, but the question whether we should use cap model or not will be discussed in section 5.3.

Other specific assumptions regarding the model parameter setup will be included in section 4.3.

In the following four sections, section 4.2 will give a brief introduction to the numerical model, for example, how the numerical model is derived from experiment model, to what extent the numerical model is accurate and a comparison between them is made. Section 4.3 describes all the setup of input data and gives some assumptions regarding the model dimension, simulation time and other important parameters. This section also gives a preliminary analysis of the influence of each parameter to the numerical results. A more detailed analysis will be presented in chapter 5. In section 4.4 the results of the cracks growth in numerical modelling will be given and in section 4.5, the results of the effects of the material parameters will be presented and this section is quite important, since it will focus on the three most vital parameters, which are friction angle, cohesion and Young modulus. Normally these three parameters are the ones that people are interested in and a lot of researches have been done to study them. This chapter also tries to find a proper description of the properties of freeze-bonds in the nature.

4.2 Brief introduction to the numerical model

A numerical model is built in order to simulate the shear box experiment and Figure 4.1 illustrates different parts of the numerical model:



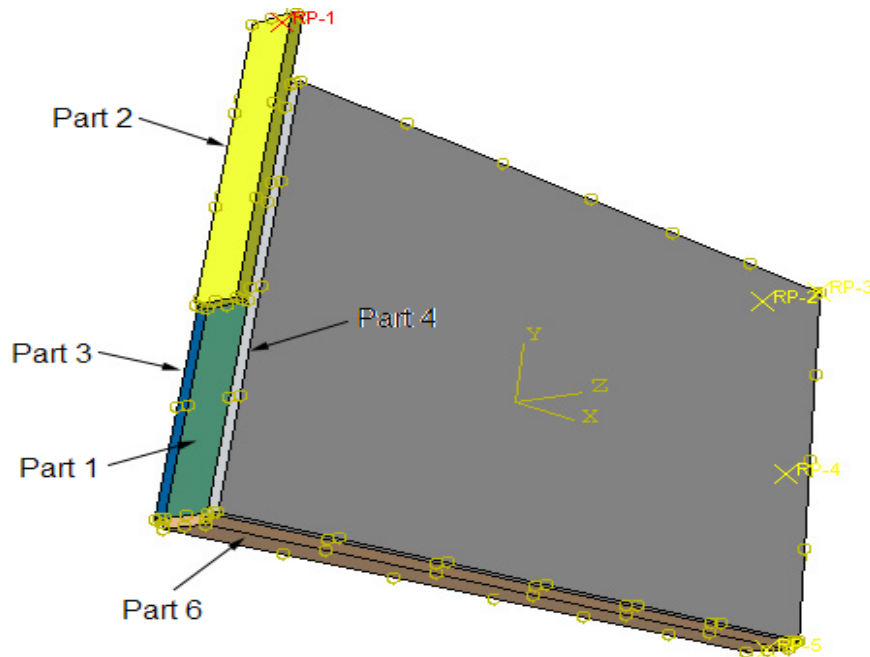


Figure 4.1 - Illustration of numerical model with coordinates

There are 6 parts in the numerical model:

Part 1: This part is modelled as ice rubble and the dimension is $600\text{mm} \times 40\text{mm} \times 400\text{mm}$ (depth). The material for this part is modelled using DP model. This numerical model uses continuum method to simulate the ice rubble and this is the main difference between numerical model and experiment tests. The reason why we use continuum method here is because continuum method is easy to analyse and it requires less computational time and memory. Besides this, if we can choose a suitable material model, the continuum method can also get results as accurate as discrete model.

Part 2: Part 2 is used to simulate the velocity controlled piston (load cell) in the experiment. A velocity in X direction is given to part 2 during the numerical modelling process, which is 1.6 mm/s and the movement in Y and Z direction of part 2 is set to be 0. In order to minimise the influence of irrelevant parts and increase the calculating speed, part 2 is set as rigid body, so that no force information will be calculated for part .

Part 3 and 4: These two parts are used to simulate the side wall of the shear box equipment. And they are also set as rigid bodies. These two parts are set to be interacted with part 1 with friction, in which the friction coefficient is 0.02. The displacements in three directions are set to be 0 in order to create a side restricted environment for ice rubble.

Part 5: This part is used to simulate the opposite part of part 2 and the displacement in all the three directions are fixed as well. It is set to be rigid body. The interaction is

the same as part 3 and 4.

Part 6: This part is used to simulate the bottom of the shear box and the displacements in all the three directions are fixed to be 0. It is rigid body. The interaction is the same as part 3 and 4. Part 6 will act as the support for the ice rubble, which will restrict the movement of ice rubble in the negative Y direction instead of positive Y direction. So the numerical model is quite similar to what happens in reality, which guarantees the accuracy of numerical model.

We can see that there are two parts where no rigid body is connected to part 1, they are the lower fixed part under part 2 and upper displaced part over part 5. The reason why the setup looks like this is because the ice rubble could hardly interact with these two parts in reality, so we can remove the rigid bodies in these two parts in order to save computational time.

Besides these, on top of part 1, pressure is added in order to simulate the normal confining pressure. 3.02 kPa and 0.86 kPa are used respectively to model high and low normal confinement according to the setup of the experiment equipment.

4.3 Setup and influence of input data

The setup of the other parameters will be discussed in this section, they are the simulation time, the rubble height, the rubble density, the normal pressure, the friction coefficient, the mesh density and the dilatation angle.

4.3.1 Simulation time

As it is discussed in section 3.4.2.3, most of the experiment data yield at 2 seconds, so our main focus is the initial 2 seconds, while the total simulation time will be 6 seconds. For one reason, in Serre et al. (2010), they define 6 seconds as the primary phase, for another reason, by choosing a longer simulation time, we can also research on what the transition phase is like.

4.3.2 Rubble height and rubble density

In experiment, the rubble height varies from 386 mm to 491 mm. Different rubble height will influence the gravity and friction, so a comparison is made in order to see in what extend the rubble height can influence the final results.

The other parameters are set like this:

Young modulus $E=1.2$ MPa, Poisson's ratio $\nu = 0.3$, DP model's friction angle $\beta = 45^\circ$, cohesion $d=1.2$ kPa, normal pressure $\sigma = 3$ kPa, friction coefficient 0.02, porosity of ice rubble $\eta = 35\%$.

So comparison of the results by applying different rubble height is given in Table 4.1:

Table 4.1 – Numerical simulation results by applying different rubble height

No.	Rubble Height (mm)	Force at 2 seconds (N)	Relative error (N)
1	400	44.1	-
2	425	45.1	1.0
3	450	46.0	0.9
4	475	47.1	0.9

We can see the influence of rubble height is minor, which can be ignored during numerical modelling, so we will assume rubble height to be 425 mm in all of the following numerical modelling.

Another influence comes from the rubble density, which is impacted by porosity. The porosity in the experiment varies from 28.9% to 42.6%. So an analysis of the influence of density is also given in Table 4.2 (with the same input parameter above):

Table 4.2 - Numerical simulation results by applying different porosity

No.	Porosity	Rubble density (kg/m ³)	Force at 2 seconds (N)	Error (N)
1	30%	630	45.7	-
2	35%	585	45.1	0.6
3	40%	540	44.6	0.5

We can find that the influence of density is also small, so we can assume the porosity to be 35% on average, with the rubble density of 585 kg/m³ during all the following calculations.

In summary, we have defined three parameters in this part, namely porosity $\eta = 35\%$, density $\rho = 585 \text{ kg/m}^3$ and rubble height $h = 425 \text{ mm}$.

4.3.3 Normal pressure

There are two normal pressures in the experiment, one is 3.02 kPa (High), another is 0.86 kPa (Low). In this part, a preliminary analysis towards the normal pressure will be given, only a qualitative comparison will be done between high and low normal pressure. A more detailed quantitative analysis can be found in section 4.5.

The other parameters are set: Elastic modulus $E = 1.2 \text{ MPa}$, Poisson's ratio $\nu = 0.3$, DP model's friction angle $\beta = 45^\circ$, cohesion $d = 1.2 \text{ kPa}$, rubble height $h = 425 \text{ mm}$, friction coefficient 0.02, porosity of ice rubble $\eta = 35\%$, density $\rho = 585 \text{ kg/m}^3$.

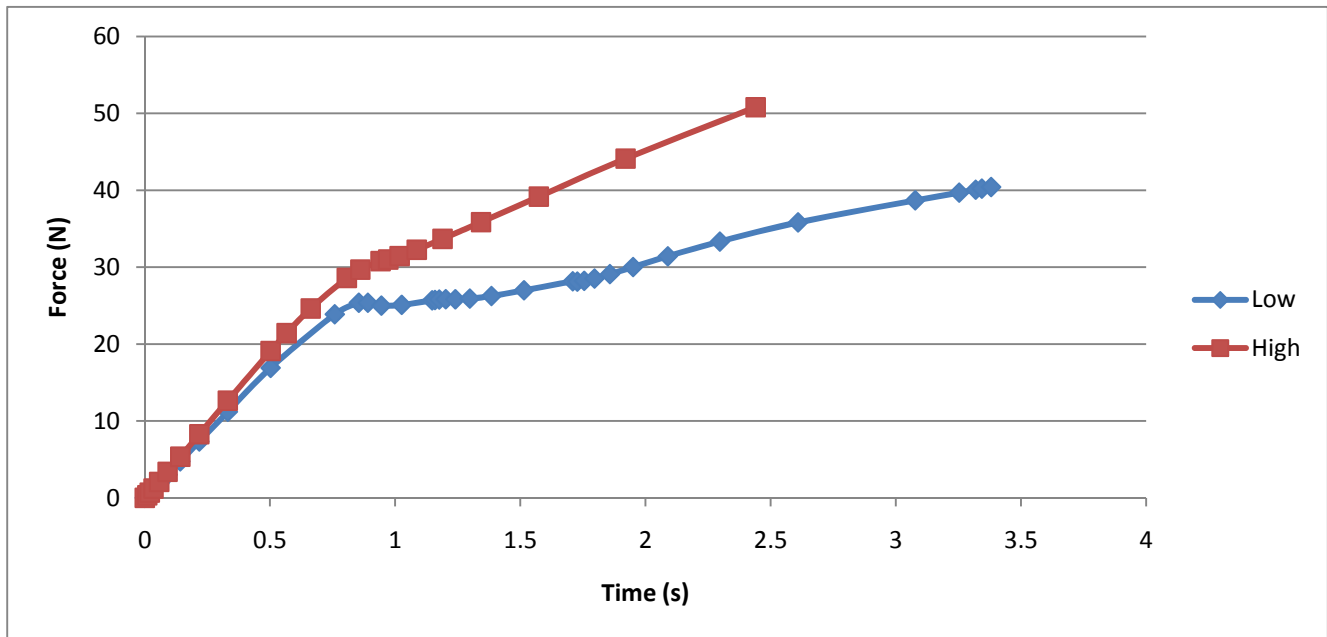


Figure 4.2 - The force under the condition of low and high confinement

From Figure 4.2, we can see that normal pressure has played a major role. It can be simply explained by the Mohr-circle in soil mechanism that high normal pressure will result in high resistant shear force.

4.3.4 Friction

The friction coefficient is not recorded during experiment, but according to the assumption made by Serré (2011), the friction coefficient can be chosen to be 0.02, which is the friction coefficient between Plexiglas and ice during his modelling. So in our case, we can also regard friction coefficient as 0.02, since the material of shear box in our case is also Plexiglas. Below we will choose friction coefficient to be 0, 0.02 and 0.04 in order to research on how large the influence of friction can be in the shear box experiment.

The other parameters are set: Elastic modulus $E=1.2$ MPa, Poisson's ratio $\nu = 0.3$, DP model's friction angle $\beta = 45^\circ$, cohesion $d=1.2$ kPa, rubble height $h=425$ mm, normal pressure $\sigma = 3$ kPa, porosity of ice rubble $\eta = 35\%$, density $\rho = 585$ kg/m³.

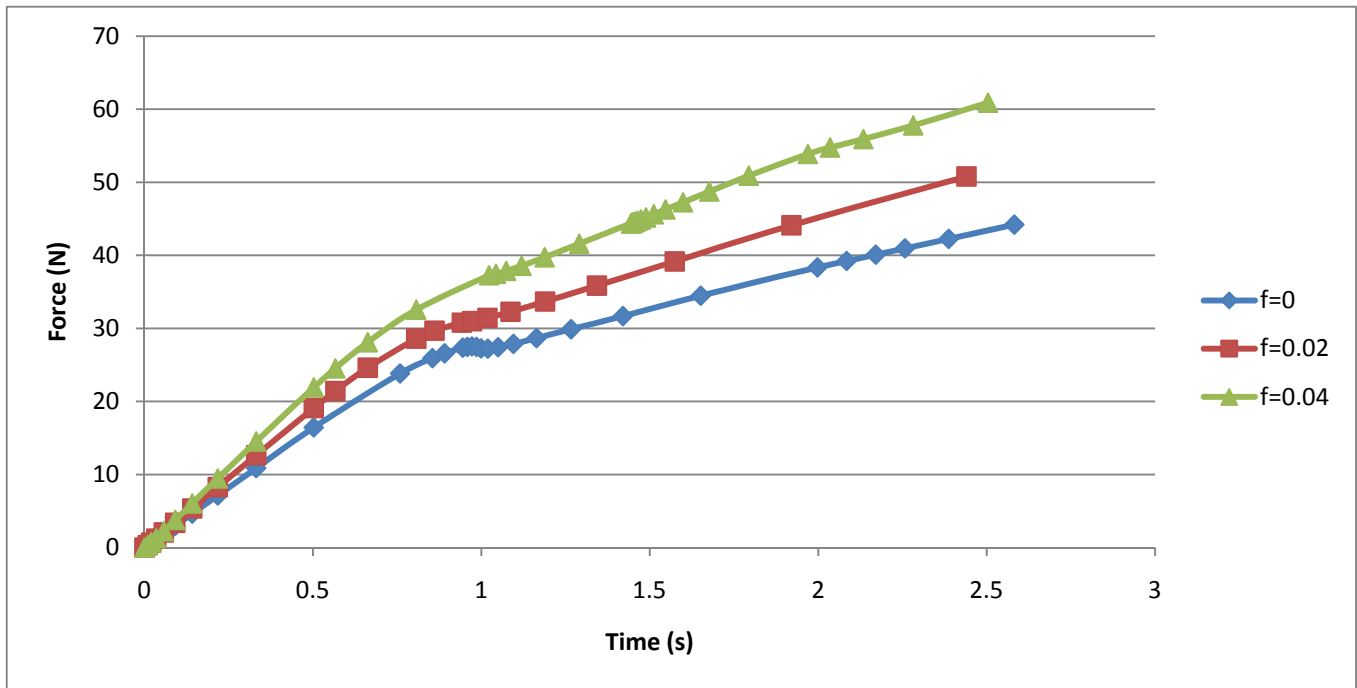


Figure 4.3 - The force under the condition of different friction coefficient

We can see from Figure 4.3 that the influence of friction coefficient is also large, but because of lacking in test data, we have to choose 0.02 as our friction coefficient. The assumption causes the uncertainty of the numerical results.

4.3.5 Mesh density

It is found that finer mesh could result in smaller forces, but the difference between fine and coarse mesh is not very large. This part will analysis the influence by choosing different mesh density, they are a coarse one (40 mm), a medium one (20 mm) and a fine one (15 mm).

The other parameters are set: Elastic modulus $E=1.2$ MPa, Possion's ratio $\nu = 0.3$, DP model's friction angle $\beta = 45^\circ$, cohesion $d=1.2$ kPa, rubble height $h=425$ mm, friction efficient 0.02, normal pressure $\sigma = 3$ kPa, porosity of ice rubble $\eta = 35\%$, density $\rho = 585$ kg/m³.

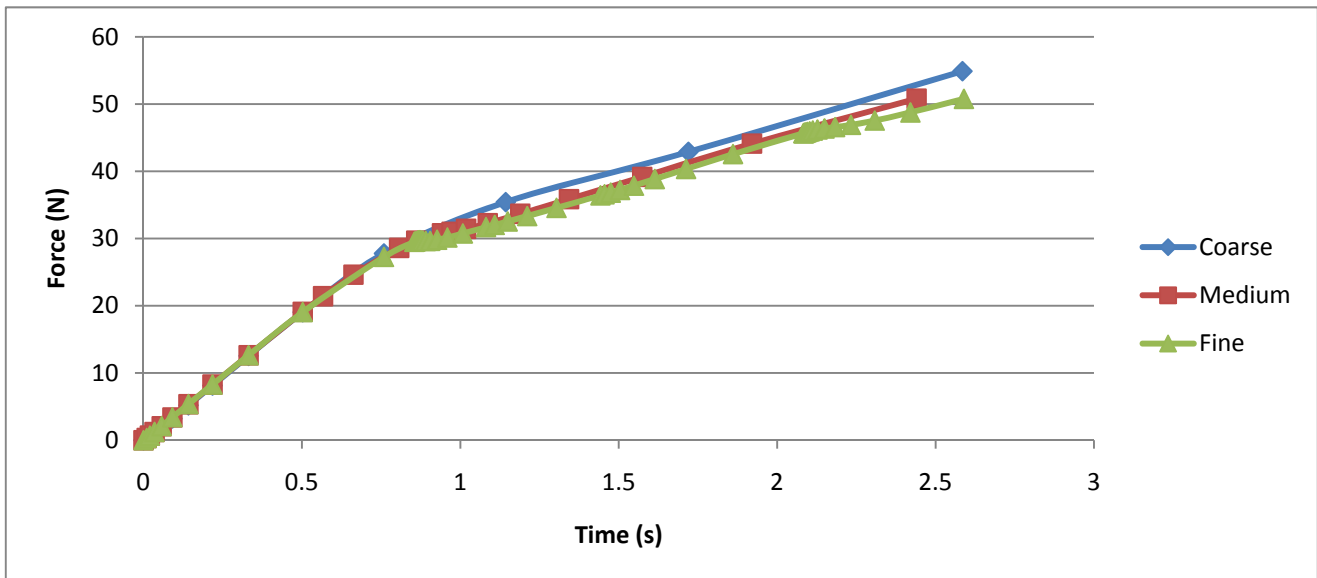


Figure 4.4 - The force by using different grain size

We can see from Figure 4.4 that the force becomes smaller when choosing finer mesh size. But by increasing the density of mesh and choosing finer mesh size, the computation time and storage space in computer will increase dramatically (40 minutes' calculation for 15 mm grain size, 5 minutes for 20 mm grain size, 0.5 minute for 40 mm grain size), but the final results do not vary a lot. So in order to find a balance between accuracy and time, this thesis will choose medium mesh density, which is 20 mm as the grain size.

4.3.6 Dilatation angle

The dilatancy characterizes the volume increase of the rubble during shearing (Serré et al., 2011). And in pressure dependent material models used for instance in Heinonen (2004) or Serré (2011) the dilatancy is represented by the dilatancy angle which determines the shape of the plastic flow potential. The experiment results had clearly shown the dilatancy of ice rubble in the secondary phase, however an important reduction of the dilatancy was observed in the Extra_High_Short confinement test. But to what extent can the dilatation angle influence the primary phase in the finite element modelling will be discussed here. Two cases are chosen: one is High_Short test, another is Extra_High_Short test.

Figure 4.5 is the result of High_Short test and the other parameters are set: Elastic modulus $E=2$ MPa, Poisson's ratio $\nu = 0.3$, DP model's friction angle $\beta = 30^\circ$, cohesion $d=4.5$ kPa, rubble height $h=425$ mm, friction efficient 0.02, porosity of ice rubble $\eta = 35\%$, density $\rho = 585$ kg/m³.

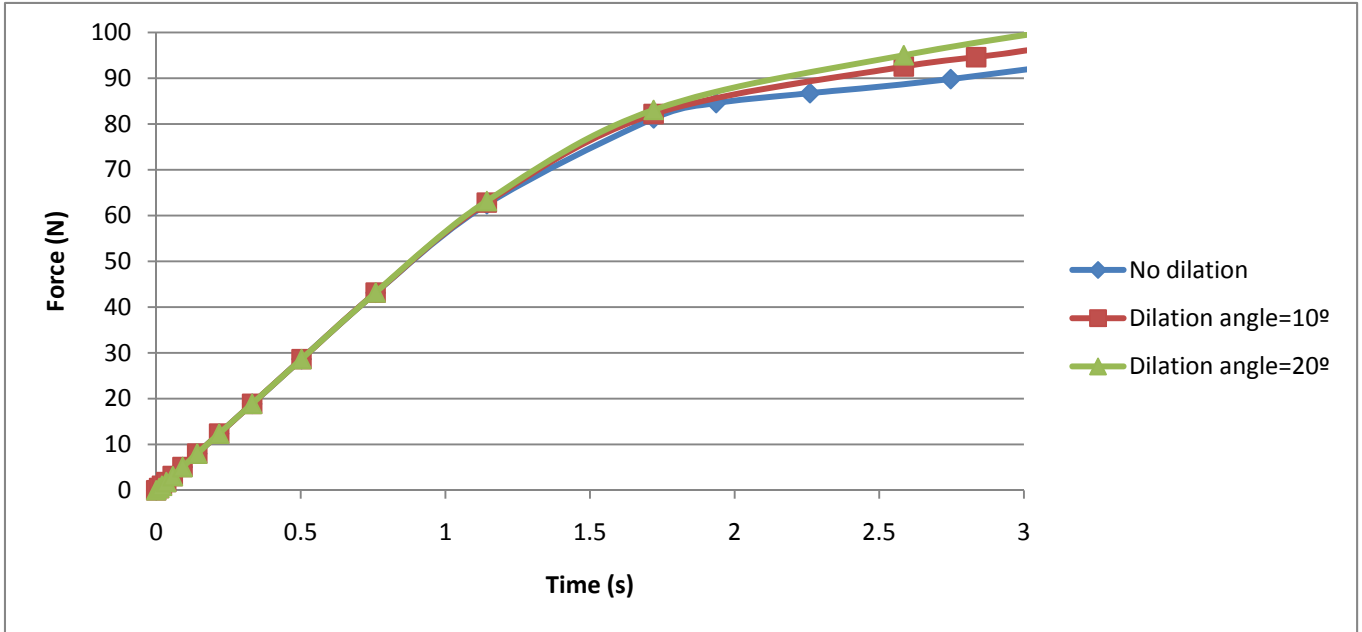


Figure 4.5 – The force under the condition of different dilatation angle in the High_Short test

Figure 4.6 is the result for Extra_High_Short test and the other parameters are set: Elastic modulus $E=3.5$ MPa, Poisson's ratio $\nu = 0.3$, DP model's friction angle $\beta = 30^\circ$, cohesion $d=8.5$ kPa, rubble height $h=425$ mm, friction efficient 0.02, porosity of ice rubble $\eta = 35\%$, density $\rho = 585$ kg/m³.

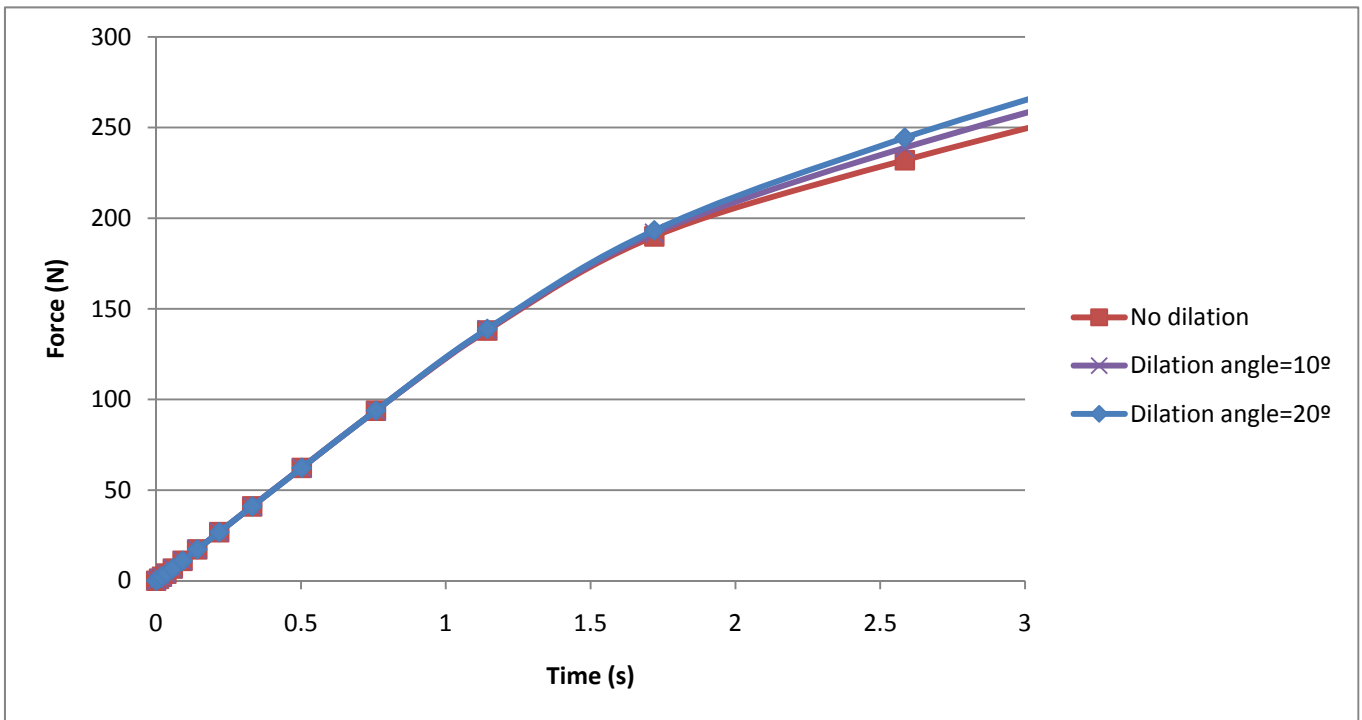


Figure 4.6 - The force under the condition of different dilatation angle in the Extra_High_Short test

So comparison of the results by applying different dilatation angle is given in Table 4.3:

Table 4.3 – Numerical simulation results by applying different dilatation angle

Case	Dilatation angle	Force at 2 seconds (N)	Relative error (N)
High_Short	0°	85.0	-
	10°	85.6	0.6
	20°	86.9	1.3
Extra_High_Short	0°	203.6	-
	10°	207.0	3.4
	20°	209.9	2.9

So we can see that the influence of dilatation angle in the primary phase is small, which can be ignored during the numerical modelling, so we will assume that there is no dilatation happening in all of the following numerical modelling.

4.3.7 Summary

In summary, the rubble height, rubble density, porosity, mesh density and dilatation angle have small influence to the results, while the normal pressure, friction coefficient and DP material parameters have major influence. Based on the assumption made in previous sections, Table 4.4 was made to summarize the setup of modelling parameters.

Table 4.4 - Modelling parameters

Simulation time	T (s)	6
Calculating time		2
Density	ρ (kg/m ³)	585
Porosity		35%
Rubble Height	mm	425
Friction coefficient	f	0.02
Elastic properties	E	To be derived in the next section
	ν	0.3
Shear yield surface	d	To be derived in the next section
	β	To be derived in the next section
Dilatation angle	ψ	none

4.4 Results of the crack growth in numerical modelling

Although ABAQUS can not model crack very efficient at the moment, one can still get an impression of where the most vulnerable place is by analysing the results of ABAQUS output file. Figure 4.7 is the result when we regard $d=1.2$ kPa, $\beta = 45^\circ$, $E=1.2$ MPa.

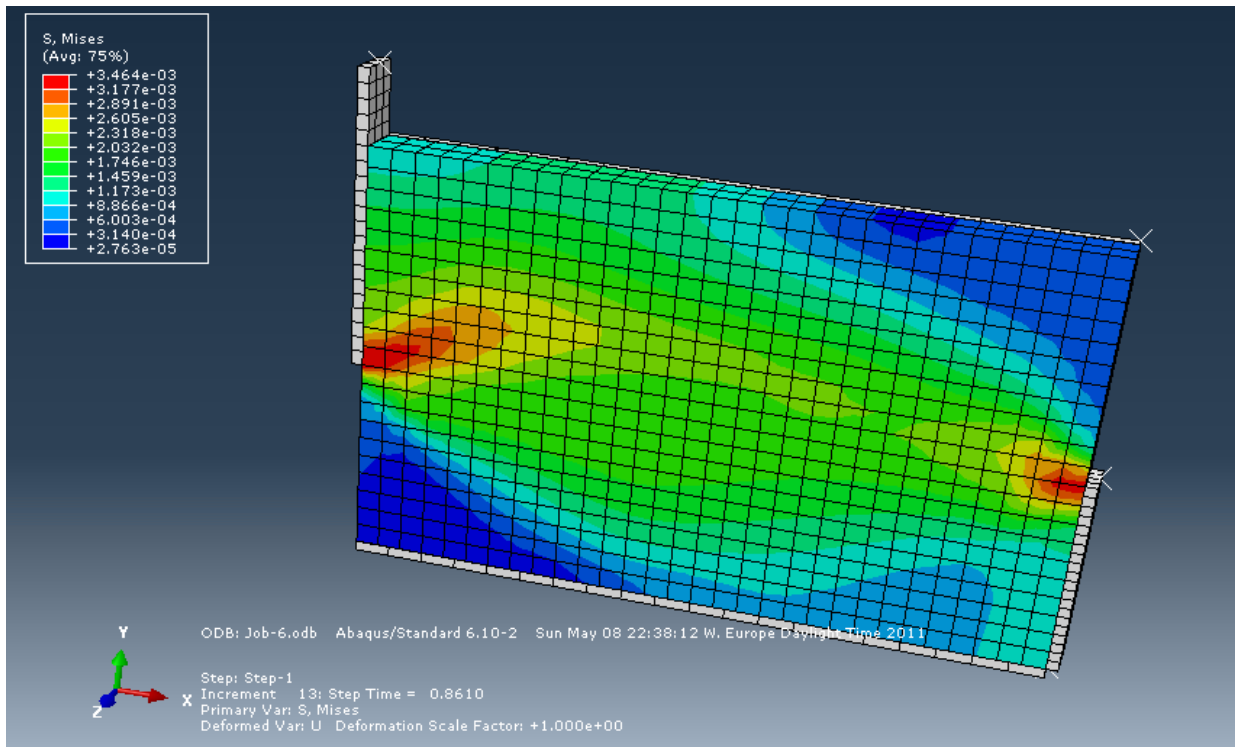


Figure 4.7 - The Mises stress in the ice rubble ($t=1$ s)

We can easily find where is the largest Mises force in the ice rubble from the pattern of Mises stress and these areas are most likely to have cracks in the experiment. In the experiment, the same pattern of crack also happens during phase 1. The crack between numerical modelling and experiment tests is nearly in the same position, which is shown in Figure 4.8.

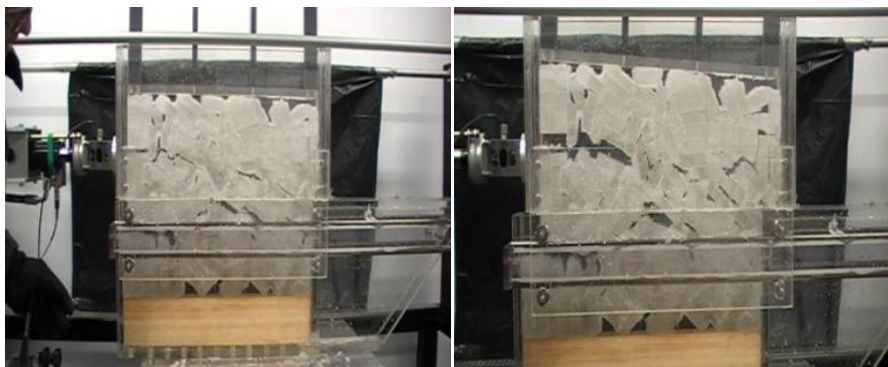


Figure 4.8 - The cracks in shear box experiment

So in summary the numerical model is good to fit in with the experiment setup, but it is also worthwhile to mention that for most of the experiment results, large block assemblies have occurred, which might also result in inaccuracy to the modelling results.

4.5 Results of the effect of the material parameters

4.5.1 General

In this section, the most important parameters will be analysed and the numerical results will be presented. We will apply Drucker-Prager model to simulate the ice rubble in our case. Young modulus, friction angle and cohesion are the three most important parameters in the whole modelling process. The aim of this section is trying to find a suitable pair of these three parameters that can match the experiment results well.

But another big problem remains unsolved in this section, that is how we can relate the results from numerical modelling and experiment modelling to the material parameters happening in nature.

First of all, section 4.5.2 will analyse the general trend of the influence of these three material parameters based on numerical modelling and give a method on how to match numerical and experiment results efficiently and accurately. Only the numerical results are considered in this section instead of experiment results. Section 4.5.3 will give detailed analysis, present the numerical modelling results and give a prediction of the material parameters based on the comparison between numerical modelling and experiment results. Section 4.5.4 will make a summary of this part.

4.5.2 A brief study of the influence of material parameters

Serré (2011) has done an analysis of punch test in lab and give the value of material parameters in his experiment: The Young modulus is 0.9 MPa, the Drucker-Prager cohesion is from 0.6 to 1.5 kPa (0.5 to 1.2 kPa Mohr-Coulomb cohesion) and the Drucker-Prager friction angle ranges from 40° to 50° (30° to 45° Mohr-Coulomb friction angle).

In Serré's experiment, the Young modulus is predetermined by another experiment, which means in his punch tests there are only two variables. But in our case, no extra tests have been done to determine the Young modulus, which means three parameters are all unknown. And this is the most difficult aspect for our numerical modelling. So we will first research on how these three unknown parameters can influence the trend of the numerical results and then find a better way to relate the results from numerical modelling and experiment together.

Since lacking in available data, we will make an assumption that the three parameters (E , d and β) will be in the same range as the results drawn by Serré, which means $E=0.9$ MPa, 0.6 kPa $<d<1.5$ kPa, $40^\circ < \beta < 50^\circ$. By making two parameters constant, we can get the following results:

- β ranging from 25° to 55° , $E=0.9$ MPa, $d=1.2$ kPa, low normal pressure
Four different value of friction angle is chosen, namely 25° , 35° , 45° and 55° , here are the results.

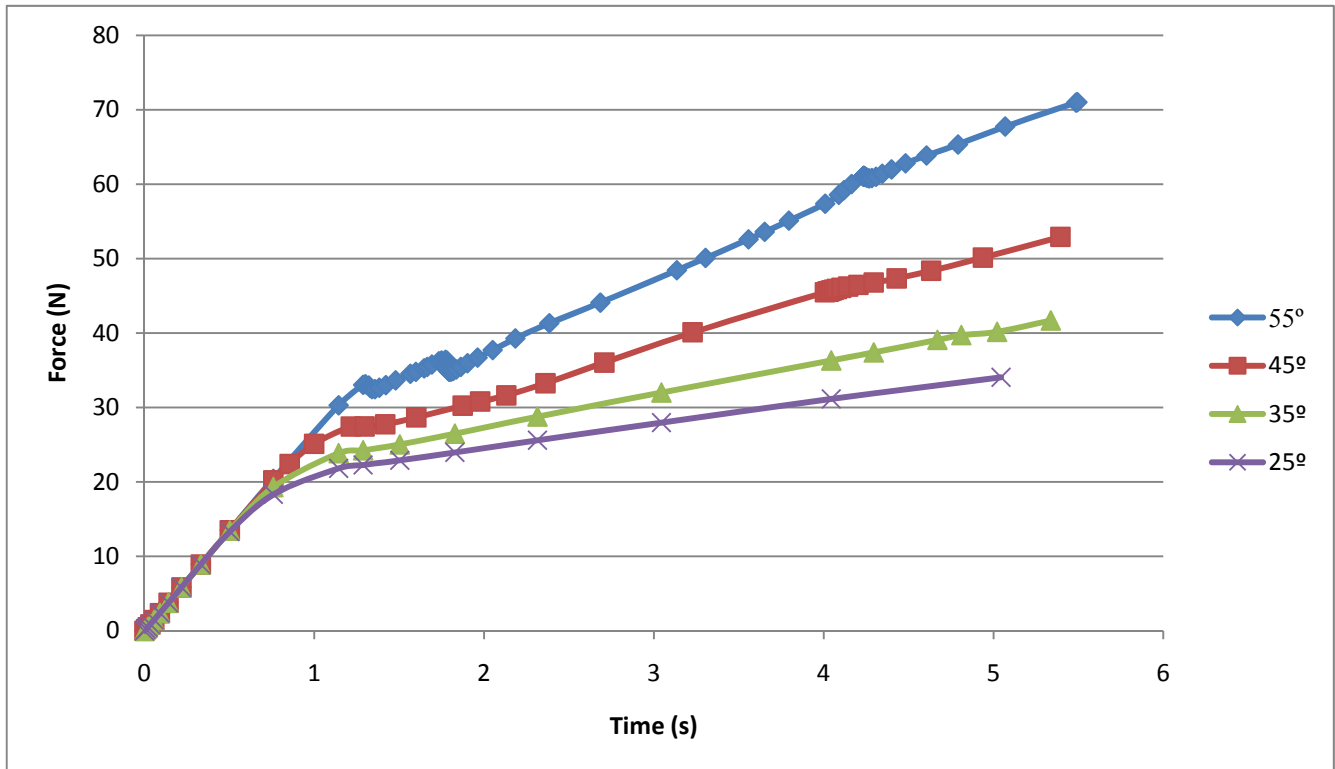


Figure 4.9 - The figure of force vs. time by choosing different friction angle

We can see from Figure 4.9 that at first, the force increase sharply and linearly, but after that, the force has come to a yielding point, which results in slowly increase. We can also see that different friction angle will influence where and when the yield point happens. Large friction angle will cause yield points later and at a higher force, while smaller friction angle will cause yield points earlier and at a lower force.

Another interesting finding is that the initial sharp force increase has the same slope, and changes of friction angle don't change this part. .

- d is from 0.6 to 1.4 kPa, $\beta = 45^\circ$, $E=0.9$ MPa, $d=1.2$ kPa, low normal pressure

Five different value of cohesion is chosen, namely 0.6 , 0.8 , 1.0 , 1.2 and 1.4 kPa, here are the results.

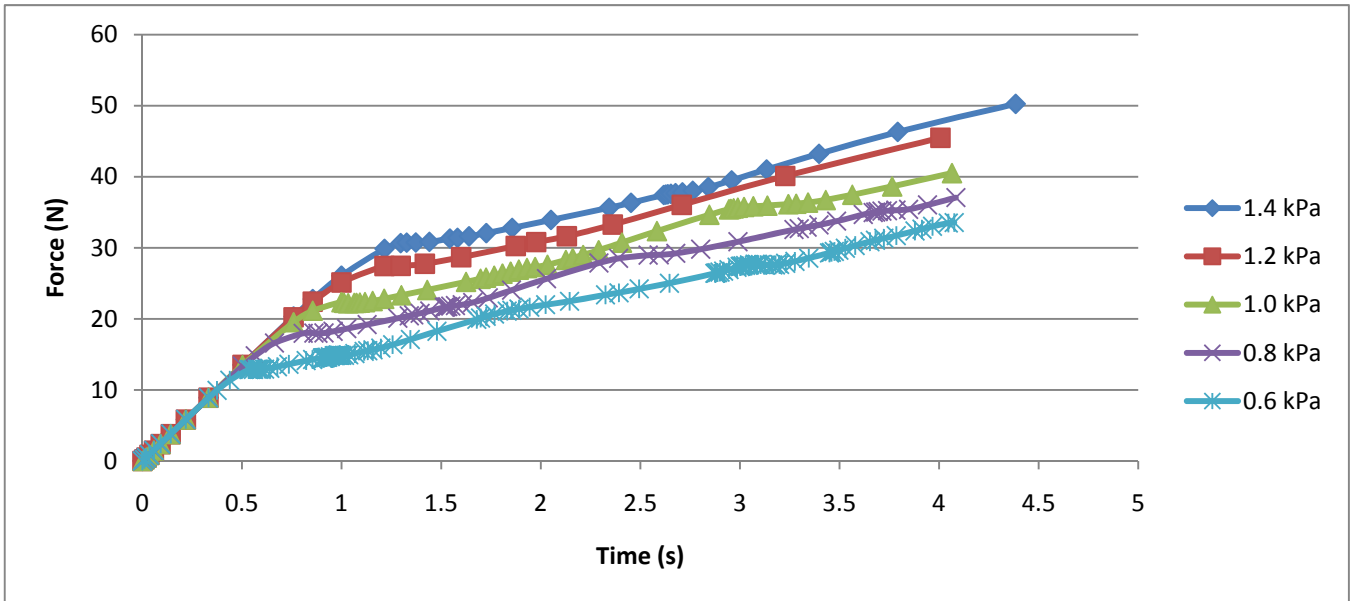


Figure 4.10 - The figure of force vs. time by choosing different cohesion

We can also see from Figure 4.10 that it has shown nearly the same trend like friction angle: different cohesion values will influence when and where the yielding points happened. And the slope remains constant no matter what the cohesion is.

So we can come to the conclusion that both cohesion and friction angle can influence the yielding point instead of the initial force slope.

3. E ranging from 0.9 MPa to 1.5 Mpa, $d = 1.2 \text{ kPa}$, $\beta = 45^\circ$, low normal pressure

Three different value of elastic modulus is chosen, namely 0.9, 1.2 and 1.5 MPa, here are the results.

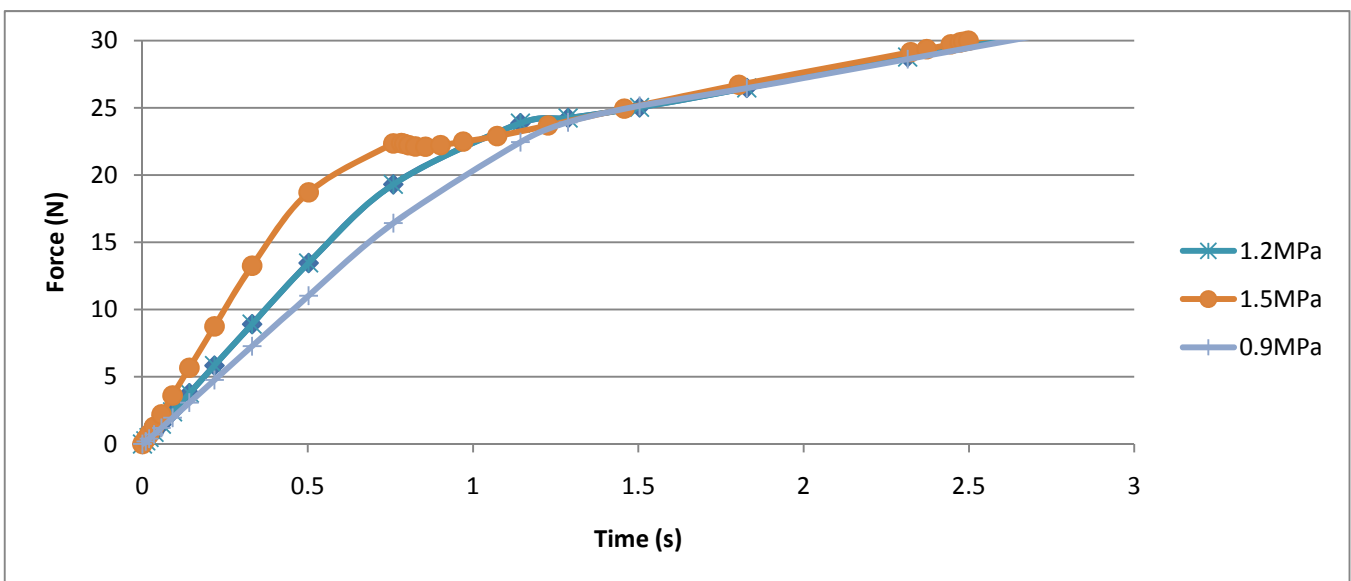


Figure 4.11 - The figure of force vs. time by choosing different Young modulus

If we zoom in and focus on the diverging point where these three lines get separated, we can see from Figure 4.11 that different Young modulus will result in different slope and also different timing when the yield points happened. Larger Young modulus means larger slope and earlier time when yield happens. But the force when these three yielding points occur is near the same, they are all around 21 N. It is also interesting to mention that different Young modulus don't influence the force afterward, the force after the yield points become almost the same, which means they are controlled by friction angle and material cohesion.

So in one word, the Young modulus will affect the slope in the initial phase, but the force when yield happens and the force afterward will not be affected by the Young modulus.

Based on the numerical results above, we can find how Young modulus, friction angle and cohesion influence the results. Young modulus will influence the initial slope, while friction angle and cohesion don't. Friction angle and cohesion will influence the force in the yield point and force afterwards, while Young modulus don't. All of them could influence the time when yield points come out. So above all is the initial study towards the material parameters.

4.5.3 A detailed study of material parameters and comparison between numerical and experiment results

Based on the analysis above, we will propose a method that can get proper results of these three material parameters in order to make good match between numerical and experiment results.

First of all, by comparing to the initial slope in the experiment data, the Young modulus can be determined, since the initial slope of increase is totally determined by Young modulus and has nothing to do with friction angle and cohesion.

Secondly, by comparing to the results on where and when the yielding point has happened, one can get a range of suitable pairs of cohesion and friction angle from numerical modelling in order to match the experiment results.

Step 1: Determine the Young modulus.

There are 6 cases from Figure 4.12 to 4.17, namely Low_Long, High_Long, Low_Short, High_Short, Dry_Low and Extra_High_Short.

Here different Young modulus are chosen in order to find the best fit of slope for each case, while we assume cohesion and friction angle to be the same in every case.

As for the Low_Long and High_Long situation, the results are (The friction angle is assumed to be 45° and the cohesion is assumed to be 1.2 kPa below):

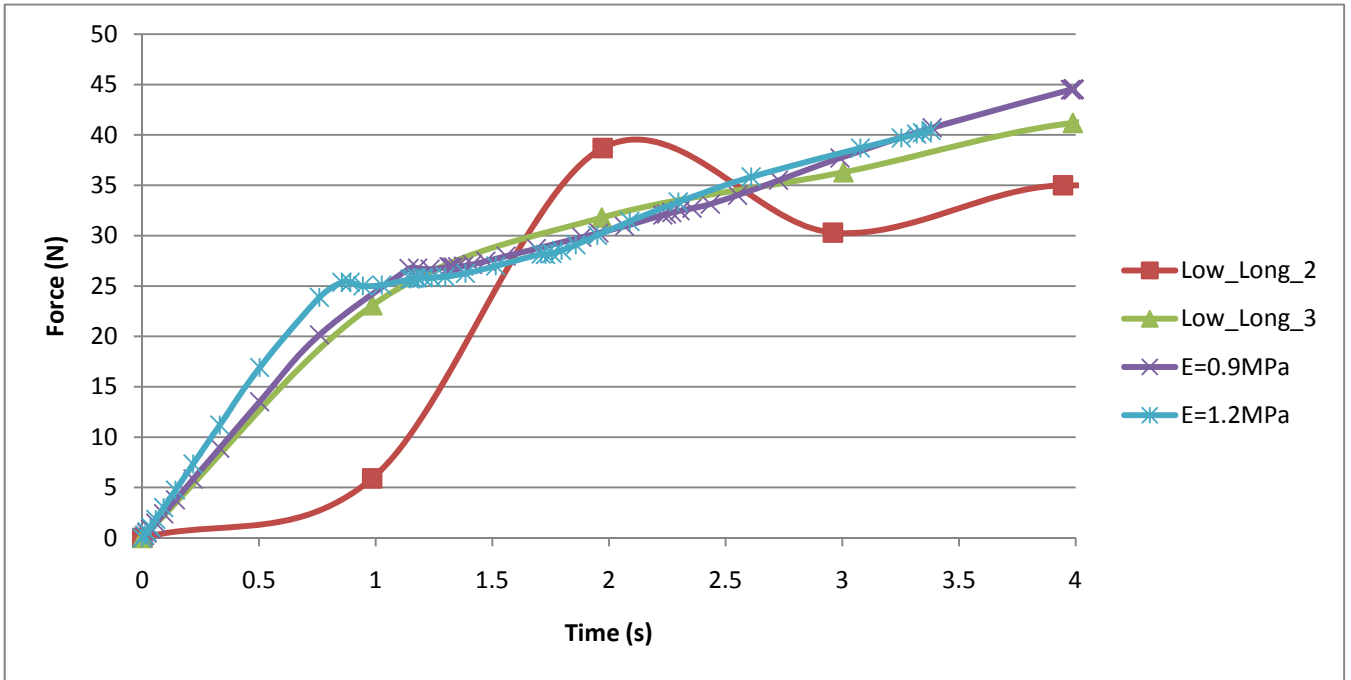


Figure 4.12 - Low_Long experiment results and numerical modelling with different Young Modulus (Low_Long_1 is not shown because of inaccuracy)

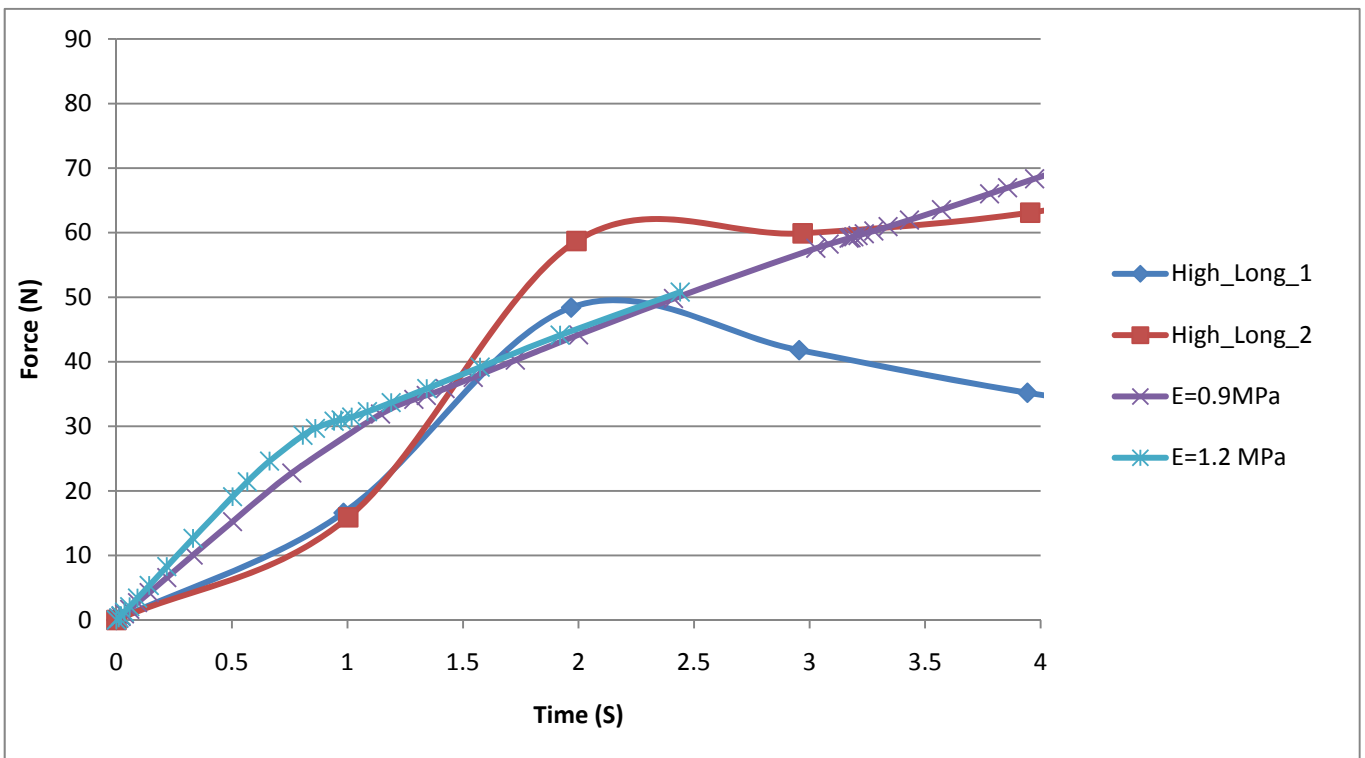


Figure 4.13 - High_Long experiment results and numerical modelling with different Young Modulus (High_Long_3 is not shown because of inaccuracy)

So from Figure 4.12 and 4.13, we can find that in the long submerging time situation, the Young modulus could be chosen as 0.9 MPa to 1.2 MPa, and this result is within the same range as the results concluded by Serré (2011). So we can assume that in the following numerical modelling of long submersion time, the Young modulus could be chosen as 0.9 MPa.

As for the short submerging time, the experiment results of force have shown rapidly increase and larger force when yield point happens, so a relative large cohesion could be used, and we choose friction angle to be 45° and the cohesion to be 4 kPa. Here are the results for short submerging time:

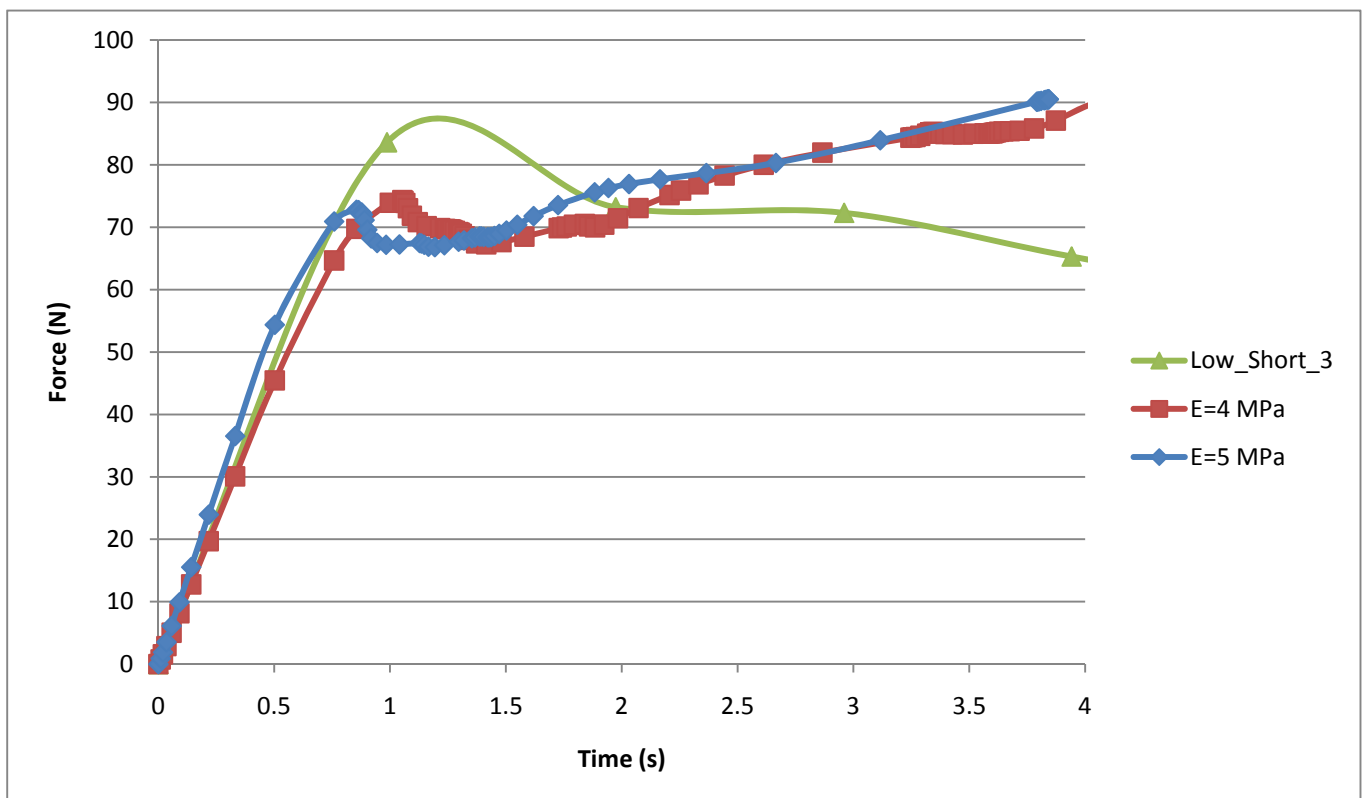


Figure 4.14 - Low_Short experiment results and numerical modelling with different Young Modulus
(Low_Short_1&2 are not shown because of inaccuracy)

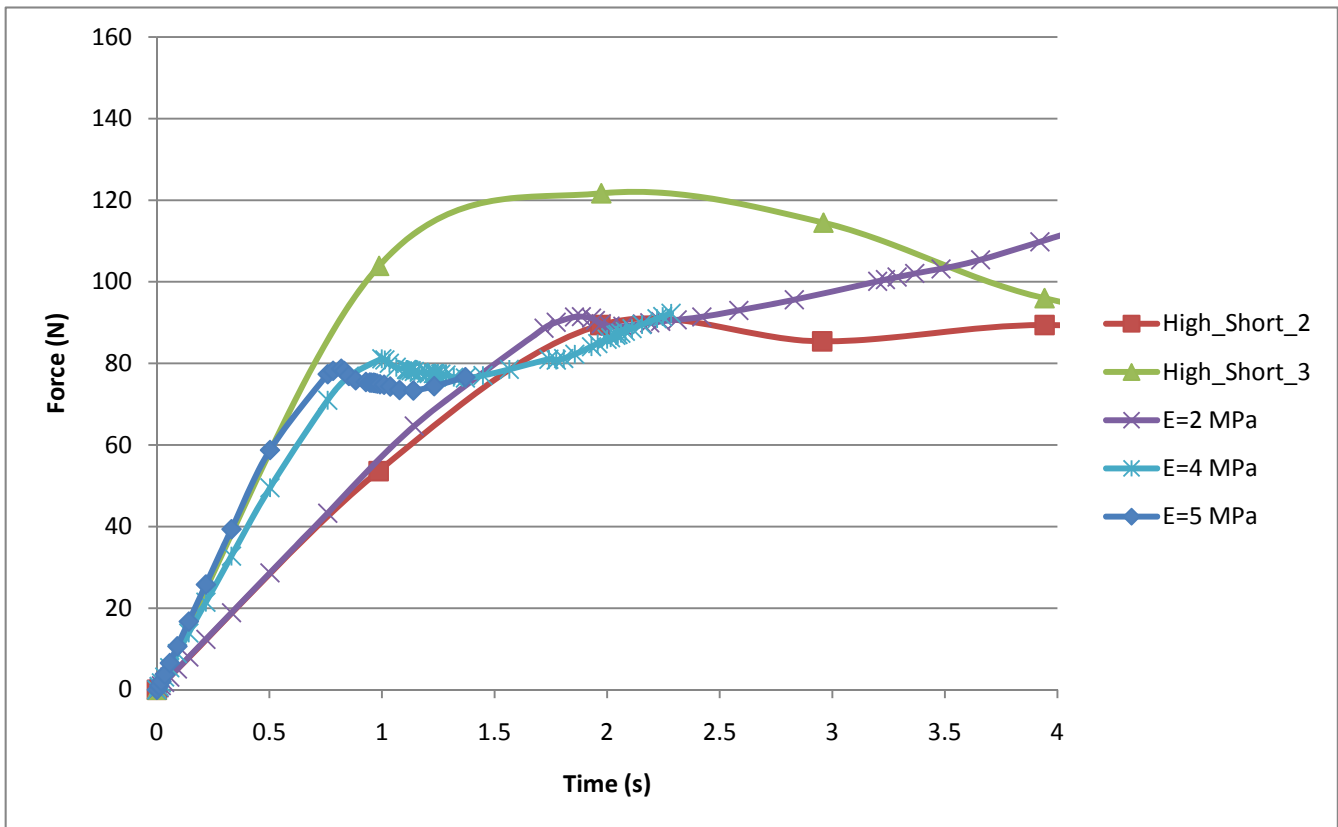


Figure 4.15 - High_Short experiment results and numerical modelling with different Young Modulus
(High_Short_1 is not shown because of inaccuracy)

We can see from Figure 4.14 and 4.15 that the Young Modulus is within the range from 2 MPa to 5 MPa and in the following modelling, we will give 4.5 MPa to the Young modulus when it comes to Low_Short experiment and 2 MPa to the Young modulus when it comes to High_Short experiment. In Serré (2011), he uses ice rubble which has finished the punch test, that means the ice rubble has been submerged in water for longer time, so he get Young modulus as 0.9 MPa in the Oedometer test. But in our case, the ice rubble is newly made and submerged into water for only 5 minutes, so it is understandable that the ice rubble in shorter submersion time will be stronger than the one in longer submersion time, which will result in larger Young modulus.

Figure 4.16 and 4.17 have shown the Young Modulus for Dry_Low test and Extra_High_Short test respectively.

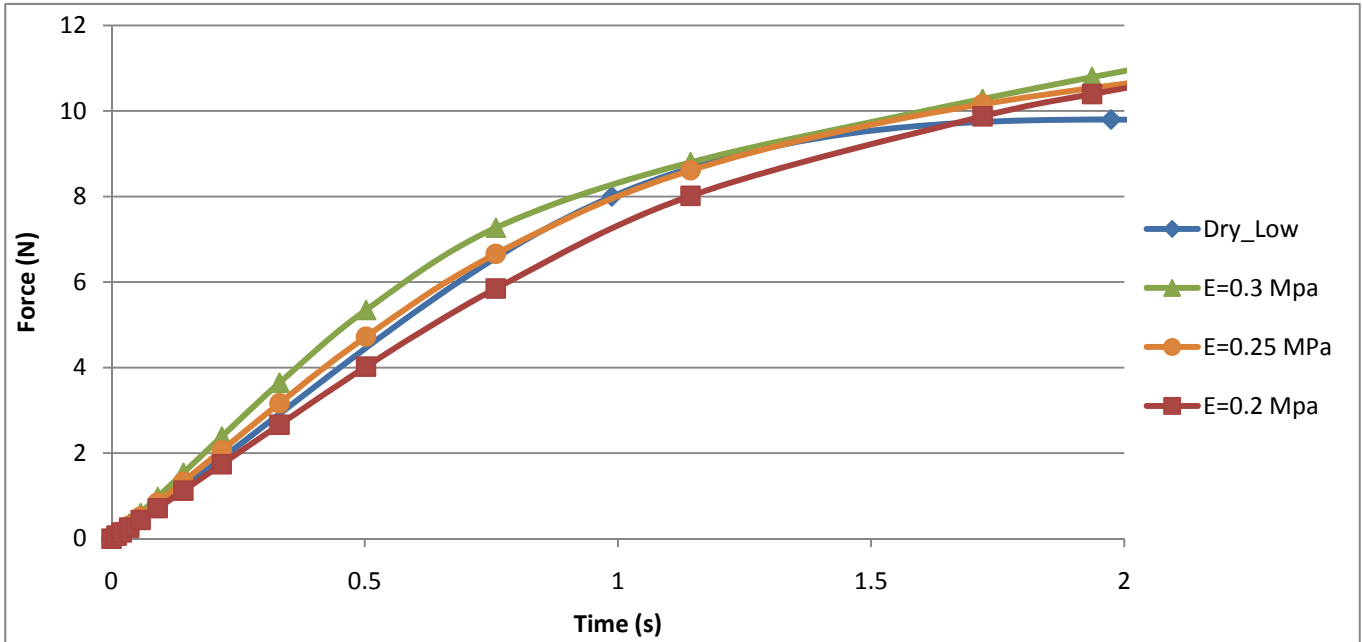


Figure 4.16 - Dry_Low experiment results and numerical modelling with different Young Modulus

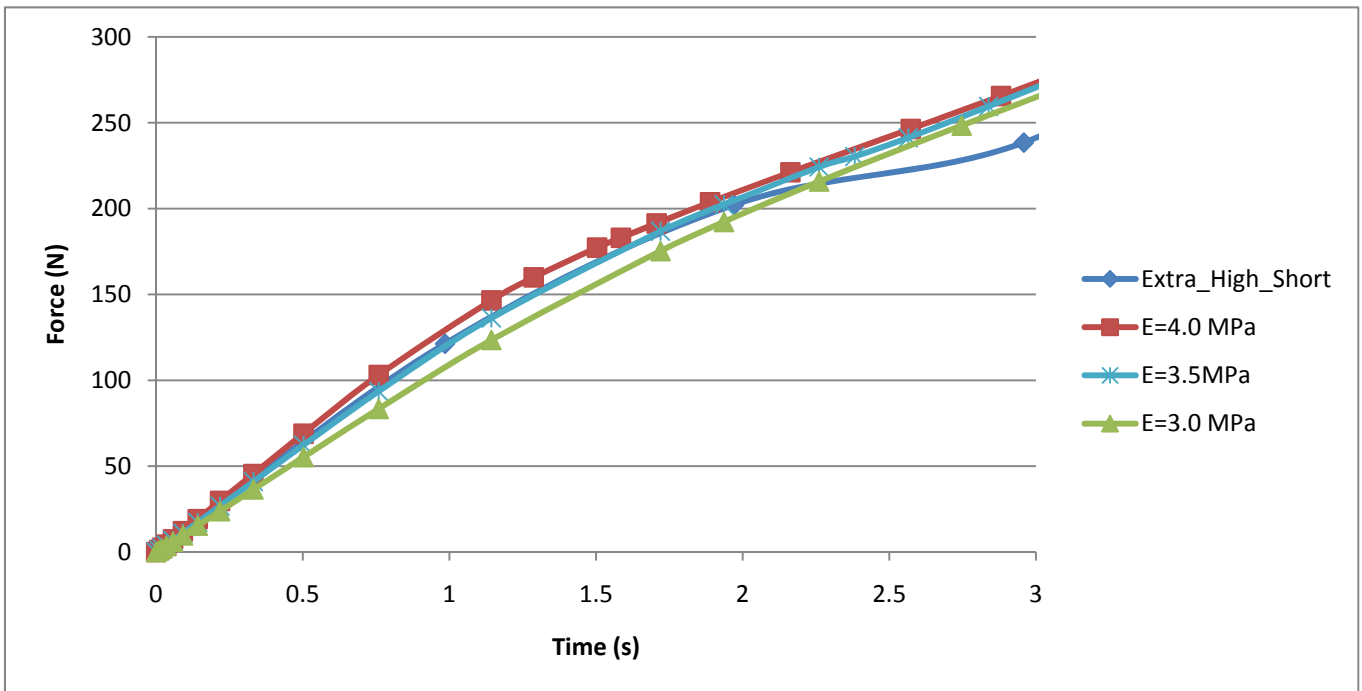


Figure 4.17 - Extra_High_Short experiment results and numerical modelling with different Young Modulus

So we can easily get the Young Modulus from the figure above for Dry_Low and Extra_High_Short tests, which are 0.25 MPa and 3.5 MPa respectively.

Table 4.5 below has summarized the Young modulus for the following numerical modelling:

Table 4.5 - The Young modulus for numerical modelling

	High_Long	Low_Long	Low_Short	High_Short	Dry_Low	Extra_High_Short
Young Modulus	0.9 MPa	0.9 MPa	4.5 MPa	2 MPa	0.25 MPa	3.5 MPa

Step 2: Determine the friction angle and cohesion

In this part, the thesis will go into details on how to choose suitable friction angle and cohesion in order to match numerical and experimental data. In the following, each of the 6 cases will be discussed respectively.

Case 1: Low_Long_2&3 (E=0.9 MPa)

Seven different friction angle is chosen, namely $25^\circ, 30^\circ, 35^\circ, 40^\circ, 45^\circ, 50^\circ, 55^\circ$ and different cohesion will be chosen in order to find the most suitable one for the experiment results. Here are two examples of the results, one is when $\beta = 45^\circ$ (medium friction angle), another is when $\beta = 25^\circ$ (low friction angle) and all the other numerical results are listed in the appendix:

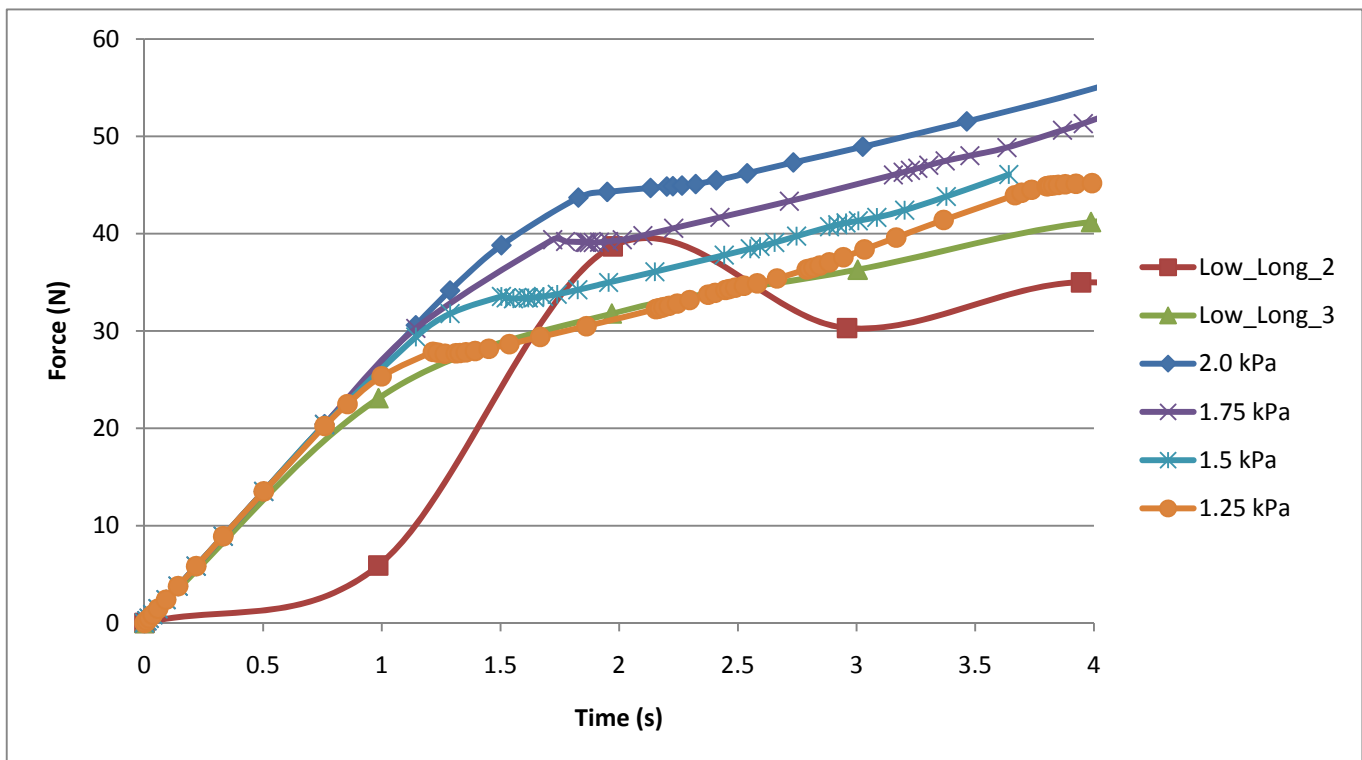


Figure 4.18 - Load-time curves in Test Low_Long with different cohesion when $\beta = 45^\circ$

In Figure 4.18 we can see that the numerical results can fit the shape of the curve-Low_Long_3 well in this case, but is a bit less fit with the curve-Low_Long_2. However, not only the time when yielding points happened, but also the force when yielding points occur are well fit between numerical and experimental results. So we can say that the setup of numerical modelling is appropriate in modelling the experiment.

But when it comes to relative low friction angle $\beta = 25^\circ$, the result is a bit different.

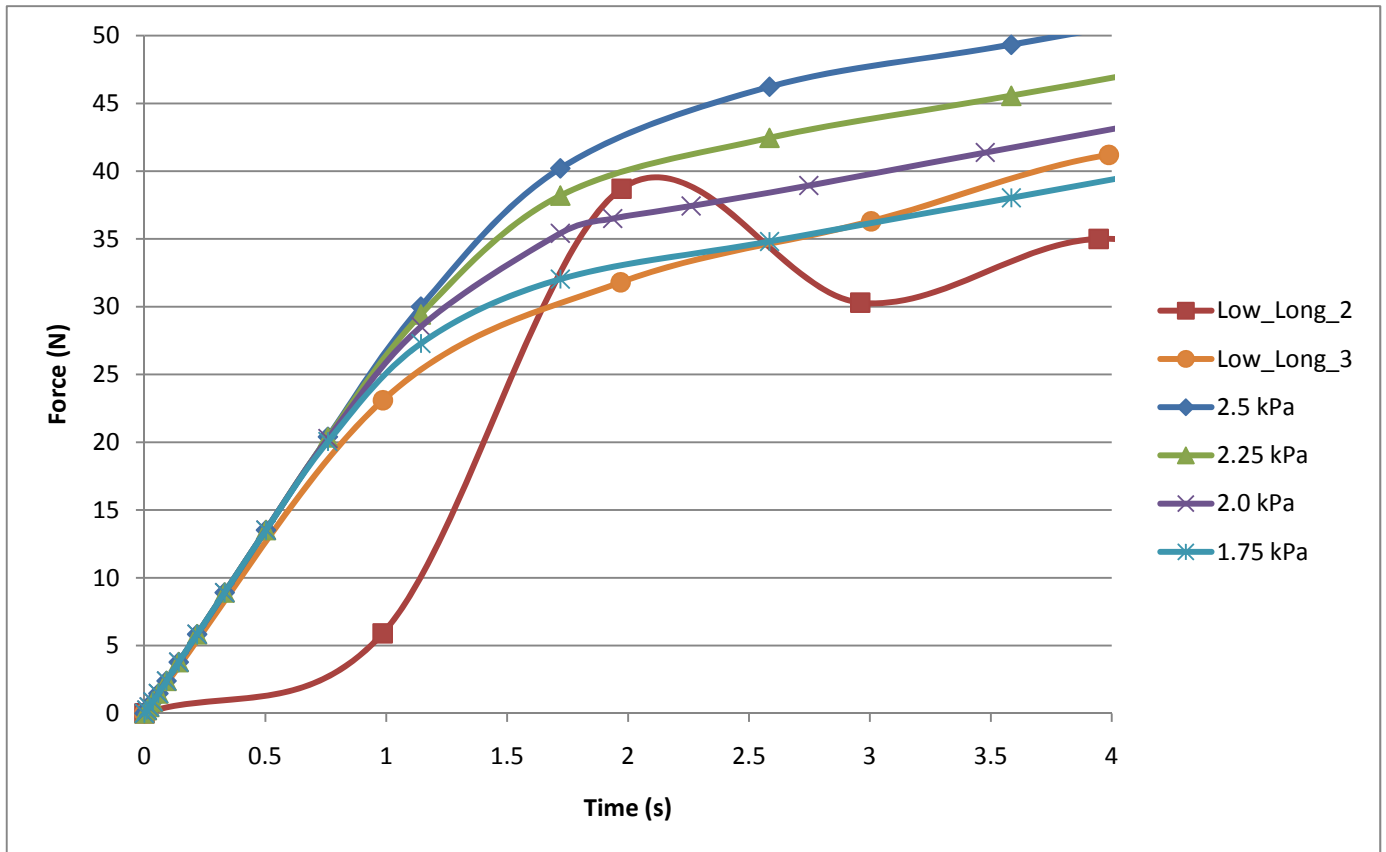


Figure 4.19 - Load-time curves in Test Low_Long with different cohesion when $\beta = 25^\circ$

We can see from Figure 4.19 that the yielding point in this case is less obvious than the previous situation, but it is still clear that the numerical model can fit the experimental results well, both shape and magnitude.

By comparing the results from Figure 4.18 and 4.19, we can find that as for lower friction angle in numerical modelling, we will need larger cohesion in order to fit well with experimental data. And a quantitative analysis will be given in the next chapter.

Case 2: High_Long_1&2 (E=0.9 MPa)

In the case, the normal pressure will be chosen as 3 kPa instead of 0.86 kPa. And the Young modulus is still 0.9 MPa. Seven different friction angle is chosen, namely 25° , 30° , 35° , 40° , 45° , 50° , 55° and different cohesion will be chosen in order to find the most suitable one for the experiment results. Two examples are given, one is when $\beta = 45^\circ$ (medium friction angle), another is when $\beta = 25^\circ$ (low friction angle) and all the other numerical results are listed in the appendix:

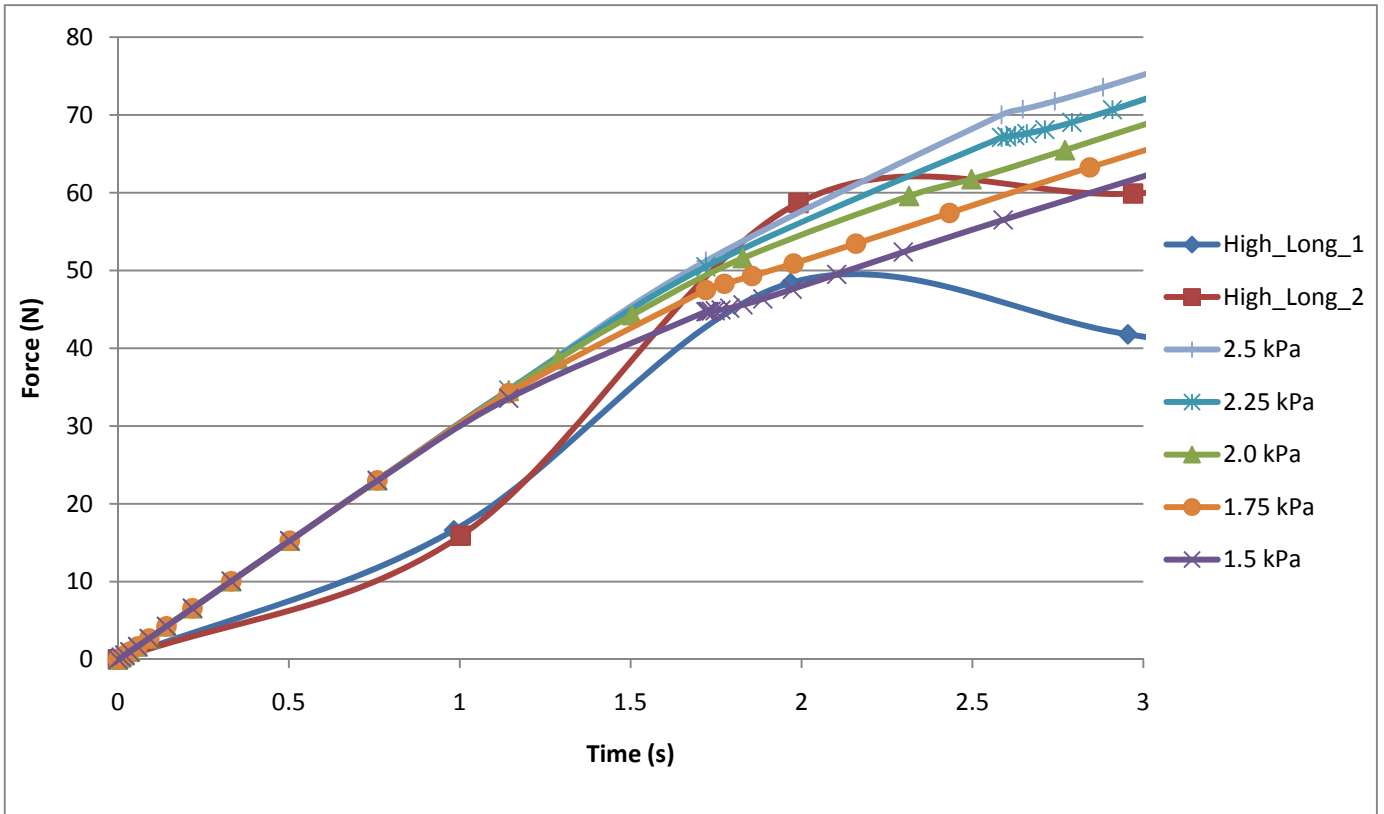


Figure 4.20 - Load-time curves in Test High_Long with different cohesion when $\beta = 45^\circ$

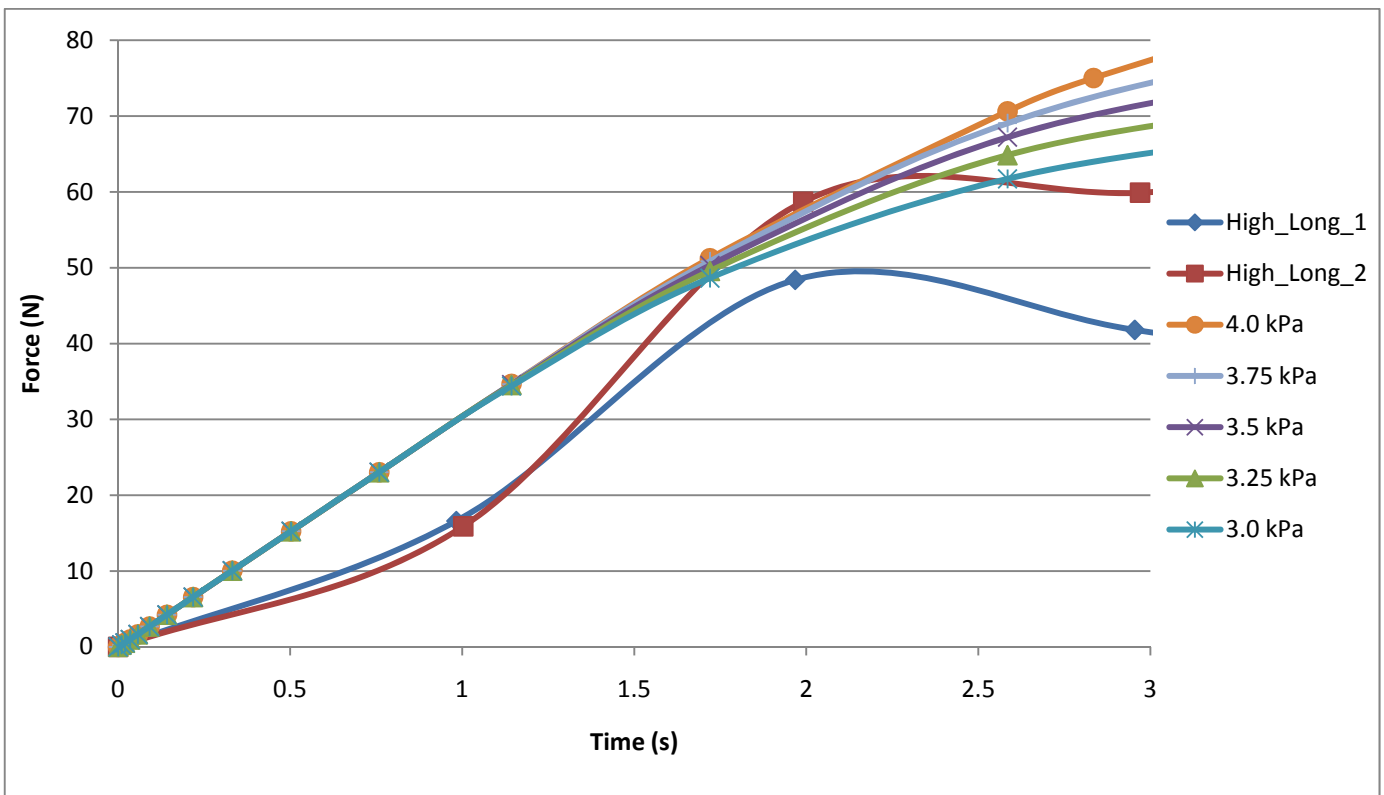


Figure 4.21 - Load-time curves in Test High_Long with different cohesion when $\beta = 25^\circ$

Case 3: Low_Short_3 (E=4.5 MPa)

Also two cases out of seven are given in order to demonstrate the numerical results.

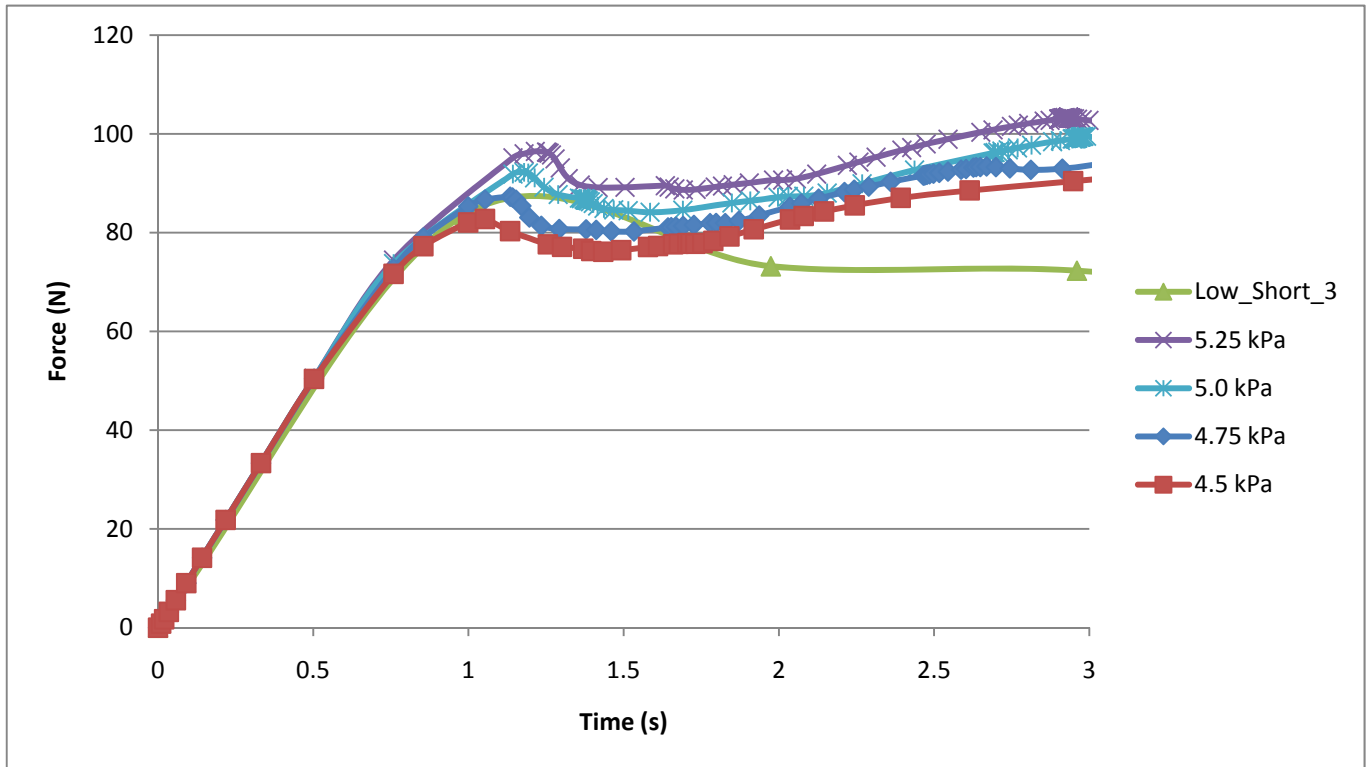


Figure 4.22 - Load-time curves in Test Low_Short with different cohesion when $\beta = 45^\circ$

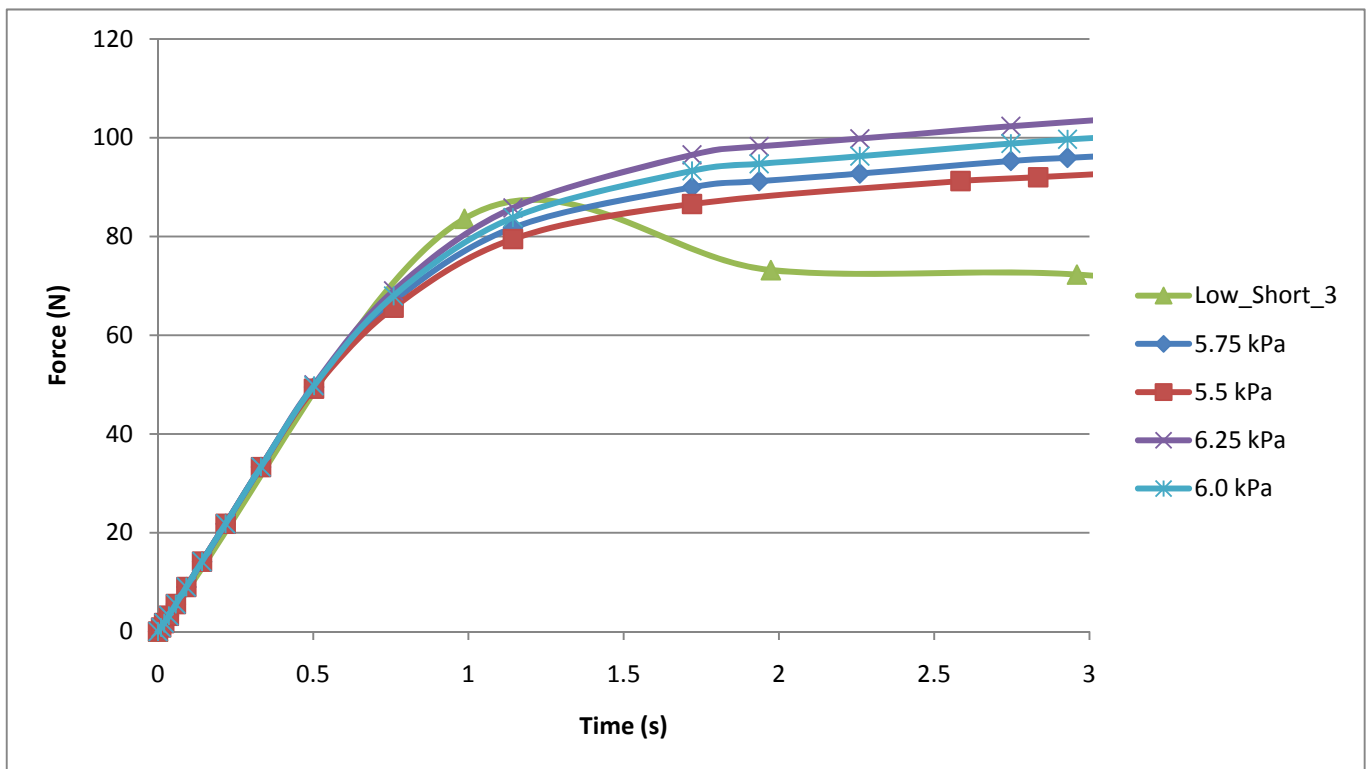


Figure 4.23 - Load-time curves in Test Low_Short with different cohesion when $\beta = 25^\circ$

Case 4: High_Short_2 (E=2.0 MPa)

Also two cases out of seven are given in order to demonstrate the numerical results.

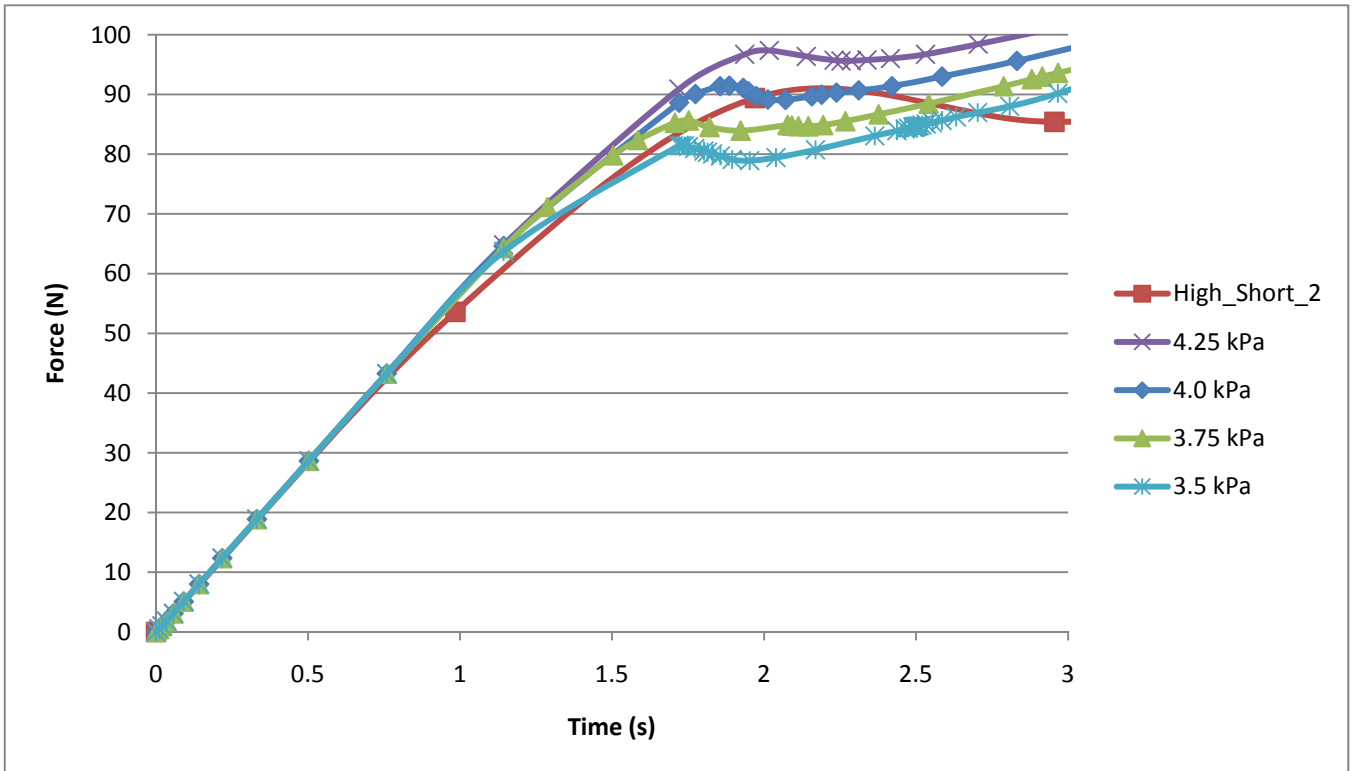


Figure 4.24 - Load-time curves in Test High_Short with different cohesion when $\beta = 45^\circ$

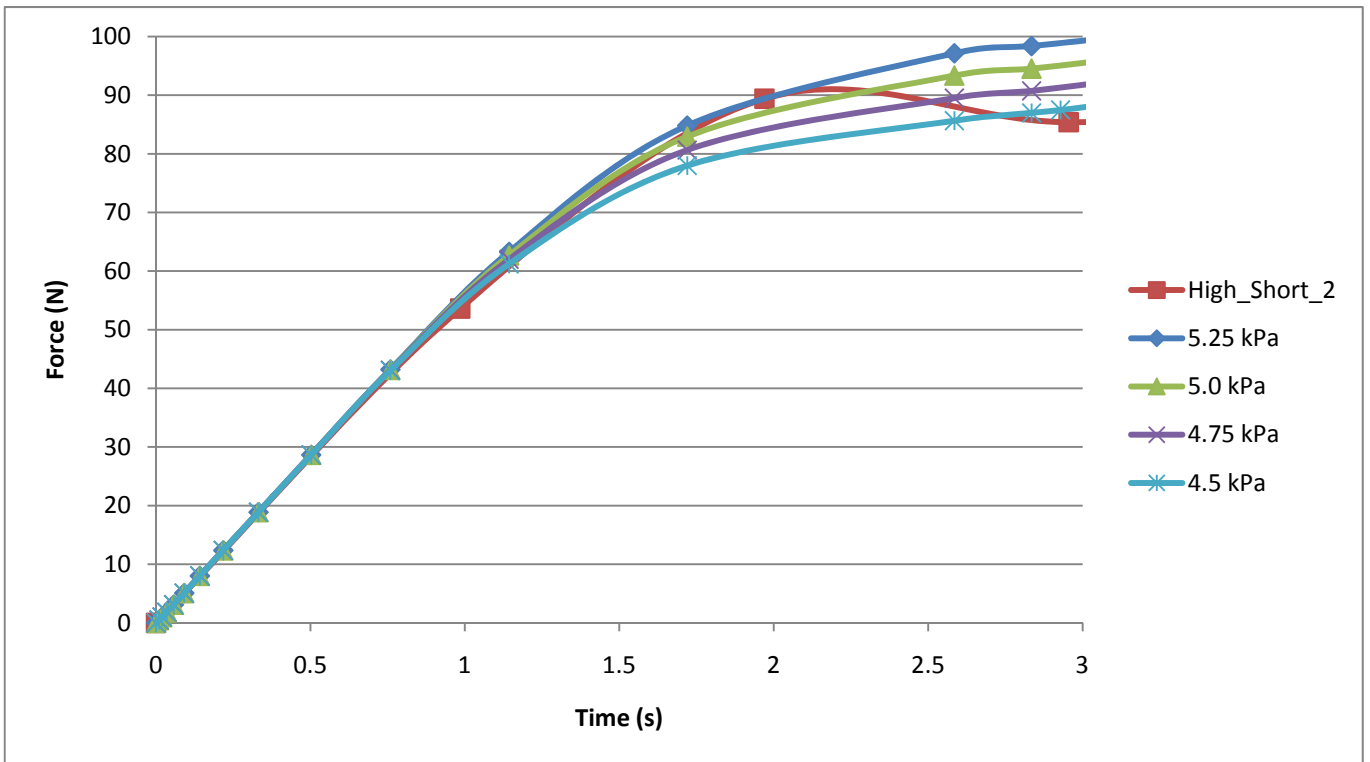


Figure 4.25 - Load-time curves in Test High_Short with different cohesion when $\beta = 25^\circ$

Case 5: Dry_Low ($E=0.25$ MPa)

Two cases out of seven are given in order to demonstrate the numerical results.

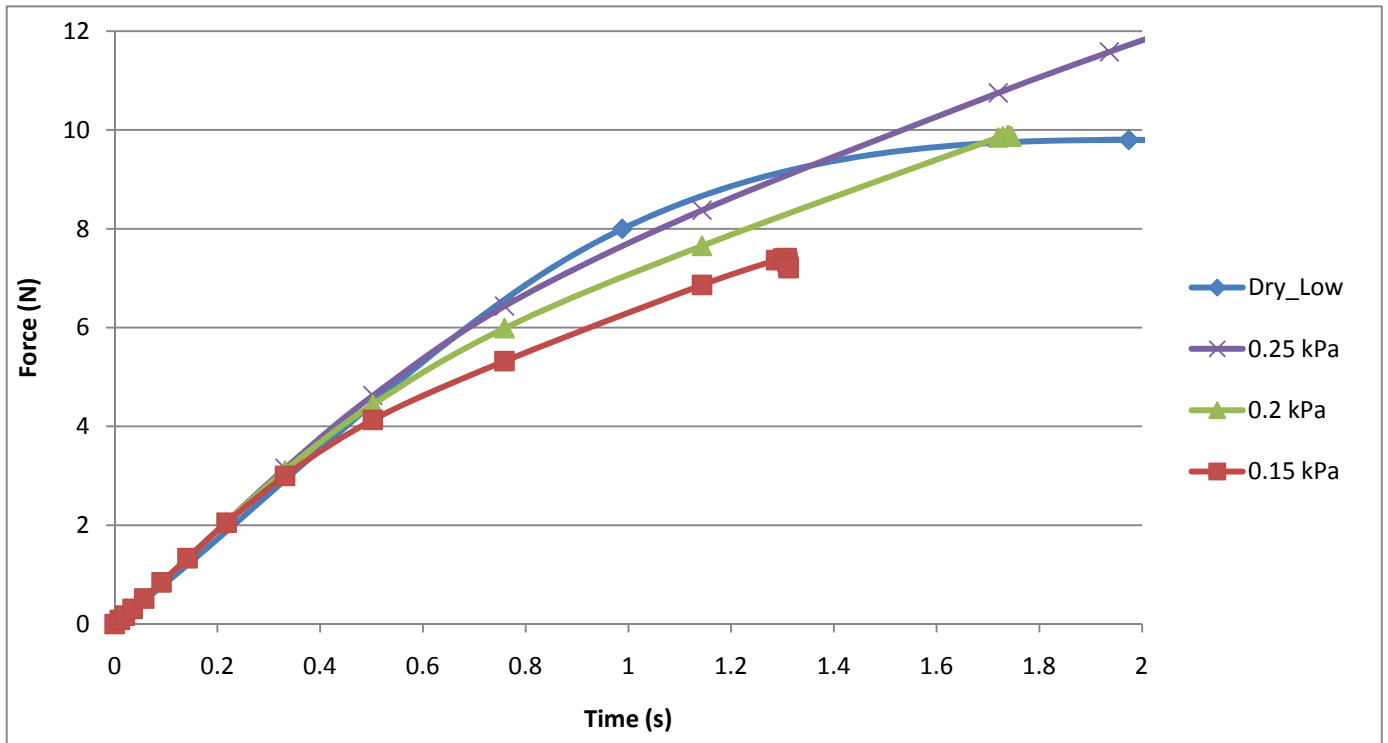


Figure 4.26 - Load-time curves in Test Dry_Low with different cohesion when $\beta = 35^\circ$

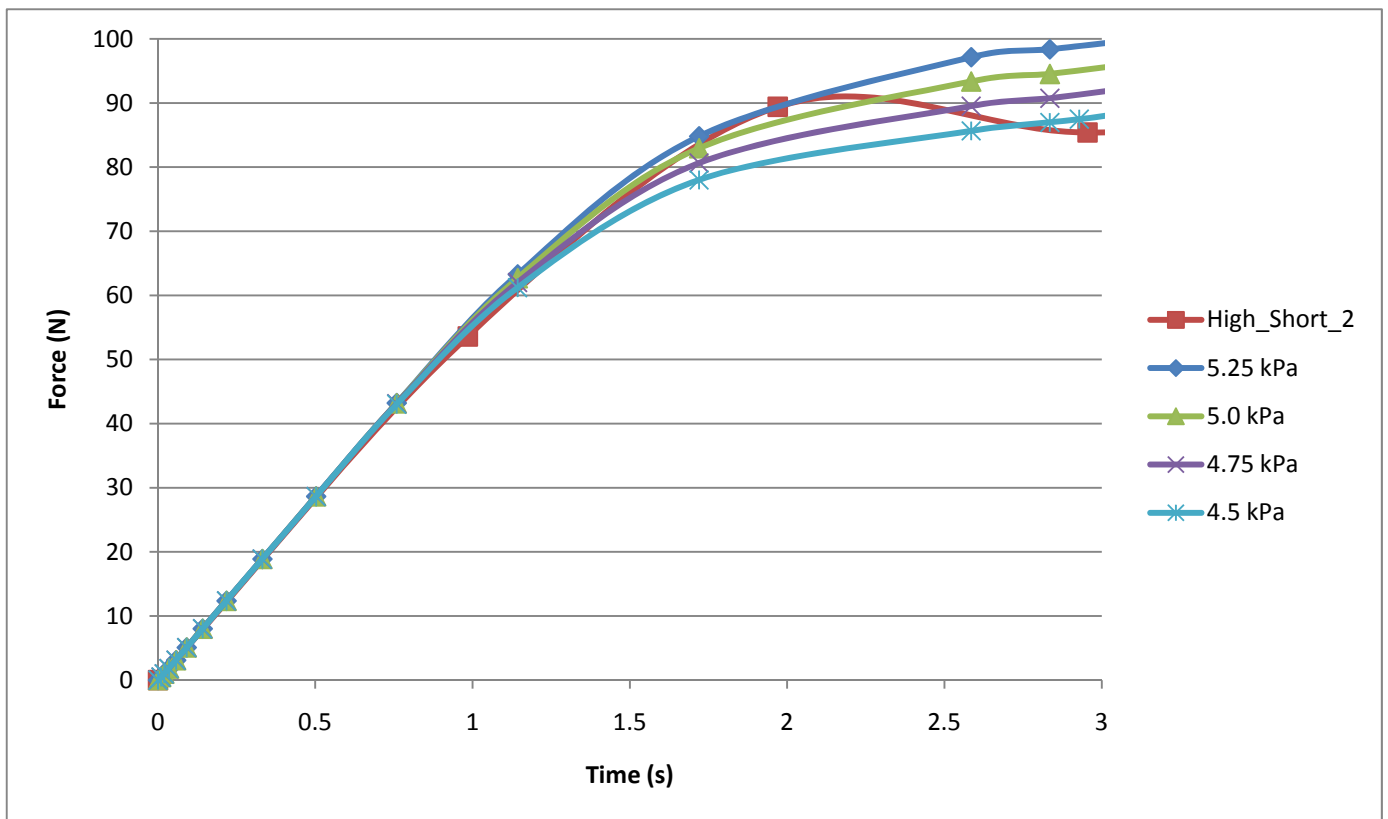


Figure 4.27 - Load-time curves in Test Dry_Low with different cohesion when $\beta = 15^\circ$

Case 6: Extra_High_Short ($E=3.5$ MPa)

Two cases out of seven are given in order to demonstrate the numerical results.

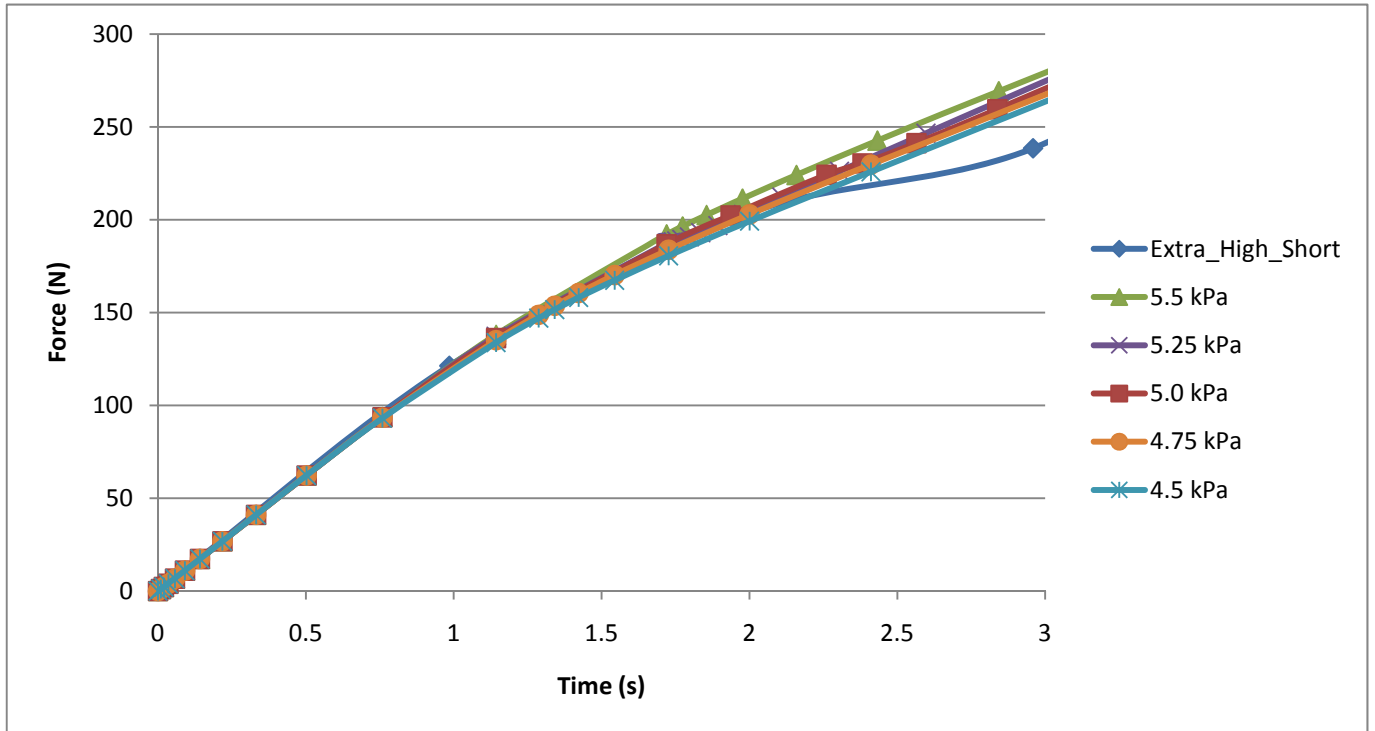


Figure 4.28 - Load-time curves in Test Extra_High_Short with different cohesion when $\beta = 45^\circ$

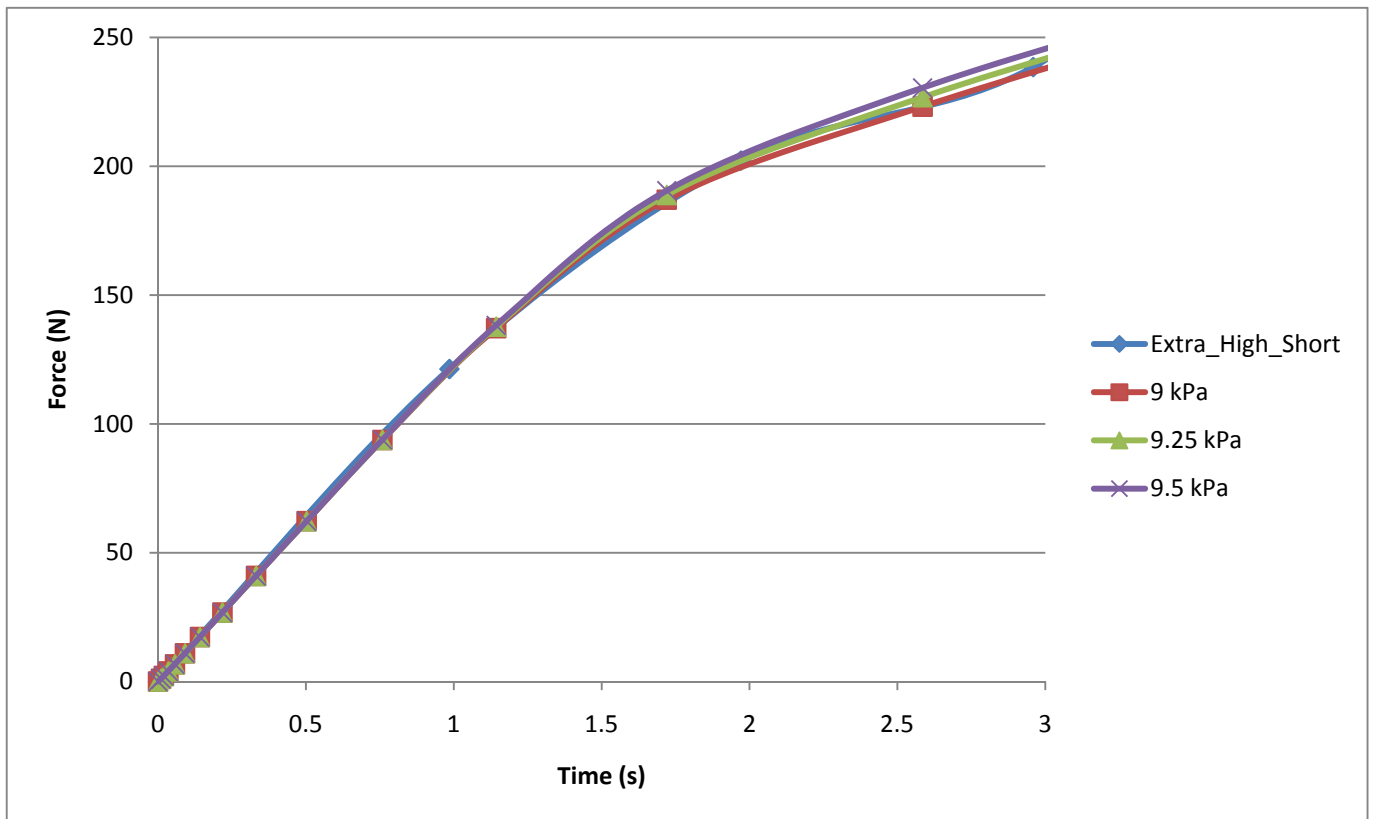


Figure 4.29 - Load-time curves in Test Extra_High_Short with different cohesion when $\beta = 25^\circ$

4.6 Summary

The numerical results are presented and discussed in this chapter, and some assumptions are made beforehand:

1. The material in the shear box is homogeneous.
2. Time dependent deformation, like creep is ignored
3. Only static analysis is carried out.
4. Cohesion softening is not used during modelling.
5. No cap model will be used in the modelling.

Based on the assumptions above, the parameter sensitivity analysis is carried out and here is the conclusion: the influence of rubble height, rubble density, porosity and dilatation angle is minor, while the influence of Young modulus, cohesion and friction angle is important. After studying these three important material parameters, a trend of them is found.

The Young modulus can only determine the slope of the initial increase, and the cohesion and friction angle will determine when the yield points happen and how large the force is when the material comes to yield. So the Young modulus can be studied first, following by the analysis of material cohesion and friction angle.

The Young modulus in each of the six cases are 0.9 MPa for Low_Long, 0.9 MPa for High_Long, 4.5 MPa for Low_Short, 2 MPa for High_Short, 0.25 MPa for Dry_Low and 3.5 MPa for Extra_High_Short. Seven friction angle are chosen for each of these four cases and different cohesion are chosen as well to fit with the experiment data. The range of the cohesion is summarized in Table 4.6 below.

Table 4.6 – Summary of the results

Case	Young Modulus (MPa)	Friction angle	Cohesion (kPa)
Low_Long	0.9	25~55°	0.8 to 2.5
High_Long	0.9	25~55°	1 to 4
Low_Short	4.5	25~55°	4 to 6
High_Short	2.0	25~55°	3 to 6
Dry_Low	0.25	15~35°	0.1 to 0.1
Extra_High_Short	3.5	15~55°	1 to 11

A further analysis of these data will be presented in the next chapter.

5. ANALYSIS AND DISCUSSION

5.1 General

This chapter will cover the following topics: Section 5.2 will analyse the material parameters based on the numerical results in chapter 4. The comparison between previous study will be presented in section 5.3 including the discussion of scaling ratio. In section 5.4, the uncertainties of numerical results will be discussed.

5.2 Analysis of material parameters

5.2.1 Young modulus

The Young modulus in our case is 0.9 MPa, 0.9 MPa, 4.5 MPa, 2 MPa, 0.25 MPa and 3.5 MPa for Low_Long, High_Long, Low_Short, High_Short, Dry_Low and Extra_High_Short tests respectively. Serré (2011) carried out Oedometer test to study the Young modulus using the ice rubble after the punch test (long submersion time) and had found E to be 0.9 MPa in all the tests.

It is important to mention that the Young modulus used in the numerical modelling in our case is the Young modulus of ice rubble, or more precisely, it is the Young modulus of the assembly of ice blocks, freeze-bonds and voids. As for the Young modulus of individual ice blocks, there is a disagreement of an order of magnitude between measurements of E in the laboratory (9 GPa) and from field observations (1 GPa). (Nimmo, 2004). But the Young modulus of individual freeze-bond is even smaller. Repetto et al. (2011c) suggests that it is in the order of 5 kPa.

In our case, it is clear the Young modulus was different for different submersion times. And the Young modulus was even different in the three individual tests in the same situation. It seems that short submersion time will result in large Young modulus. The colder the ice is, the stronger the freeze-bonds will be, thus resulting in larger Young modulus. The ice blocks are also getting weaker and most probably less elastic with increasing submersion time. Besides this, in the numerical modelling results, Young Modulus also shows the dependency on the normal pressures. Larger normal pressure means larger Young Modulus. But from a modelling point of view the fact that the Young modulus's dependent on the boundary conditions is quite a difficult phenomenon to include, so whether or not the confinement will influence the Young Modulus still needs discussion. Apart from these, there are a lot of other things that can influence the Young modulus of freeze-bonds, like the temperature, the porosity, the salinity, the block thickness and so on. But how could they affect the Young modulus of freeze-bonds is not known yet and goes beyond the scope of this thesis, so it will not be included at the moment.

So it is difficult to give a certain value of Young modulus and even a certain range of Young modulus is impossible to be given since a lot of parameters can influence the magnitude of E for freeze-bonds. So it is suggested that Oedometer test or other tests could be carried out in each shear box experiment in order to give an individual Young modulus for different test setup and situation and also the Young modulus could be determined from the time vs. force figure using the theory that this thesis proposed: The initial slope could only be influenced by the Young modulus.

5.2.2 Friction angle and cohesion

In chapter 4, a series of cohesion is given for the numerical modelling in order to match a series of different friction angle. Here the results have been summarized with both numerical and experimental data in one figure, the cross points can be found between the simulated and the measured lines representing admissible combinations of cohesion and the friction angle for each test case.

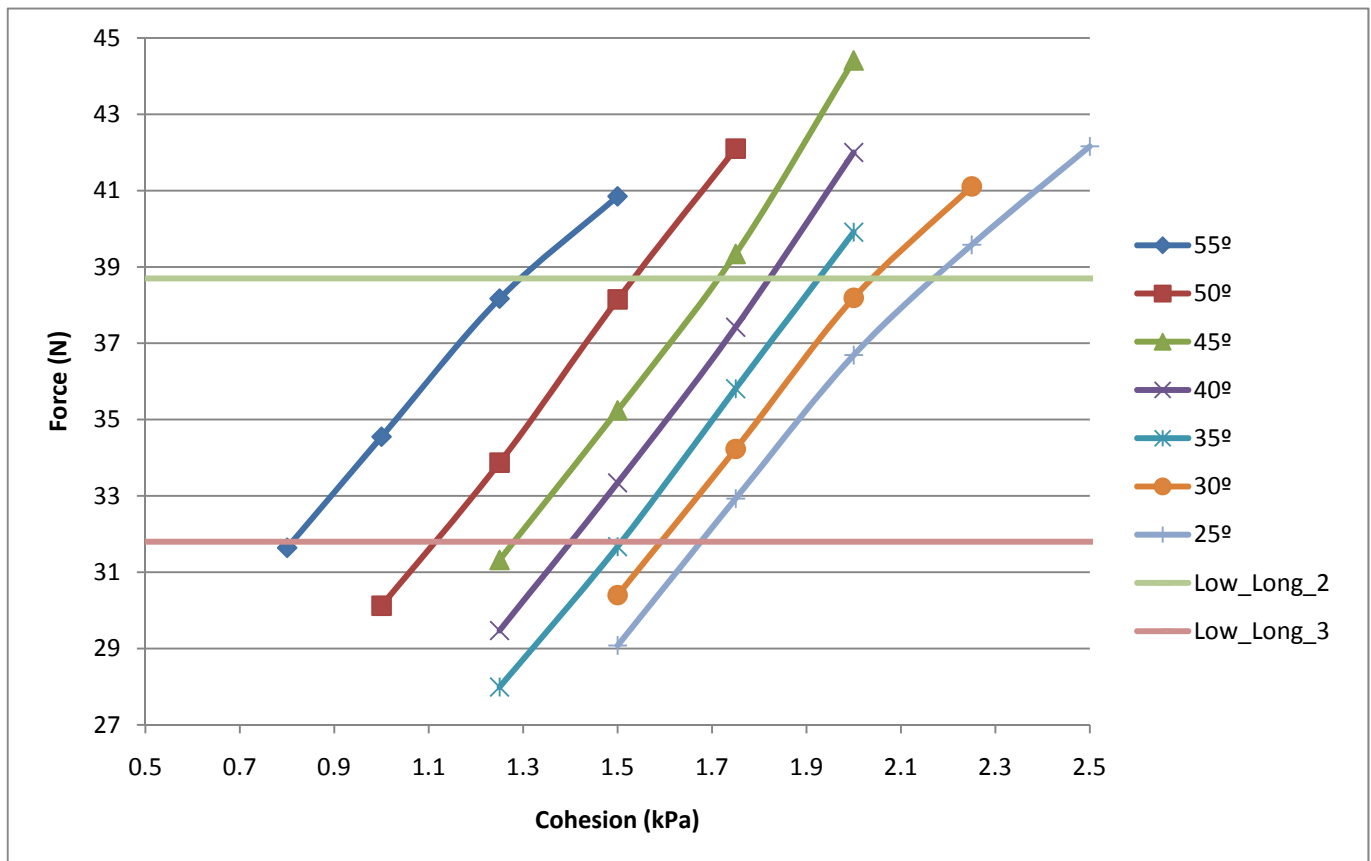


Figure 5.1 - Force at yielding point in Low_Long test versus corresponding initial cohesion with different values for the internal friction angle

We can see from Figure 5.1 that there will be a series of pairs of cohesion and friction angle that can match the experimental results, but based on the present available data, it is difficult to find the most realistic pair of cohesion and friction angle. But if we assume that the friction angle in Phase 1 and Phase 3 is the same, we can use the

derivation of friction angle from Phase 3 (see section 3.3.4), and suggest an unique pair of cohesion and friction angle for the different tests. Let us calculate the average friction angle in Phase 3:

For long submersion time: the average friction angle is $(8.6^\circ + 29.4^\circ + 30.8^\circ)/3 = 22.9^\circ$, if we neglect the peculiar small angle 8.6° , the average friction angle will be around 30° .

For short submersion time: the average friction angle is $(55.6^\circ + 33.4^\circ + 73.8^\circ)/3 = 54.3^\circ$, if we neglect the peculiar large angle 73.8° , the average friction angle will be around 45° .

This result is quite interesting that it implies the friction angle has something to do with submersion time and the result also gives a certain friction angle to each case and based on that, the cohesion can be determined as well. But in reality, there are a lot of uncertainties during the calculation, like the inequality between rubble friction angle and individual freeze-bonds friction angle, the experiment itself has made a lot of simplicity and assumption in order to model freeze-bonds in reality. All of these has shown that the friction angle calculated above would be qualitatively and descriptively, rather than quantitatively.

Here are the matching pairs of cohesion and friction angle between numerical and experimental modelling for the other five cases:

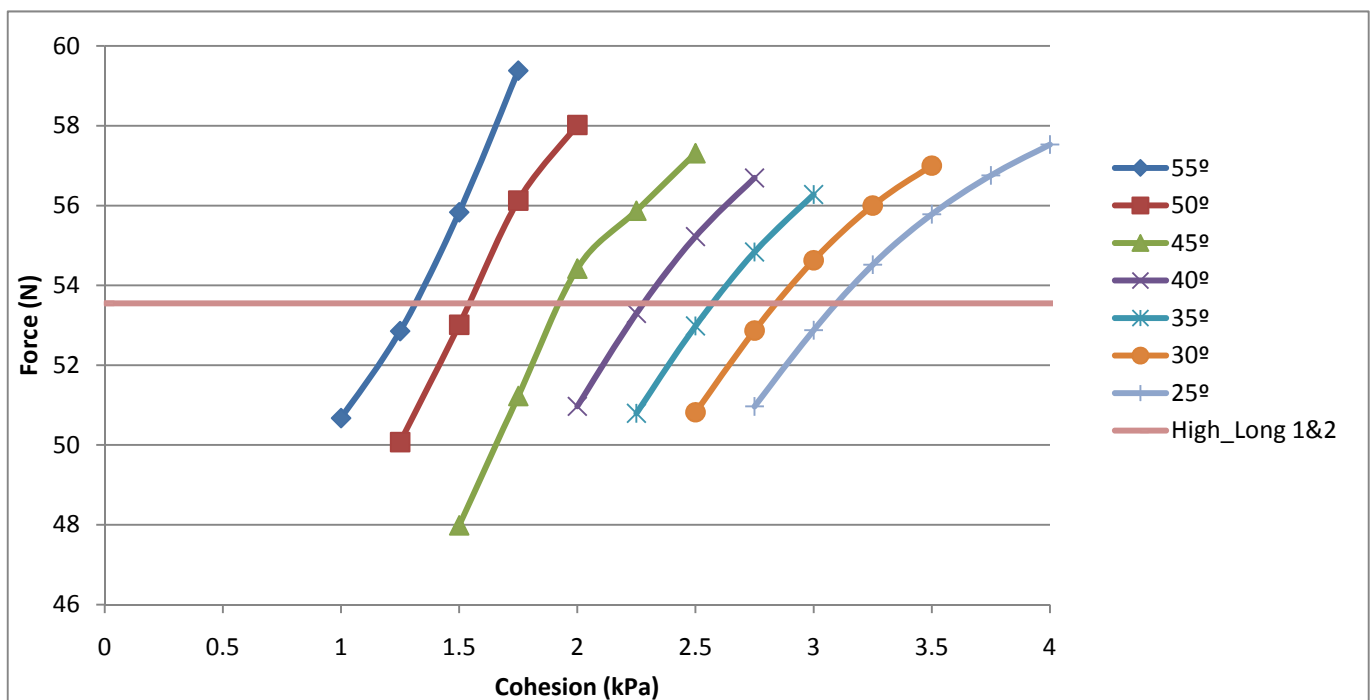


Figure 5.2 - Force at yielding point in High_Long test versus corresponding initial cohesion with different values for the internal friction angle

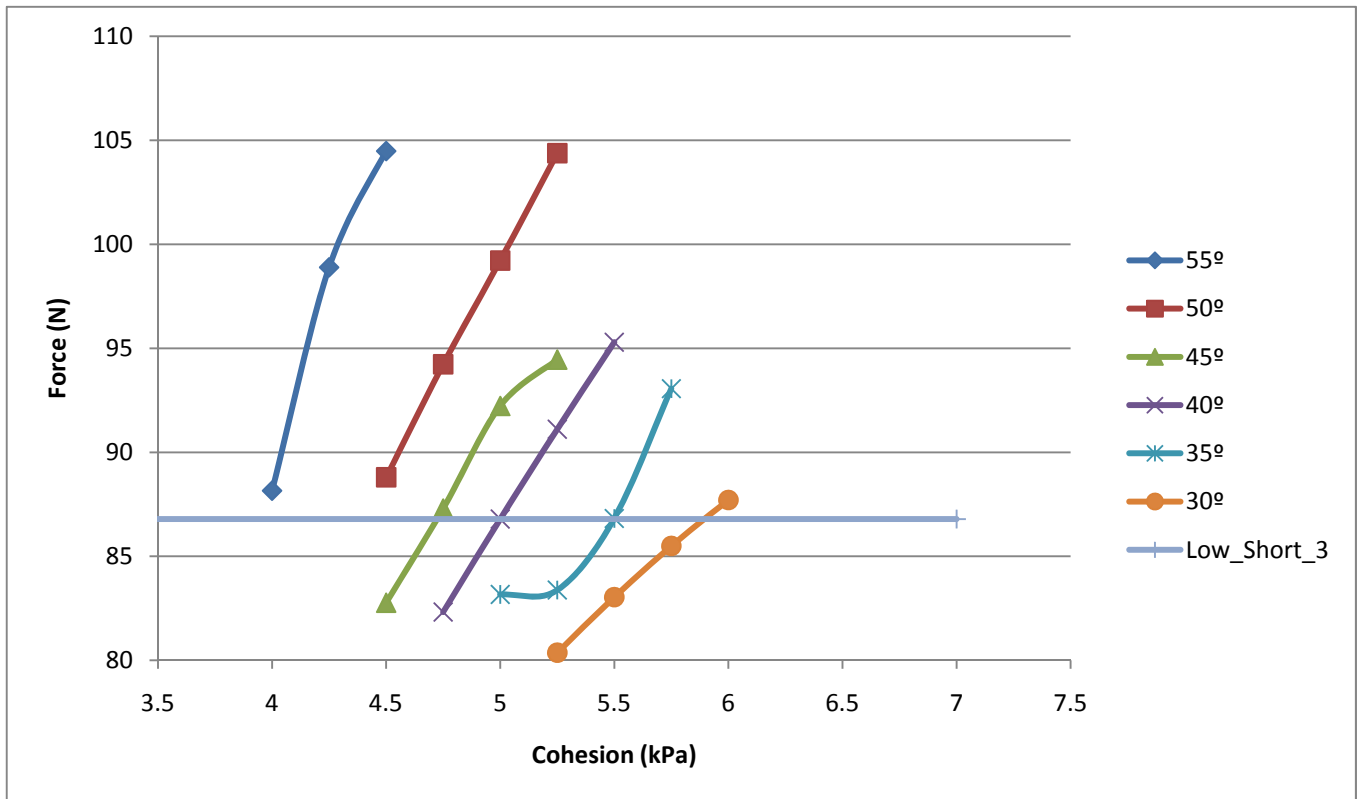


Figure 5.3 - Force at yielding point in Low_Short test versus corresponding initial cohesion with different values for the internal friction angle

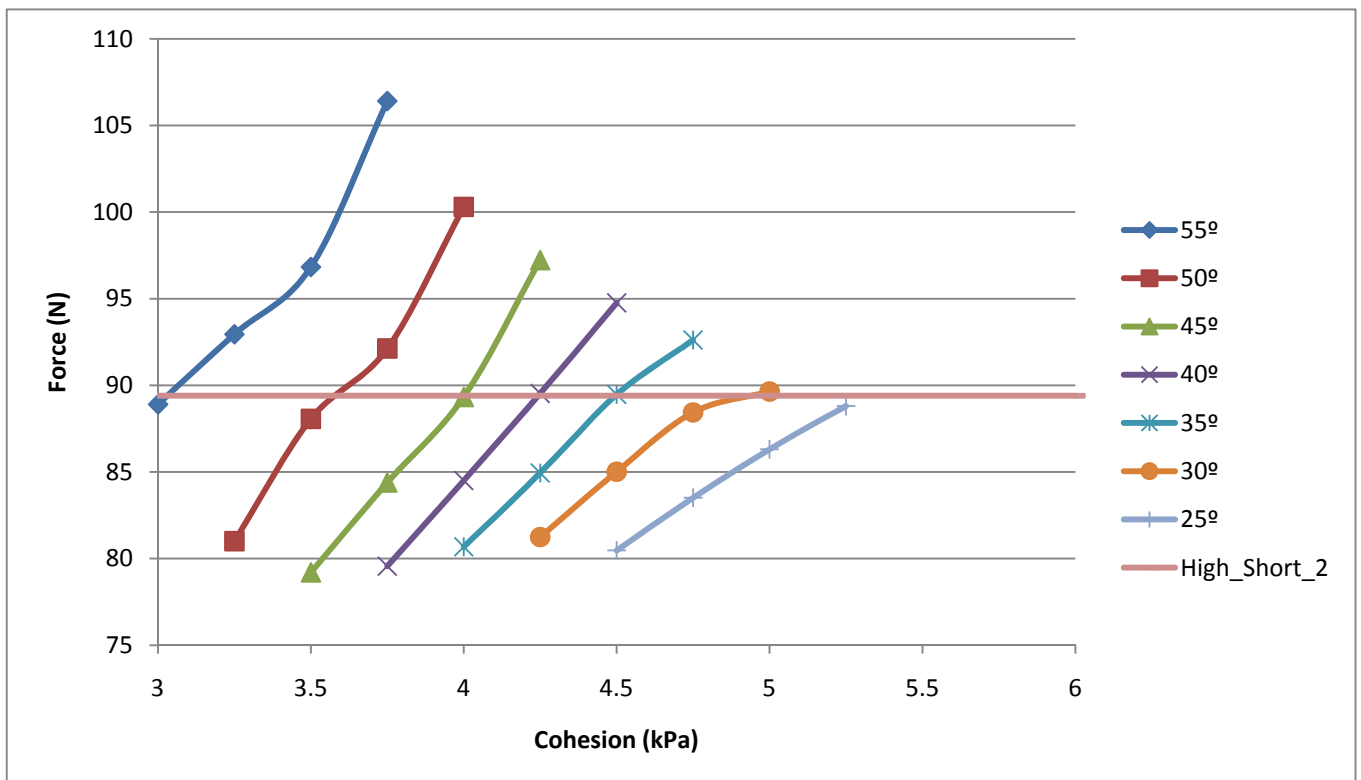


Figure 5.4 - Force at yielding point in High_Short test versus corresponding initial cohesion with different values for the internal friction angle

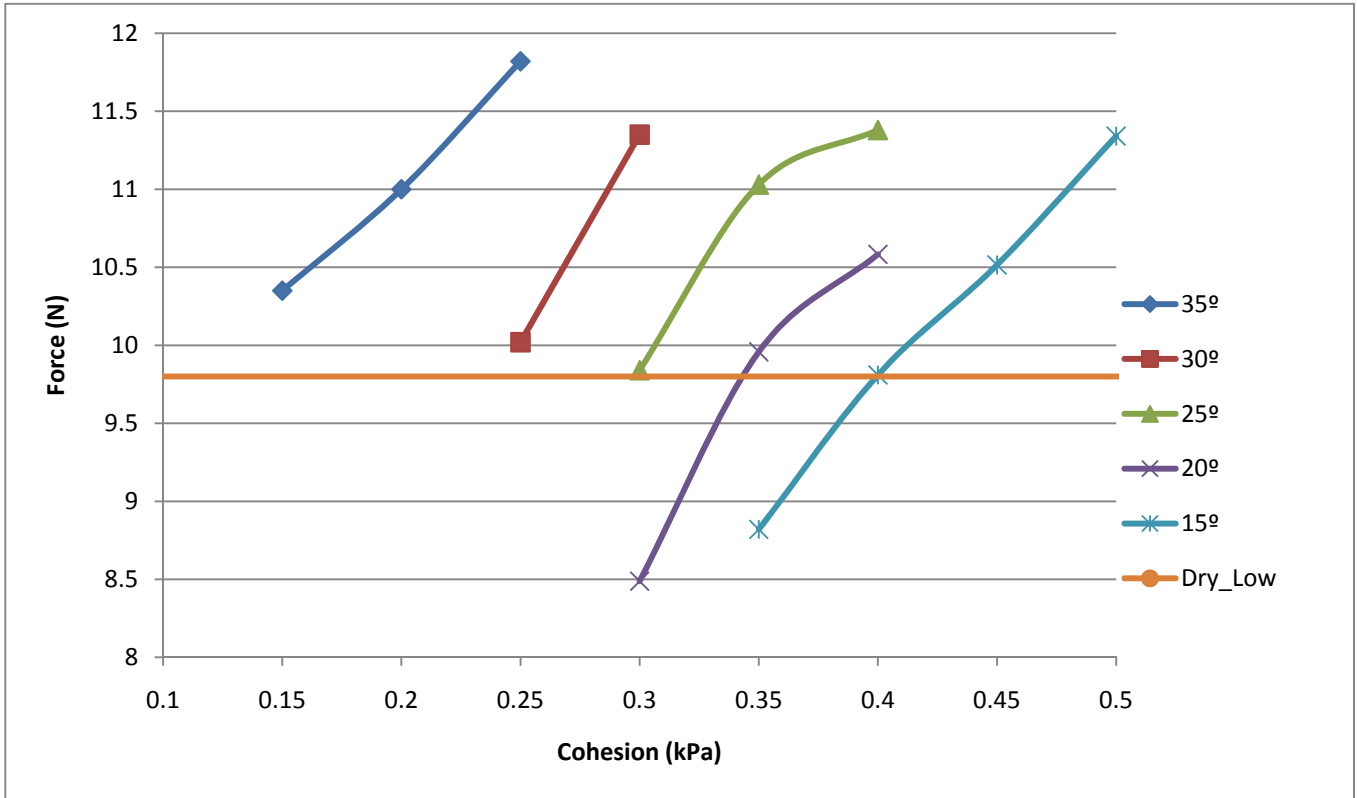


Figure 5.5 - Force at yielding point in Dry_Low test versus corresponding initial cohesion with different values for the internal friction angle

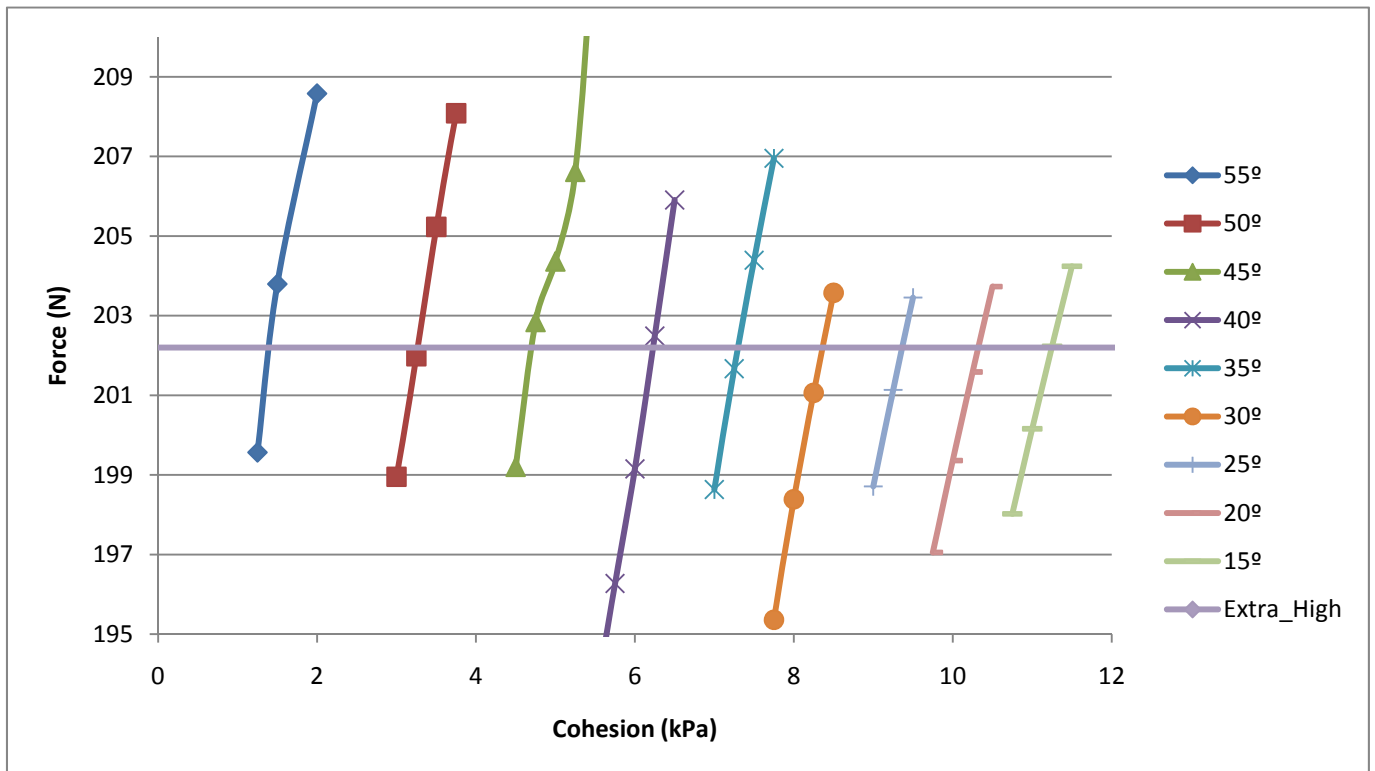


Figure 5.6 - Force at yielding point in Extra_High_Short test versus corresponding initial cohesion with different values for the internal friction angle

The dependency study between cohesion and the friction angle is carried out. All of the six experiment results will be plotted in our figure, which shows the direct relationship between cohesion and the friction angle.

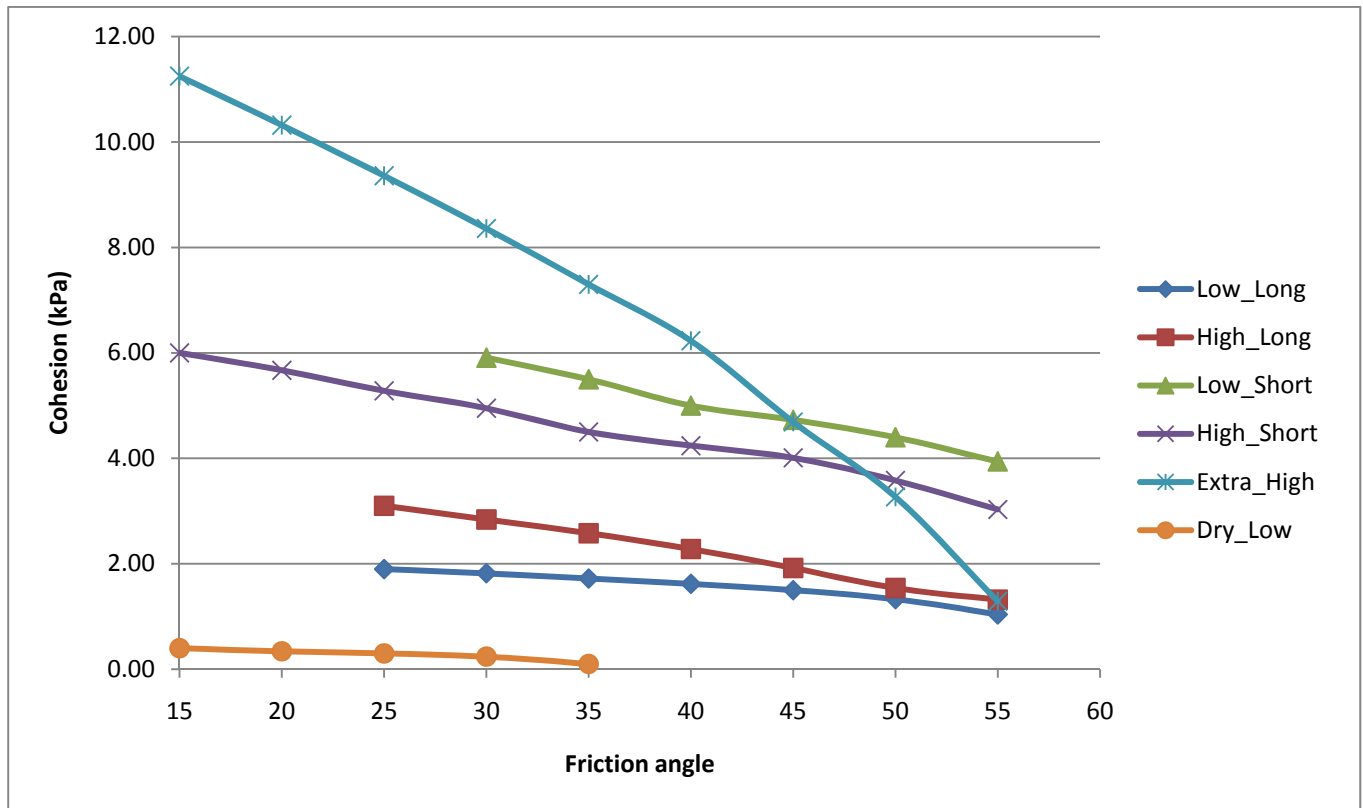


Figure 5.7 - Curve describing possible combination of the corresponding cohesion and friction angle

A form is also given here for convenience with all of the possible combinations of cohesion and friction angle together.

Table 5.1 - Possible combinations of cohesion and friction angle of numerical model for different test in order to fit with experiment data

	Cohesion for Low_Long test (kPa)	Cohesion for High_Long test (kPa)	Cohesion for Low_Short test (kPa)	Cohesion for High_Short test (kPa)	Cohesion for Dry_Low test (kPa)	Cohesion for Extra_High_Short test (kPa)
55°	1.04	1.32	3.94	3.03	1.29	
50°	1.33	1.54	4.4	3.58	3.27	
45°	1.5	1.92	4.73	4.01	4.69	
40°	1.62	2.28	5	4.24	6.23	
35°	1.72	2.58	5.5	4.5	7.30	0.10
30°	1.82	2.84	5.91	4.95	8.36	0.24
25°	1.9	3.1	-	5.28	9.36	0.30
20°				5.67	10.32	0.34
15°				6.00	11.25	0.40

We can see from Figure 5.7 that a linear dependency between cohesion and friction angle is found. The larger friction angle results in lower cohesion to simulate the shear box experiment. Some of the cases gave similar results among themselves, but two different groups are within this figure. The cohesion for short submersion time is almost twice as large as the cohesion for long submersion time, which shows the freeze-bond is stronger for short submersion time than for long submersion time.

Normally the two short or two long time experiment will results in more or less the same cohesion between themselves, since the ice rubble they use is in the same environment, but for Figure 5.7, we can see that the cohesion seems also to be influenced by the normal pressure, large normal pressure will give large cohesion. The might be explained by the unqualified size of RVE in this experiment. During the shear box experiment, a lot of large block assemblies are formed, which might indicate that the shear box size was below the RVE. This part of the deficit of the experiment setup has been discussed in section 3.

5.3 Analysis of the application of cap hardening model

Heinonen (2004) has described the cap hardening model: Since the classical models (MC and DP) in ABAQUS can not model the dilatation correctly, the yield criterion must be modified to take the compaction failure into account. By adding a cap yield surface to the shear criterion, one bounds the yield surface in hydrostatic compression. This cap yield criterion with volumetric hardening controls the dilatation while material fails either by shearing or by compaction.

In section 4.1, we assume that no cap hardening happens during the numerical modelling process, but is this assumption correct or not? This section will pick up some elements from the numerical model. By plotting the p-q figure on the deviatoric plane, one can examine the stress-state of these picked elements and get a deeper understanding on whether a cap model is needed or not.

We have picked up two elements in the model, one is exactly on the shear plane and in front of the moving piston, another is about 200mm away from element one in the horizontal direction. After examining the p-q figure on these two elements in six different test situations, three different categories of the results can be given:

Case 1: The High_Short, High_Low, Low_Short and Low_Long showed the same pattern of p-q figure and here I use High_Long as an example. (Friction angle is 40° , cohesion is 3 kPa and simulation time is 6 seconds)

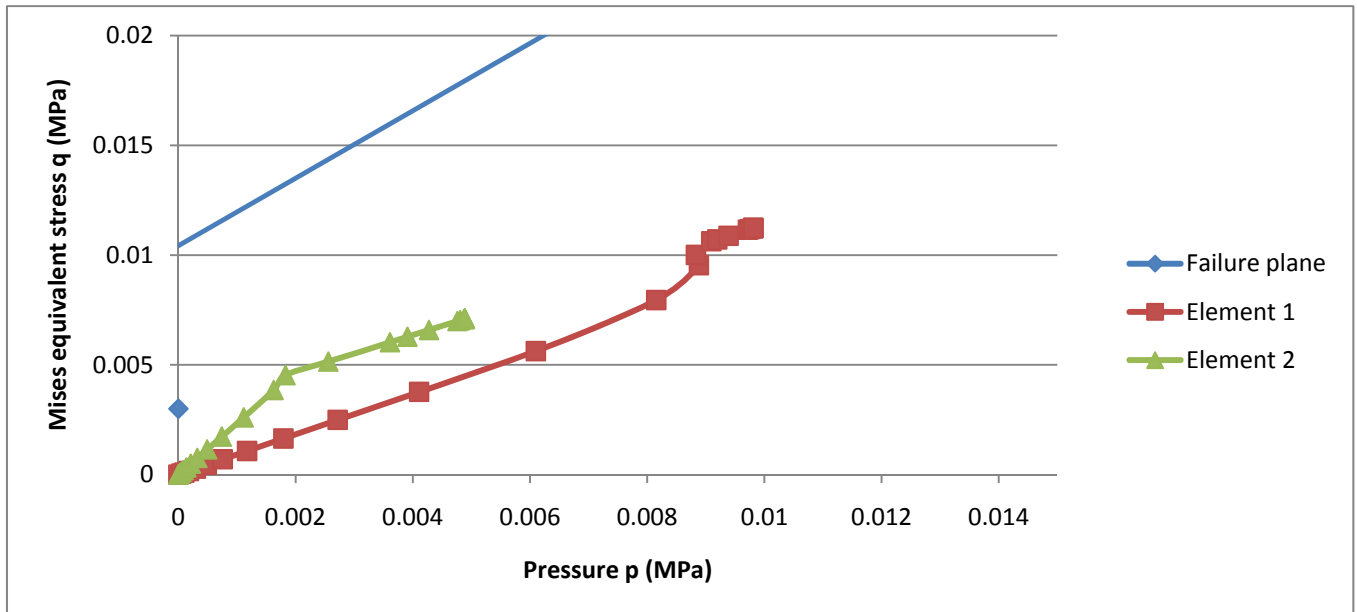


Figure 5.8 – Failure plane and stress state for High_Long test (Simulation time 6 s)

The common character in these four tests can be drawn from Figure 5.8: Both of element 1 and 2 have come to failure at last, but the pressure stress p is much larger for element 1 than for element 2. And the maximum value for the pressure of element 1 is within the range of 10 kPa as for 6 seconds' simulation time. But if we only consider the initial 2 seconds as the primary phase, then the pressure p will be smaller.

Case 2: The Extra_High_Short test (Friction angle is 15° , cohesion is 11.5 kPa and simulation time is 6 seconds)

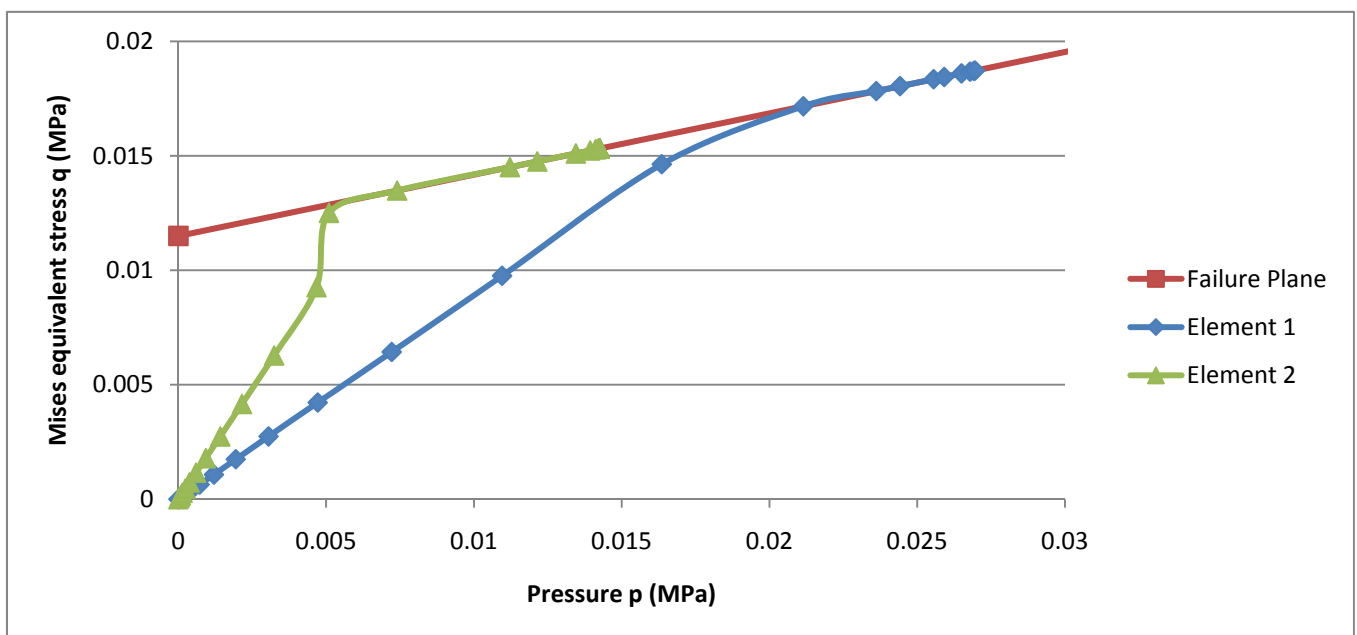


Figure 5.9 - Failure plane and stress state for Extra_High_Short test (Simulation time 6 s)

We can see from Figure 5.9 that although the pressure stress p is still much larger for element 1 than for element 2, the absolute value is much larger at this time than case 1. Here the maximum pressure even reaches 30 kPa for element 1 and 15 kPa for element 2.

Case 3: Dry_Low test (Friction angle is 25° , cohesion is 0.4 kPa and simulation time is 3 seconds)

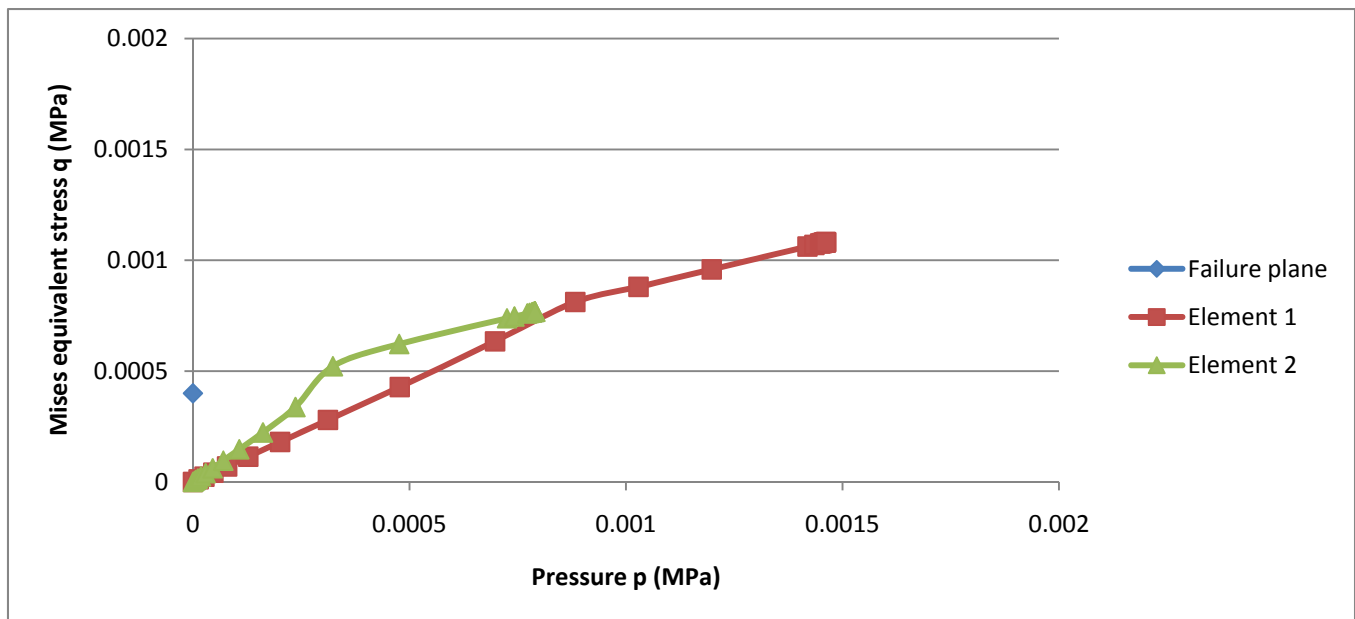


Figure 5.10 - Failure plane and stress state for Dry_Low test (Simulation time 3 s)

We can see from Figure 5.10 that neither of these two elements have been sheared to failure in this case and the pressure stress p is still much larger for element 1 than for element 2. But the maximum pressure in this case is 1.5 kPa for element 1 and 0.8 kPa for element, which is much smaller at this time than case 1 and 2.

So a criteria must be given in order to judge whether cap hardening should be used or not. Serré (2011) has done an oedometer test in order to study the cap hardening law, and the results are summarized in the following table:

Table 5.2 – Cap hardening (Serré, 2011)

Volumetric plastic strain	Hydrostatic yield stress (kPa)
0.05	1.3
0.1	3.8
0.15	7.5
0.2	13.7

Comparing to Serré's results, we can find that in case 1, the element near the shear plane has relative large volumetric plastic strain, while the element away from the shear plane hasn't been influenced a lot by cap hardening. While in case 2, both of the

two elements have gone through large volumetric plastic strain and in case 3, neither of these two elements have large volumetric plastic strain.

So we can conclude that as for High_Long, High_Short, Low_Long and Low_Short tests, the cap hardening only plays an important role in a small range of the ice rubble, particular near the shear plane and moving piston, while the whole behaviour is not dominated by cap hardening. But the cap hardening influence the stress-state of Extra_High_Short test quite a lot, both the element near and away from the shear plane have large volumetric plastic strain, so we can conclude that the present assumption on neglecting cap hardening in the Extra_High_Short test is not appropriate and the finite element model is not suitable for simulating this case. And the Dry_Low test is not influenced by the cap hardening at all, so we can still use the present material model to simulate this case. But in this thesis, we have only considered the primary phase, so if we want to model the secondary and third phase of the shear box experiment, we should consider the cap hardening law in all of these six cases.

5.4 Scaling and comparison with recent studies

The relatively recent studies of Serré (2011) and Heinonen (2004) about experimental and FEM studies of punch tests on ice ridges have been used to compare with the present analysis. Both Serré (2011) and Heinonen (2004) used Drucker-Prager elasto-plastic ABAQUS FE model.

It is important, but difficult to scale the cohesion derived from experiment and numerical modelling to the cohesion of full scale ice rubble. In the paper of Serré (2011), he argued that: the gravity and material forces are major contributors to the rubble action. A combination of Froude and Cauchy scaling then be used for the scaling of the rubble actions and ice mechanical properties. He also assumed that ice ridges can be scaled with the Froude scaling law. Based on this assumption, we can compare the cohesions computed in the present paper with the other two recent studies. The friction angle is chosen to be 50° .

Many differences exist within these three experiment, like the equipment setup, the way the ice rubble is built and data analysis methods, but the biggest difference between them is that the present study uses shear box experiment to model the material properties, while the other two experiments use punch tests. Although the method to study cohesion and friction angle is different, but the results can still be comparable since all of them have used the same material model-Drucker-Prager model and they analysis the same thing, which is shear-bonds among ice rubble. It is also important to mention that the scale from Heinonen (2004) to Serré (2011) relates to the keel depth, whereas the scale between the present shear-box tests and Heinonen's full-scale tests (2004) relates to the block thickness.

Table 5.3 - Comparison between present study and recent study of Drucker-Prager cohesion, for variable scaling parameters. (Full scale (FS) and model scale (MS))

	Scale	h_{kMS} (m)	h_{kFS} (m)	d_{MS} (kPa)	d_{FS} (kPa)
Heinonen (11/1999)	1:1	N/A	6.4	N/A	10
Serré (Ridge 1000)	1:12.8	0.5	6.4	0.6	7.7
Serré (Ridge 2000)	1:16	0.5	6.4	1.5	24
Low_Long	1:10	-	-	1.33	13.3
High_Long	1:10	-	-	1.54	15.4
Low_Short	1:10	-	-	4.4	44
High_Short	1:10	-	-	3.58	35.8

Table 5-3 shows that Low_Long and High_Long experiment have the cohesion which is more or less the same as the full scale model. And the cohesion from the Low_Short and High_Short is larger than all of the previous study, and around 4 times larger than the full scale test of Heinonen (2004). It can be explained that the ice rubble in the present study is newly build for Low_Short and High_Short experiment, which might have strong freeze-bonds which does not exist in the real world. Besides, the full scale ice rubble in Heinonen's study is formed from thinner ice than in the Arctic situation, which tend to produce more rafting in the keel. Another important thing to mention here is that the scale factor between shear box experiments and Heinonen's full-scale data are based on block thickness and not keel depth, so the results are not comparable between Serré's (2011) and this experiment.

So a lot of questions exist nowadays to research on the properties of ice rubble, like how to give a proper description of cohesion and friction angle for freeze-bonds in reality, the different cohesion and friction angle in different positions, the scaling problem and the problem on how to compare experiment data with full scale tests properly.

5.5 Analysis of uncertainties

5.5.1 Experimental uncertainties

The size of RVE is probably the main reason for the uncertainties in the experiment. Since the size of the RVE hasn't met the requirement for modelling, the behaviour of individual ice block may introduce large variations into the global behaviour of the rubble.

The data recording process has also introduced uncertainties into the experiment. Since no information is available about when the piston starts to push the shear box,

we will not know when the force starts to increase, which will especially influence the accuracies of the primary phase, which is only 6 seconds as it is defined. Secondly, the sampling frequency might also influence the experiment, the data has been recorded every one second, sometimes although the maximum force between numerical and experimental modelling is the same, the path of force between every second is not the same anyway. Thirdly, there are three individual tests under the same condition, but the data between each other varies quite a lot, in some cases, the difference is even 10 times between each other. And the experimental data which is used to compare with numerical modelling is chosen from either the average of the three individual tests or from one test which seems to be the most reasonable. So a lot of repetitive tests are needed in order to reduce the uncertainties.

Besides this, the experiment setup might also introduce uncertainties into the results. The shear plane is fixed, thus will bring in the influence of individual ice block. The movement of the piston against the ice rubble might introduce stress concentration and the stress is not uniform across the shear plane. And the concepts that governing the rubble behaviour is still not fully known. All of these above reasons could bring uncertainties into the experiment process.

5.5.2 Numerical modelling uncertainties

The numerical model has made a lot of assumptions which tries to make the model simple, but the problem is that the ice rubble could be quite complicated both in experiment and reality. First of all, the Young Modulus might not be homogeneous and isotropic across the whole sample. Influenced by porosity, salinity, and the internal structure, the Young modulus is rather heterogeneous. Secondly, the influence of rubble height, density, porosity is neglected and given a constant value during numerical modelling, which will also introduce uncertainties. Thirdly, the friction between ice rubble and Plexiglas is not tested during experiment and assumed to be 0.02 in numerical modelling, which can also result in uncertainties. The main uncertainties might be the choice of material model, in this case, we choose one of the simplest case in Drucker-Prager model, which assumes the model to be linear, no dilatation, no cohesion softening and hardening. But after calculating the stress-state for the elements in the finite element model, it is found that the present model is not suitable to simulate the Extra_High_Short test, which is influenced by cap hardening a lot. Last but not the least, the scaling of ice rubble properties is still a matter of research, which brings uncertainty into the results transferring from numerical and experimental modelling to the results of full-scale cases.

5.6 Summary

In this chapter, analysis of numerical results is given, together with the comparison between numerical and experimental modelling. Besides, the deficit of the experimental and numerical model is also given.

Within the interpretation of the numerical simulation of the shear box experiment:

1. A finite element model was built in ABAQUS 6.10-2 and Drucker-Prager material model is applied in order to simulate the freeze-bonds of ice rubble. Three important material parameters are studied, which are Young modulus E , DP model friction angle β and DP model cohesion d and other less important parameters are assumed as constant, which are ice rubble height, ice density, ice porosity, loading velocity, friction cohesion between ice and Plexiglas and no dilatation happens during the numerical modelling.
2. Effects of model dimension, ice rubble properties, boundary conditions and the influence of finite element mesh dependency were studied as well.
3. Three important material parameters in numerical modelling were retrieved by trial and error method to match with experimental results, so a lot of possible pairs of cohesion and friction angle were summarized, but which pair suits more accurately with the freeze-bonds in reality can not be known from the present experiment. And it has shown that the match between experiment and numerical results is acceptable. Both the force when yielding points occur and the simulation time when the yielding points occur can match with each other well.
4. By analysing phase three in the experiment, two possible cohesion angle were given under the case of long and short submersion time conditions. But whether or not this angle calculated in phase 3 of the experiment is the same as the friction angle of freeze-bonds still needs further study.
5. Comparison with two recent studies which research on freeze-bonds properties were made and the scaling problems were also discussed in order to relate the model of experimental and full scale together, so that the results from experimental and finite element modelling could be used to study the freeze-bonds in reality.
6. Cap hardening law was examined and the present assumption of neglecting volumetric plastic strain is not appropriate in the Extra_High_Short test.
7. The uncertainties of the results within both the experimental model and finite element model were suggested.

6. CONCLUSION AND RECOMMENDATION FOR FUTURE WORK

6.1 Conclusions

The freeze-bonds between ice blocks is an important feature of ice rubble and it has given the rubble ice its peculiar aspects in comparison with other geotechnical materials such as sand and gravel. At present, the research about freeze-bonds has met some difficulty. Almost no analytical and numerical method can be used to model freeze-bonds directly. Serré et al. (2011) has carried out a shear box experiment that relate qualitatively the freeze-bonds properties to the rubble deformation behaviour. In the thesis I have analysed this experiment and then built a numerical model that has simulated the shear box experiment for the primary phase. Conclusions are made in experimental testing and numerical simulation respectively in the following sections.

6.1.1 Testing

My main conclusions from analysing the experimental data are:

1. There are high dispersions of the experiment results, and it can be explained that the RVE (representative volume element) is not sufficient large to avoid uncertainties and the behaviour of individual ice block could have determined the force.
2. Serré et al. (2011) has used the theory from Hellmann' paper in 1984 in order to describe the three phases in their own experiment. But the boundary conditions between them are different, Serré et al has used constant normal pressure, while Hellamnn has restricted the volume of ice rubble and the normal pressure is recorded increasing during the experiment. So it seems that Hellamnn's theory can not be borrowed to explain the experiments of Serré et al. (2011).
3. It is doubtful that the data from phase two can be used to model the property of ice-bonds accurately, since large variation of data has shown dramatic influence of individual rubble piece instead of the influence of freeze-bonds. So numerical simulation by using Drucker-Prager model might not be applicable for phase two in this shear box experiment.
4. The friction angle of ice rubble has been found from phase three after analysis and the angle is around 30° for long time submersion tests and 45° for short time submersion tests. But whether or not this angle is equal to the friction angle of freeze-bonds is impossible to determine from the data at present.

6.1.2 Numerical simulations

The main findings of the numerical simulations are:

1. The Drucker-Prager material model can be used at this time to model the primary phase of the shear box experiment.
2. The parameters of ice rubble, ice density, rubble porosity, mesh density and dilatation angle have limited influence on the numerical results, and they can be set as constant throughout the whole numerical modelling process.
3. Young modulus can only determine the slope of the force, while DP model cohesion and friction angle can determine when the yielding points occur and the force when the yield points occur.
4. The deformation of the ice rubble within the shear box and the possible cracks pattern from numerical simulation is more or less the same as what is observed in shear box experiment.
5. The Young modulus which matches the experimental results are 0.9 MPa for 20 hours submersion time, 2 to 4.5 MPa for 0.17 hour submersion time, 0.25 MPa for the non-submersion tests and 3.5 MPa for 0.17 hour submersion test in extra High pressure.
6. The friction angle which matches the experimental varies from 25° to 55° and the corresponding cohesion are different for each situation: 3.0 kPa to 1.3 kPa for long submersion time and 5.3 kPa to 3.0 kPa for short submersion time in high pressure test, 2.0 kPa to 1.0 kPa for long submersion time and 6.0 kPa to 4.0 kPa for short submersion time in low pressure test. The cohesion for the other two particular cases are also analysed and it is found that the cohesion for the non-submersion time test is less than 0.3 kPa in the experiment, while the cohesion for the extra high normal pressure test varies a lot, from 11.25 kPa when cohesion angle is 15° to 1.3 kPa when the cohesion angle is 55°.
7. The present material model is not suitable to simulate the Extra_High_Short test, since in this case, the cap hardening effect has played an important role.
8. It is assumed that ice ridge can be scaled with Froude scaling law. And two recent studies have been compared with the present one. It is found that the cohesion for short submersion time in the present study is around 3 times larger than that in the long submersion time. And it is also found that the rubble cohesion for long submersion time in the present study is more or less the same as the cohesion of full scale model done by Heinonen (2004). And the rubble cohesion for short submersion time in the present study is around 2 times larger than the cohesion from Ridge 2000

(short submersion) in the punch test done by Serré (2011), and 3 to 4 times larger than the full scale model done by Heinonen in 2004.

6.2 Recommendation for future work

The recommendation has covered both analytical and numerical analysis of experimental data from shear box test, the detailed explanation for these pieces of suggestion could be found in the previous chapters.

6.2.1 Recommendation for experiment modelling

In general, two aspects of the present experiment need to be improved: one is to test more necessary parameters, another is to improve the equipment setup in order to avoid some deficits of the present equipment. Here are the recommendations for future work in these two aspects.

1. Young modulus could be measured using Oedometer test, together with the test of friction between ice rubble and shear box.
2. The friction angle of ice rubble could be measured by pile test, which can find the repose angle, critical angle and failure angle respectively in order to provide basic information for the analysis of material parameters.
3. Another two individual tests could also be designed to analysis the influence of friction angle and cohesion. The first one is designed by using Plexiglas blocks with the same size of tested ice rubble, and the same pile tests could be carried out to see what the friction angle is for the Plexiglas blocks and compare the result with the pile test results of ice rubble. The second test is to freeze the Plexiglas, submerge it into water for a while and let the freeze-bonds grow between the Plexiglas blocks and after that, put the Plexiglas blocks into the shear box, carrying out the same shear box experiment as the ice rubble. These two experiments could be used as a group of comparable tests, which can be used to compare with the tests using ice rubble. The results must be interesting and worth researching, since no such tests have been done before using Plexiglas blocks instead of ice block.
4. Studies need be done in order to get better understanding of freeze-bonds process in both natural sea ice and experiment model and also the scaling problem should be a concern for further study, so that the data from natural sea ice and experiment could be comparable and more reliable results can be found in the future.
5. A larger shear box could be used in order to meet the requirement for larger RVE.
6. Another shear box could be designed as it is discussed in section 3.4.3 in order to create multiple possible shear plane to avoid the influence of individual rubble piece.

6.2.2 Recommendation for numerical modelling

A lot of assumptions are used in the numerical modelling in this case and only the primary phase is analysed in this present paper. All of these are the restrictions for the present numerical modelling. Based on this, some recommendations are given:

1. In the present study, we use continuum model, and it is also recommended that discrete model can be used to simulate this shear box experiment again in order to compare with the present continuum model.
2. In the present study, we use Lagrange finite element model to simulate primary phase, and this method could only simulate small displacement, so that the implement is restricted in ice rubble numerical modelling. It is recommended that Phase two and three could be simulated using Eulerian finite element model. Besides this, cohesion softening, non-linear failure model, cap model and dilatation angle could also be considered when modelling phase two and three in the future.
3. A better way to model cracks needs to be found especially when modelling phase two and three in the shear box experiment. At present, how to model cracks is still not totally solved yet, but cracks happen a lot during phase two and three and have dominated the behaviour of ice rubble, so only by finding a good way to model cracks, can one get enough accurate results of numerical modelling for phase two and three.
4. We can see from previous analysis that the data is not easy to analyse because the results have shown a scattered pattern, so the method to study freeze-bonds within ice rubble should be probabilistic instead of deterministic. So more experiment should be done in order to get database which is enough large as the input data.
5. The results in this thesis give a series pairs of cohesion and friction angle in order to match the numerical modelling results with the experimental results, but in reality the friction angle couldn't be in a range from 25° to 55° for example. So further numerical study needs to be done in order to go into details of the mechanism of freeze-bonds failure, so that a particular friction angle and cohesion could be defined as what it is in nature.

REFERENCE

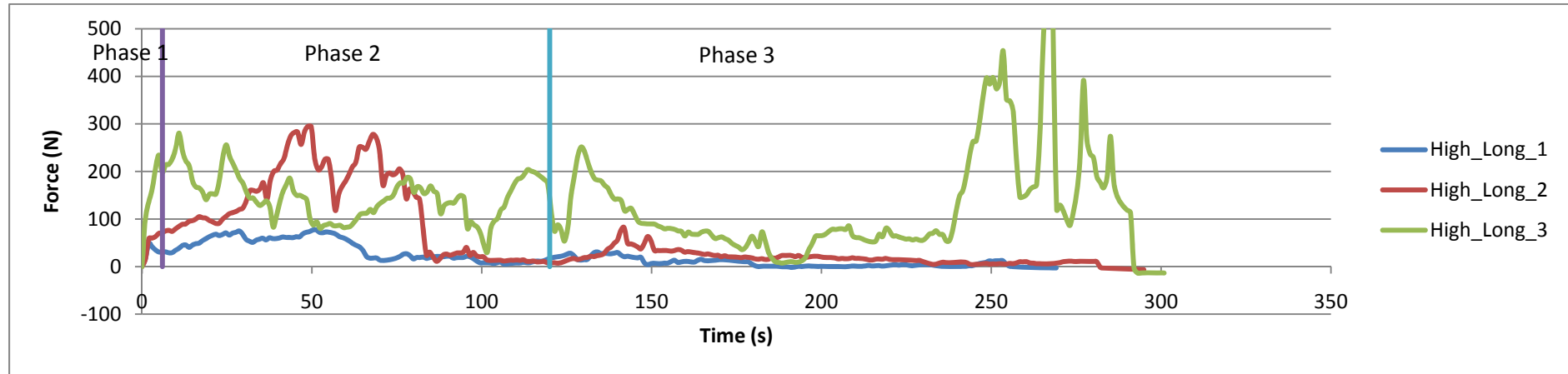
- ABAQUS Documentation for Version 6.10.
- Analysis of geotechnical problems with ABAQUS. 2003. ABAQUS, Inc.
- Heinonen, J., 2004. *Constitutive modelling of ice rubble in first-year ridge keel*. PhD thesis, Helsinki University of Technology.
- Hellmann, H., 1984. Basic investigations of Mush Ice, *Proc. of the 7th International Symposium on Ice (IAHR)*, Hamburg, Germany Vol. 3, pp. 37–55.
- Høyland, K. V., Kjestveit, G., Heinonen, J. and Määttänen, M., 2000. LOLEIF ridge experiments at Marjaniemi; The size and strength of the consolidated layer. *Proc. Of the 15th International Symposium on Ice (IAHR)*, Gdansk, Poland, pp. 45-52.
- Høyland, K. V., 2002. The consolidation of first-year sea ice ridges. *Journal of Geophysical Research*, Vol. 107, No. C6.
- Høyland, K. V., 2007. Morphology and small scale strength of ridges in the North-western Barents Sea. *Cold Regions Science and Technology*, Vol. 48, issue 3, pp 169-187.
- Høyland, K. V., 2010. Thermal aspects of model basin ridges. *Proc. of the 20th International Symposium on Ice*, Lahti, Finland.
- ISO/FDIS 19906, 2010. *Petroleum and natural gas industries - Arctic offshore structures, ISO TC 67/SC 7*. Final Draft International Standard, International Standardization organization, Geneva, Switzerland, pp. 443.
- Jensen, A., Løset, S., Høyland, K. V., Liferov, P., Heinonen, J., Evers, K. U. and Maattanen, M., 2001. Physical modelling of first-year sea ice ridges-part II: mechanical properties. *The 16th International Conference on Port and Ocean Engineering under Arctic Conditions (POAC)*, Ottawa, Canada, vol. 3, pp. 1493–1502.
- Kankaanpää, P., 1998. *Distribution, morphology and structure of sea ice pressure ridges in the Baltic Sea*. PhD thesis, Department of Geography, University of Helsinki, Fennia, Helsinki, pp. 101.
- Lemaitre, J. and Chaboche, J. L., 1990. *Mechanics of Solid Materials*. Cambridge University Press, Cambridge, UK.
- Liferov, P. and Bonnemaire, B., 2005. Ice rubble behaviour and strength: Part I. Review of testing and interpretation of results. *Cold Regions Science and*

- Technology*, Vol. 41, issue 2, pp. 135-151.
- Liferov, P., 2005. Ice rubble behaviour and strength: Part II. Modelling. *Cold Regions Science and Technology*, Vol. 41, issue 2, pp 153-163.
- NASA Earth Observatory, 2009. <http://earthobservatory.nasa.gov/Features/SeaIce/>
- F. Nimmo, 2004. *What is the Young's Modulus of ice?* Department of Earth and Space Sciences, University of California Los Angeles, USA.
- Prodanovic, A., 1979. Model tests of ice rubble strength. *Proc. of the 5th International Conference on Port and Ocean Engineering under Arctic Conditions (POAC)*, Trondheim, Norway, Vol. 1, pp. 89-105.
- Repetto-Llamazares, A. H. V., Serré, N. and Høyland, K. V., 2011a. Experimental studies on 2D rubble failure Part II: Freeze-bond experiments and comparison with numerical simulations. *Proceedings of the 21st International Conference on Port and Ocean Engineering under Arctic Conditions (POAC)*, Montréal, Canada.
- Repetto-Llamazares, A. H. V., Høyland, K. V. and Evers, K-U., 2011b. Experimental studies on shear failure of freeze-bonds in saline ice Part I: Set-up, Failure Mode and Freeze-bond Strength. *Cold Regions Science and Technology*, Vol. 65, pp. 286-297
- Repetto-Llamazares, A. H. V., Høyland, K. V. and Kim, E. 2011c. Experimental studies on shear failure of freeze-bonds in saline ice Part II: Ice-ice friction after failure and failure energy. *Cold Regions Science and Technology*, Vol. 65, pp. 297-307
- Sanderson T. J. O., 1988. *Ice Mechanics, Risks to Offshore Structure*. BP Petroleum Development Ltd, London. Graham and Trotman Limited, London, pp. 253.
- Sayed, M., Timco, G. W. and Sun, L., 1992. Testing model ice rubble under proportional strains, OMAE, Vol 4, *Arctic Technology*, 1992, pp. 335-341.
- Serré, N., Repetto-Llamazares, A. H. V. and Høyland, K. V., 2011. Experiments on freeze-bonds and rubble strength Part I: Shear box experiments. *Proceedings of the 21st International Conference on Port and Ocean Engineering under Arctic Conditions (POAC)*, Montréal, Canada.
- Serré, N., 2011. Mechanical properties of model ice ridge keels. *Cold Regions Science and Technology*, doi:10.1016/j.coldregions.2011.02.011
- Shafrova, S., 2007. Initial failure of the ice rubble in plane strain direct shear tests. *Proceedings of the 19th International Conference on Port and Ocean Engineering under Arctic conditions (POAC)*, Dalian, China, Vol. 1, pp.

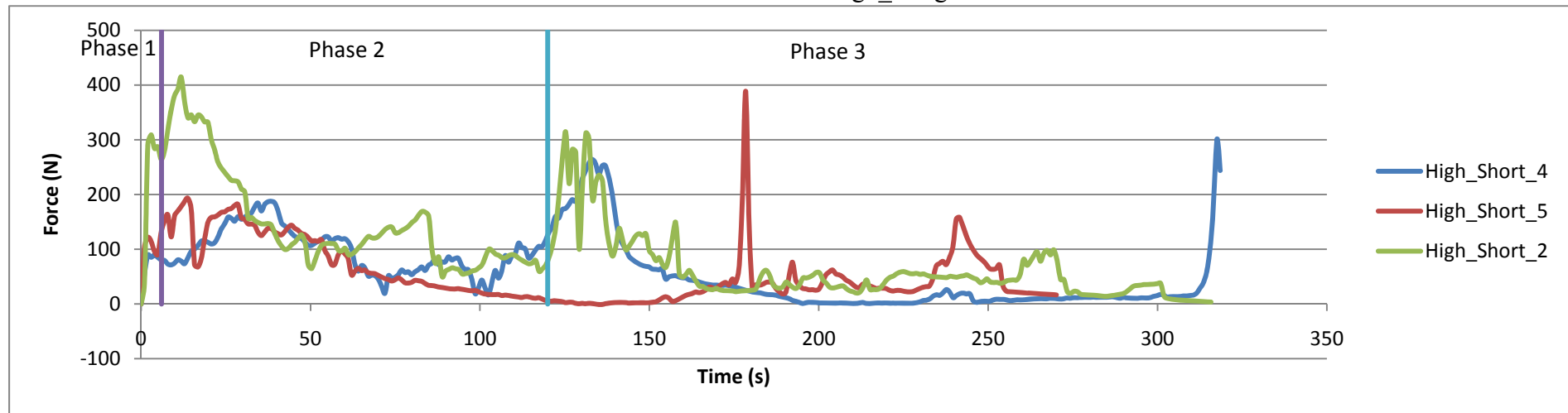
256-266.

- Timco, G. W. and Burden, R. P., 1997. An analysis of the shapes of sea ice ridges. *Cold Regions Science and Technology*, Vol. 25, issue 1, pp. 65-77.
- Timco, G.W., and Cornett, A.M., 1999. Is ϕ a constant for broken ice rubble? *Proc. of the 10th Workshop on River Ice Management with a Changing Climate*, Winnipeg, Manitoba, Canada, pp. 318–331.
- Urroz, G.E. and Ettema, R., 1987. Simple shear box experiments with floating ice rubble. *Cold Regions Science and Technology*, Vol. 14, issue 2, pp. 185–199.
- Urroz, G.E. and Ettema, R., 1989. On internal friction and cohesion in unconsolidated ice rubble. *Cold Regions Science and Technology*, Vol. 16, issue 3, pp. 237-247.
- Urroz, G.E. and Ettema, R., 1991. Friction and cohesion in ice rubble reviewed. *Proceedings of the 6th International Speciality Conference Cold Regions Engineering*, Hanover, USA, pp. 316-325.
- Weiss, R. T., Prodanovic, A. and Wood, K. N., 1981. Determination of ice rubble shear properties, *Proc. of the International Symposium on Ice (IAHR)*, Quebec, Canada, Vol. 2, pp. 860-872.
- Yasunaga, Y., Kioka, S., Matsuo, Y. and Saeki, H., 2001. Tests on strength of consolidated parts of Hummock ice model. *The 16th International Conference on Port and Ocean Engineering under Arctic Conditions (POAC)*, Ottawa, Canada, pp. 1503-1511.

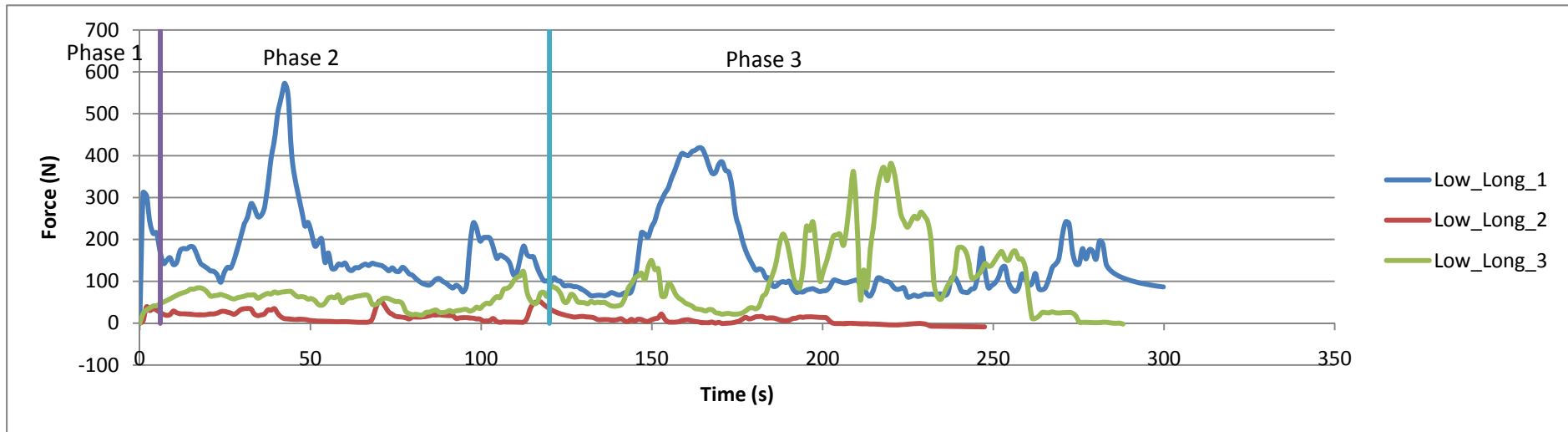
Appendix 1: The force-time series of the 14 tests



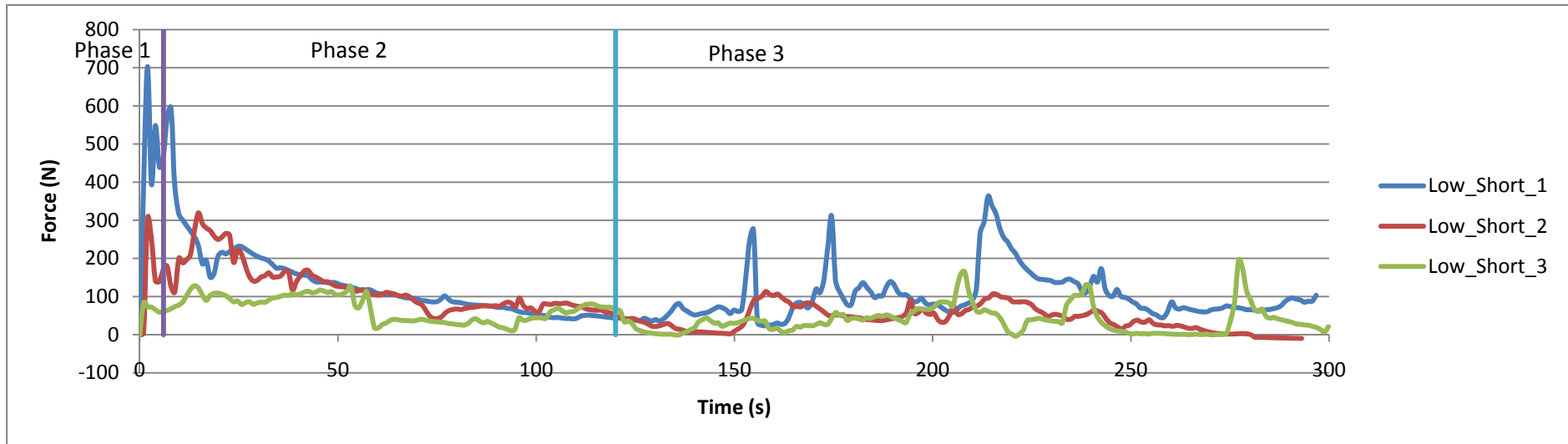
A1: Force-time series for High_Long tests



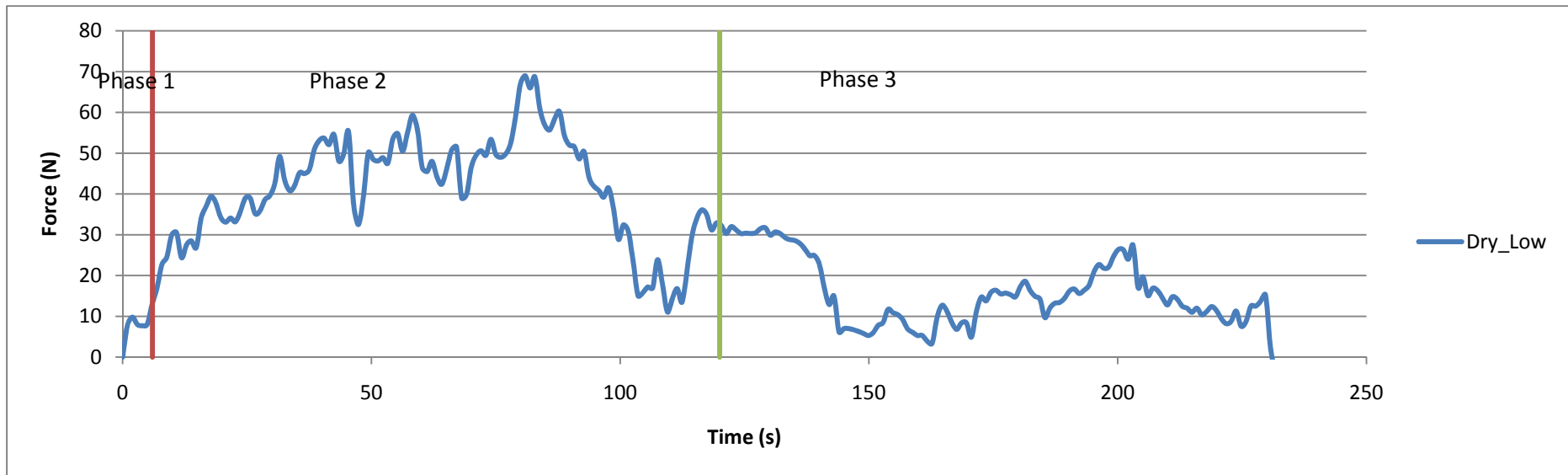
A2: Force-time series for High_Short tests



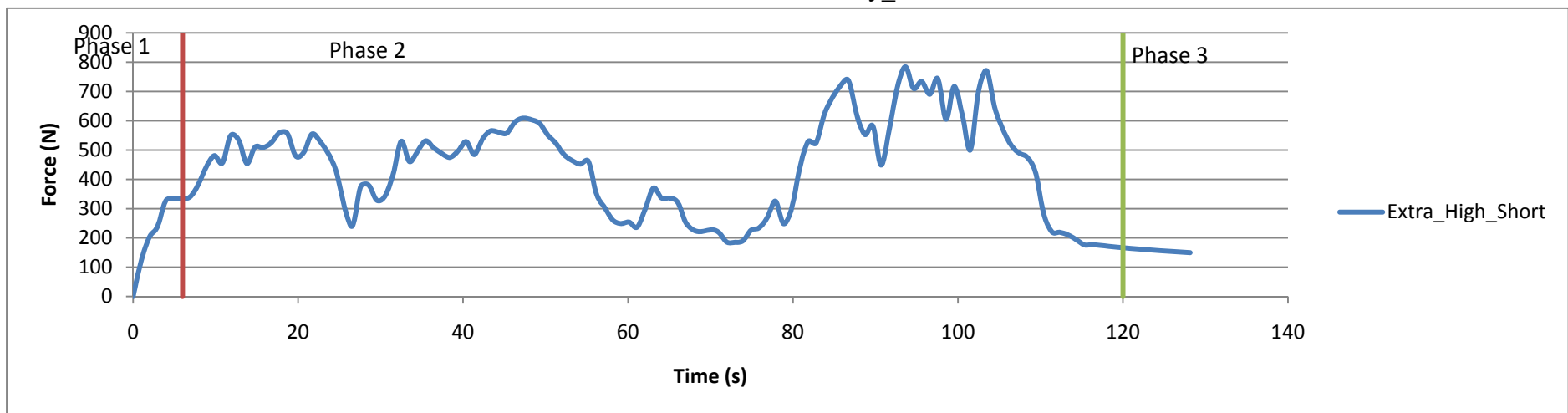
A3: Force-time series for Low_Long tests



A4: Force-time series for Low_Short tests

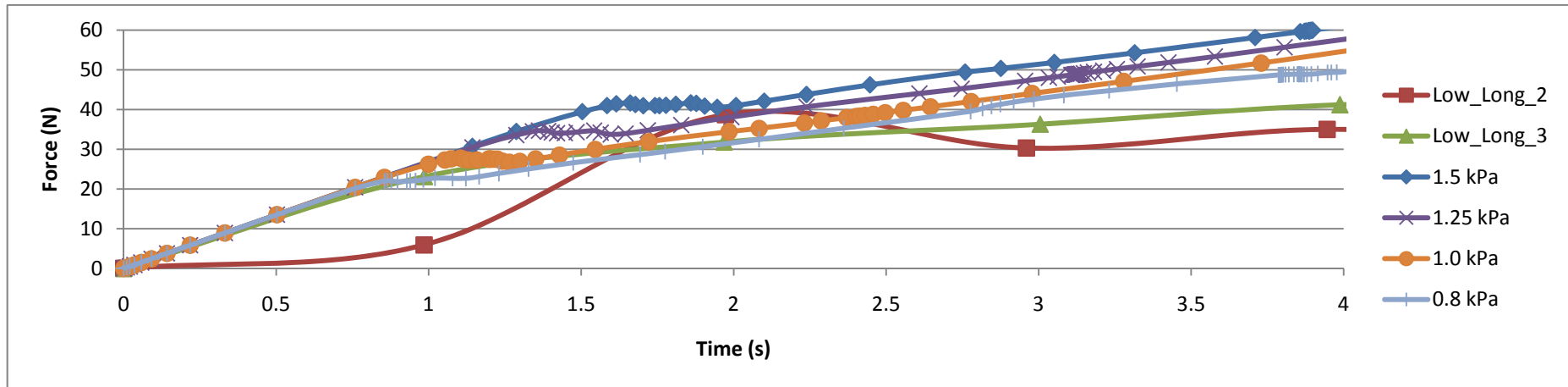


A5: Force-time series for Dry_Low tests

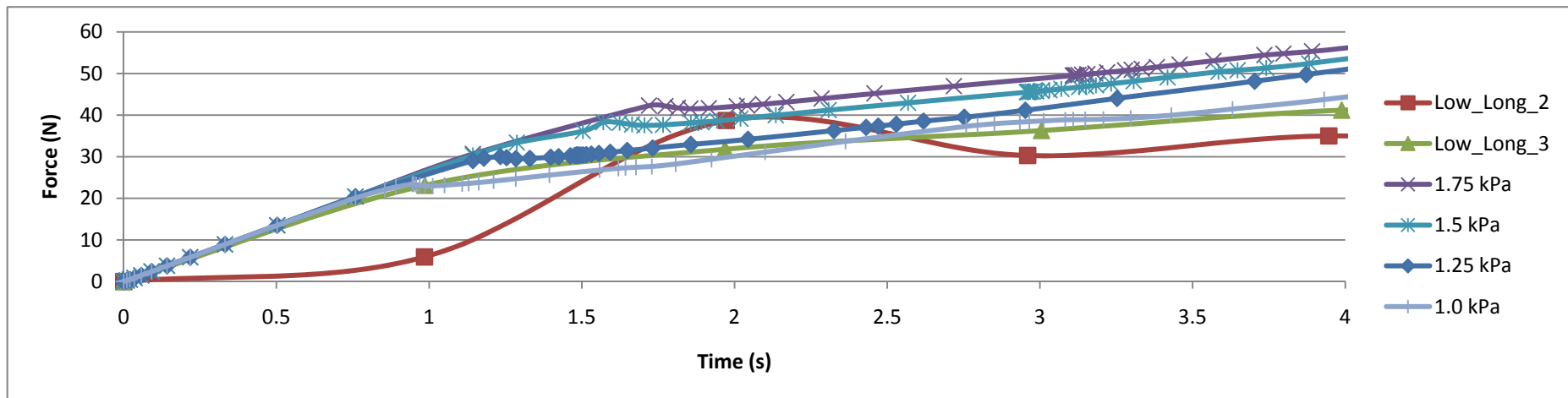


A6: Force-time series for Extra_High_Short tests

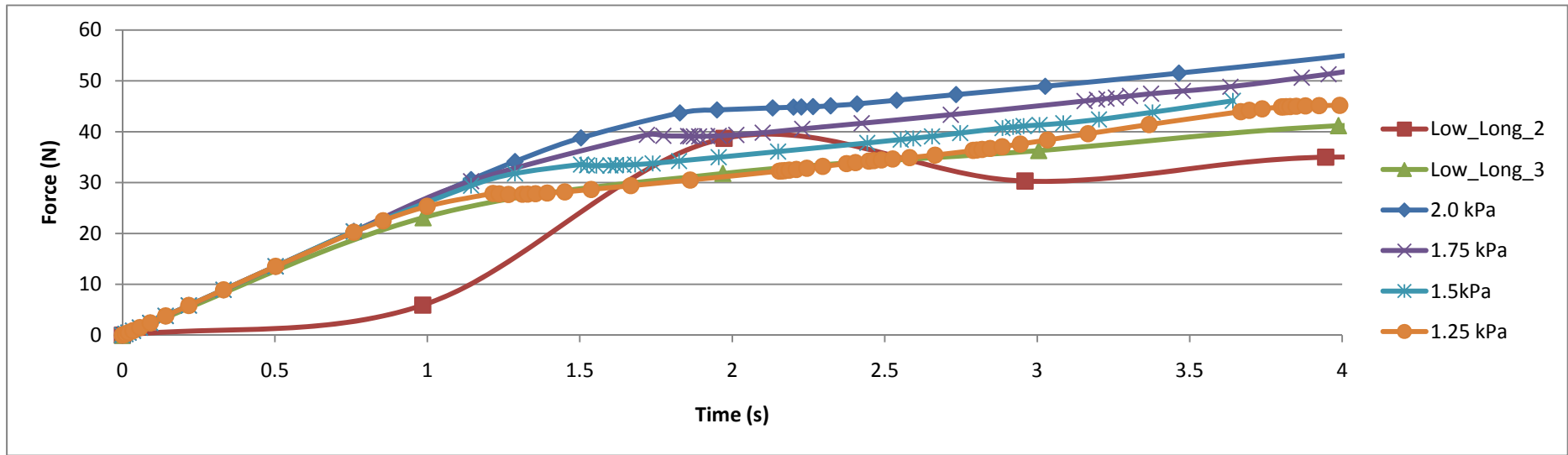
Appendix 2: Results of numerical simulation



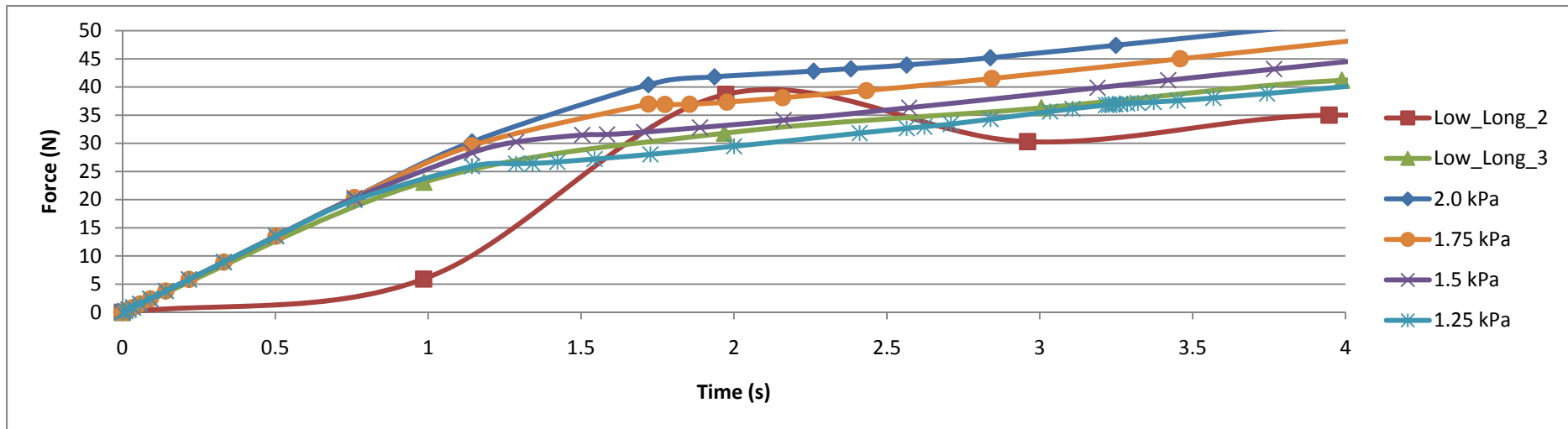
A7: Load-time curves in Test Low_Long with different cohesion when $\beta = 55^\circ$



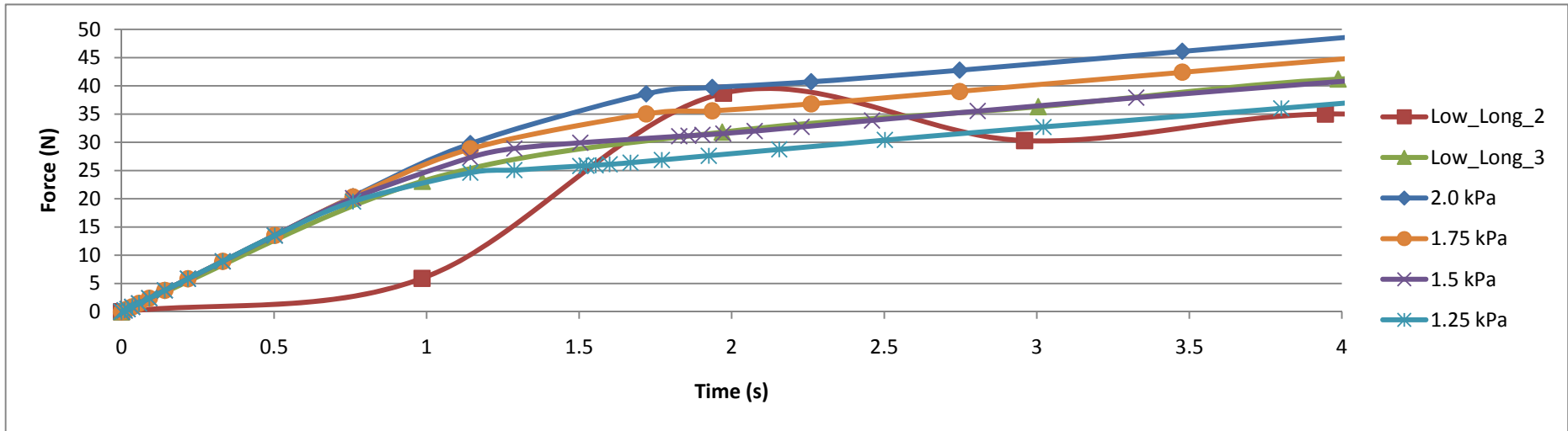
A8: Load-time curves in Test Low_Long with different cohesion when $\beta = 50^\circ$



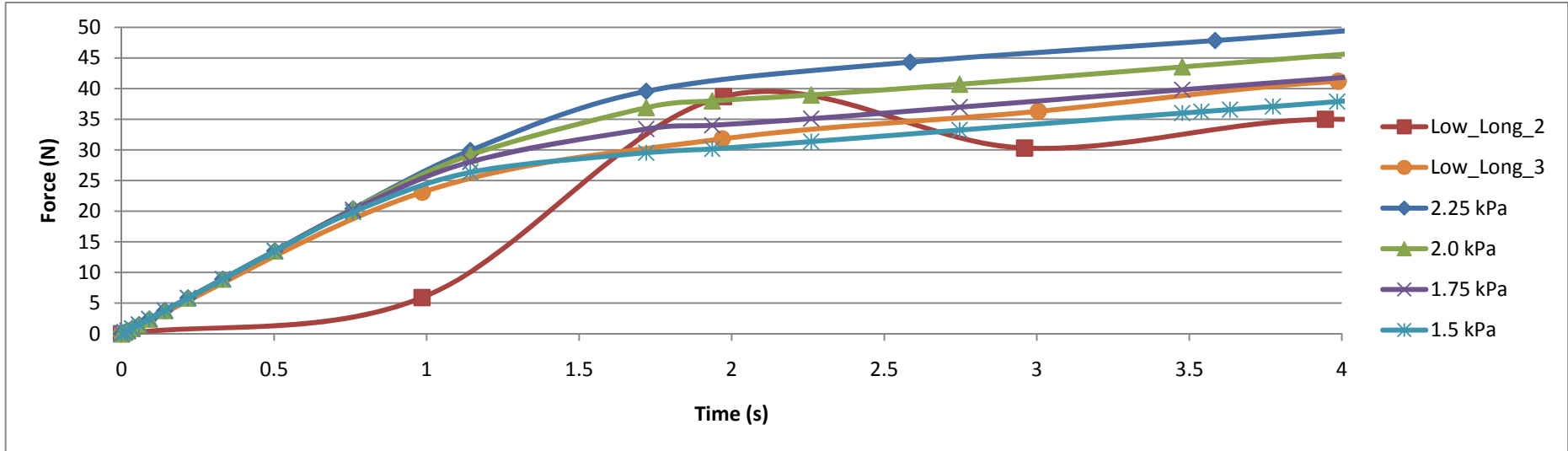
A9: Load-time curves in Test Low_Long with different cohesion when $\beta = 45^\circ$



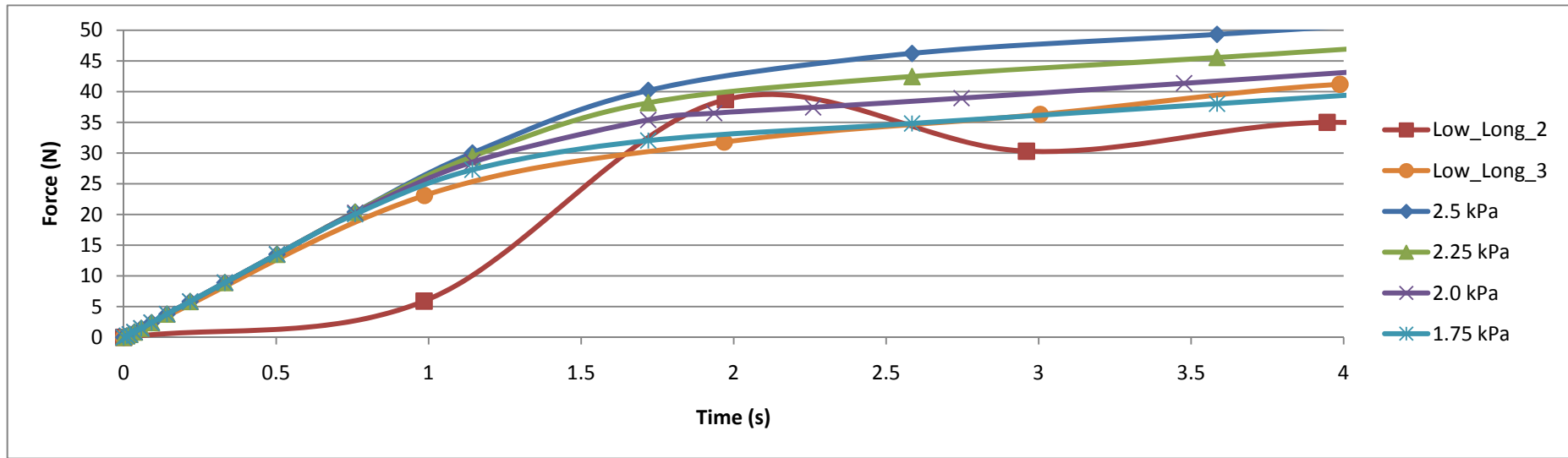
A10: Load-time curves in Test Low_Long with different cohesion when $\beta = 40^\circ$



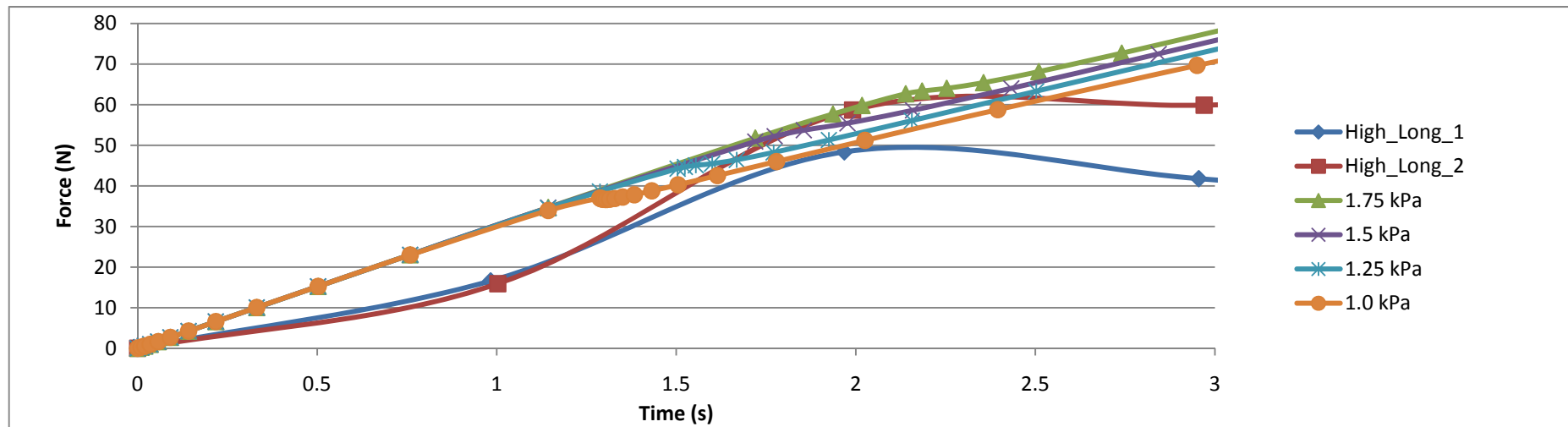
A11: Load-time curves in Test Low_Long with different cohesion when $\beta = 35^\circ$



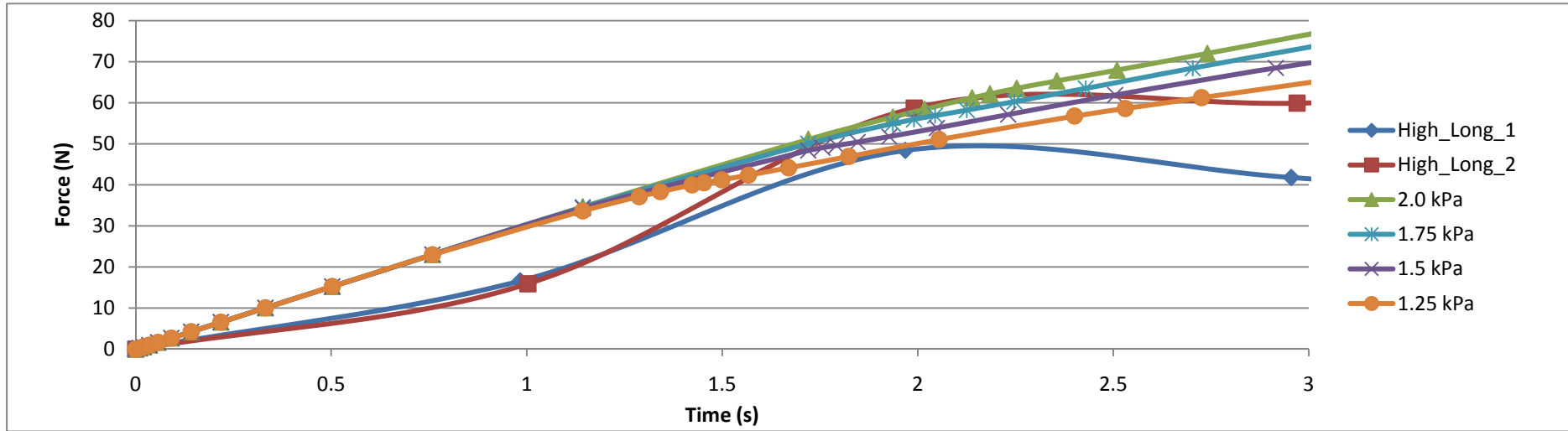
A12: Load-time curves in Test Low_Long with different cohesion when $\beta = 30^\circ$



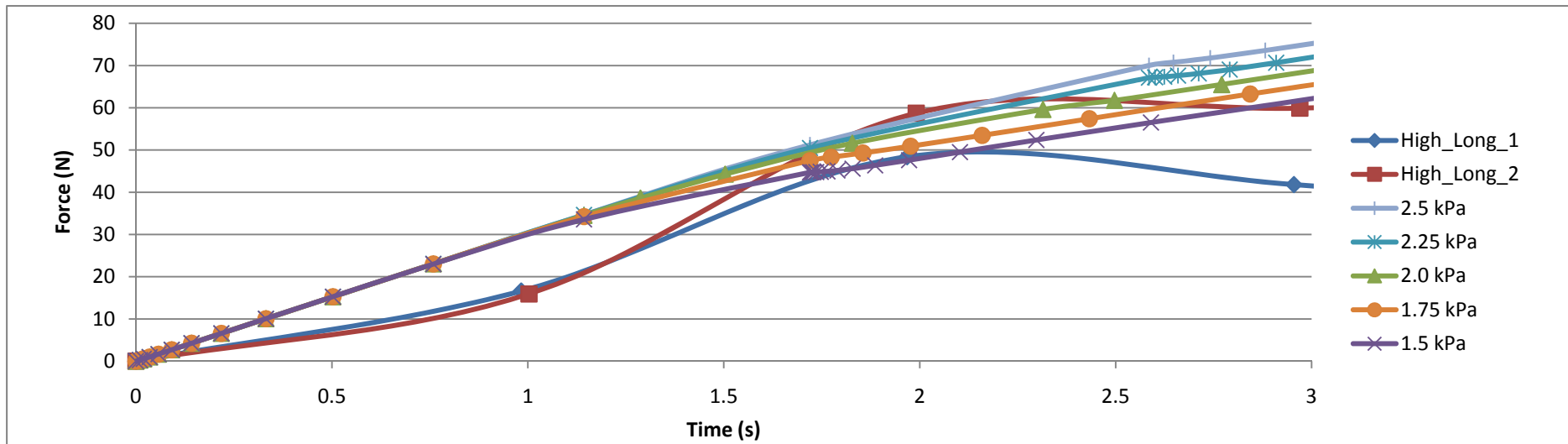
A13: Load-time curves in Test Low_Long with different cohesion when $\beta = 25^\circ$



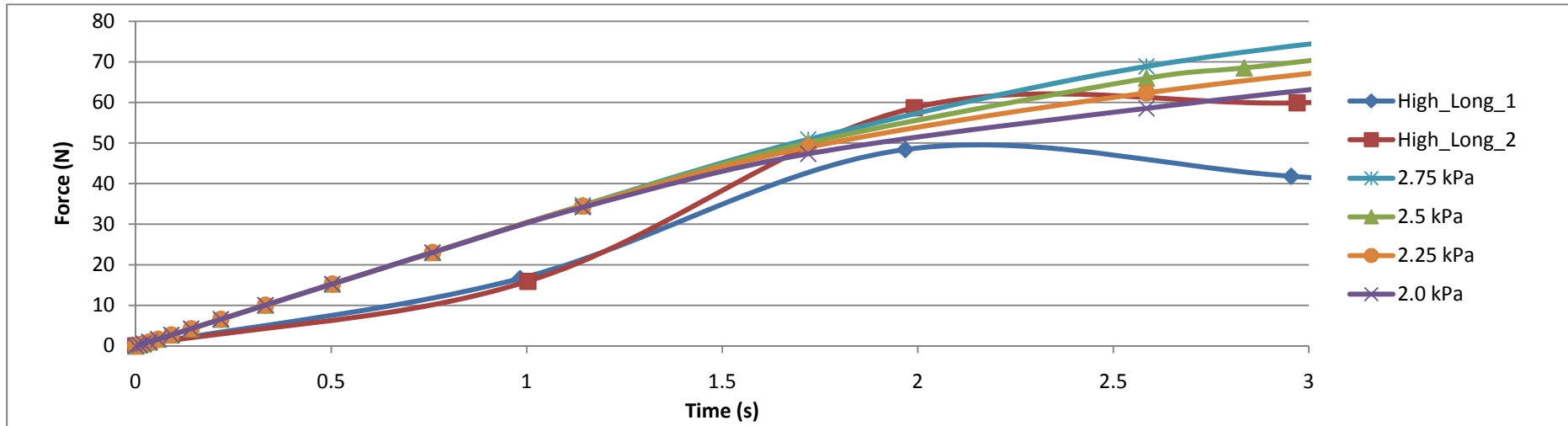
A14: Load-time curves in Test High_Long with different cohesion when $\beta = 55^\circ$



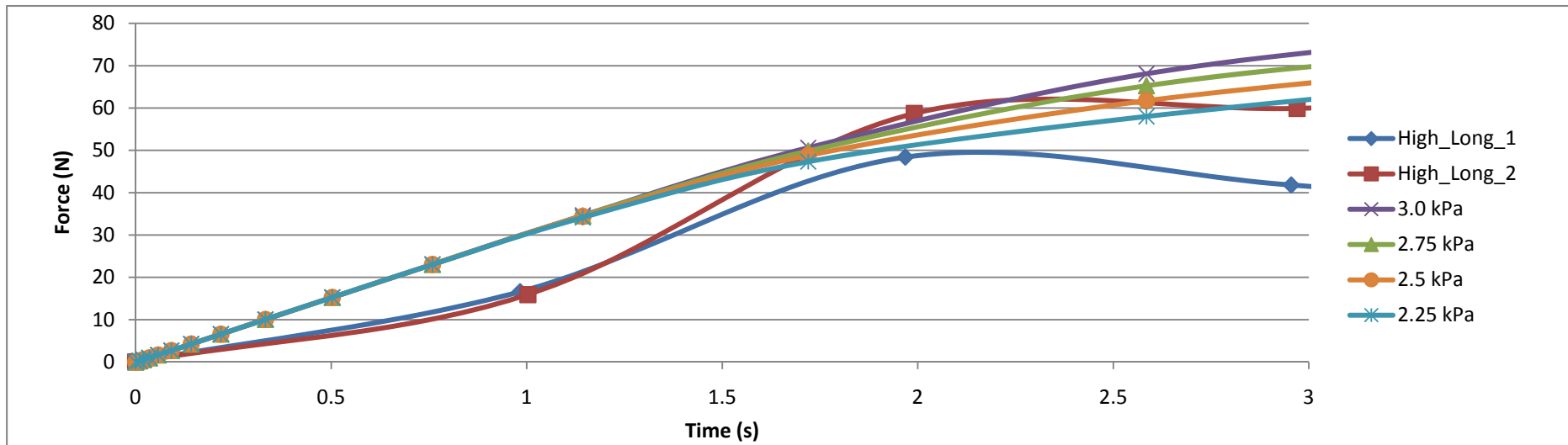
A15: Load-time curves in Test High_Long with different cohesion when $\beta = 50^\circ$



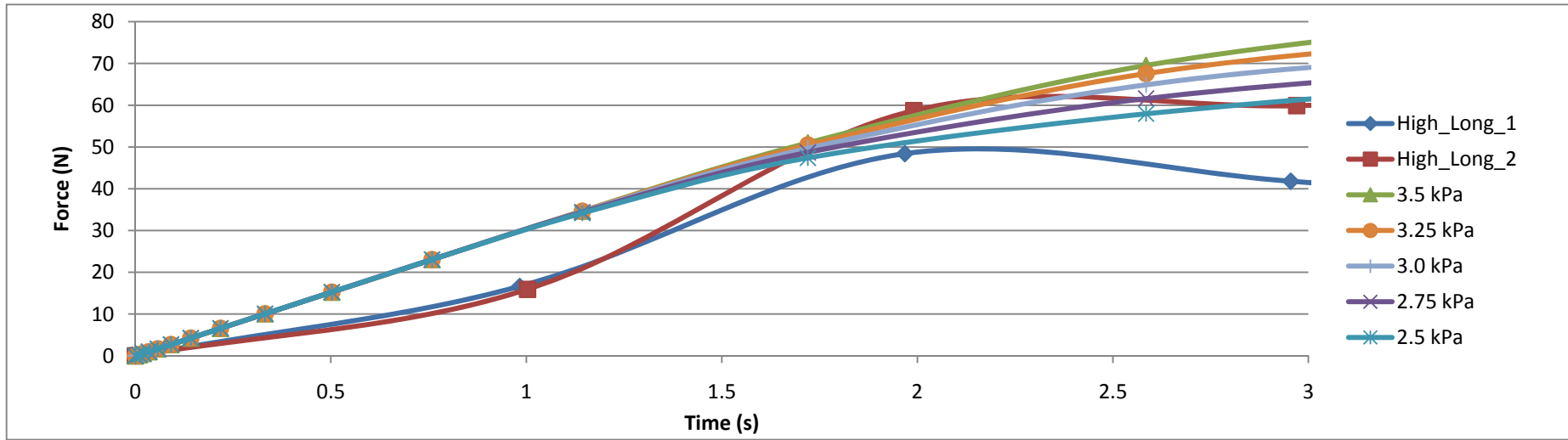
A16: Load-time curves in Test High_Long with different cohesion when $\beta = 45^\circ$



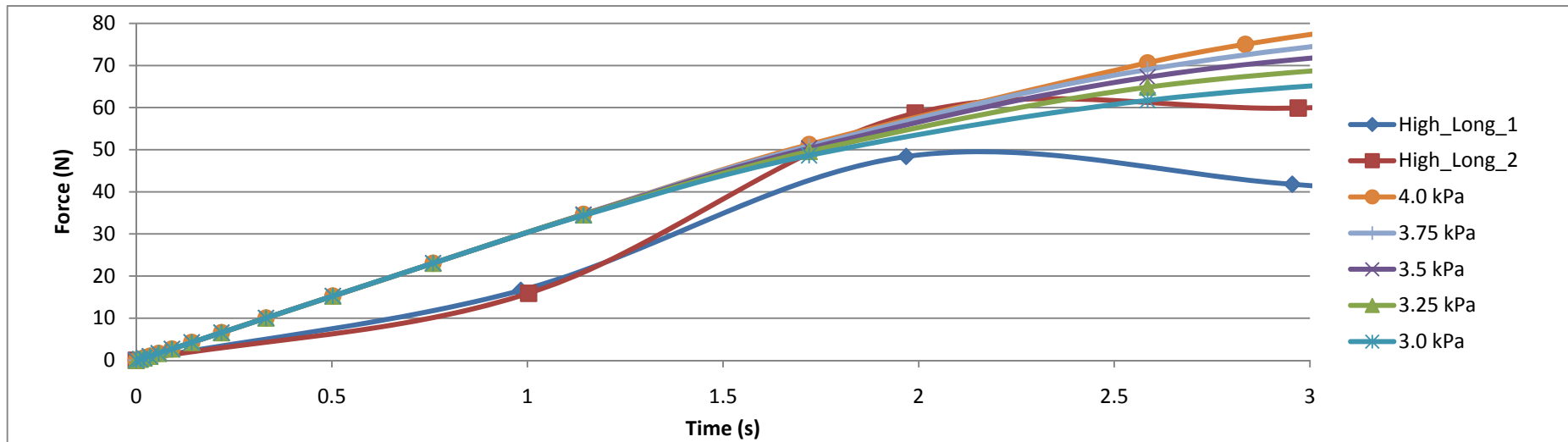
A17: Load-time curves in Test High_Long with different cohesion when $\beta = 40^\circ$



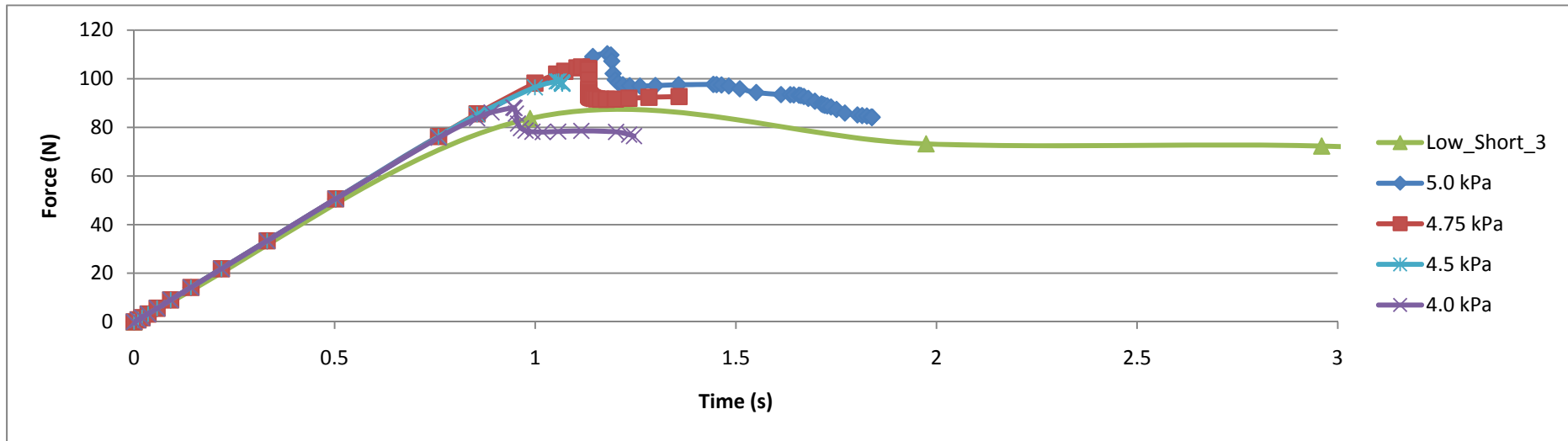
A18: Load-time curves in Test High_Long with different cohesion when $\beta = 35^\circ$



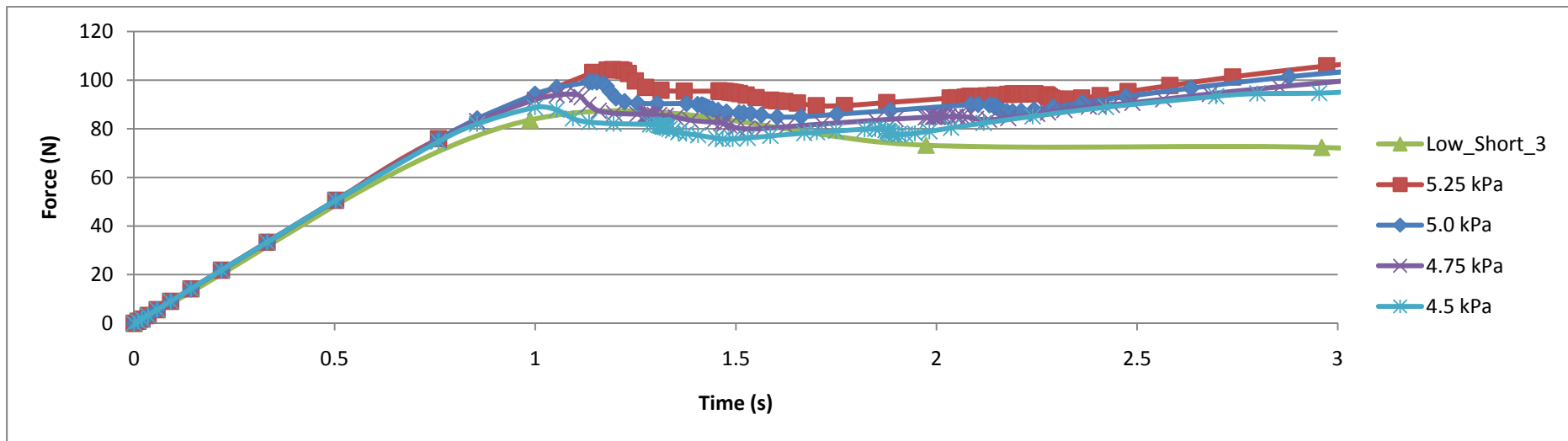
A19: Load-time curves in Test High_Long with different cohesion when $\beta = 30^\circ$



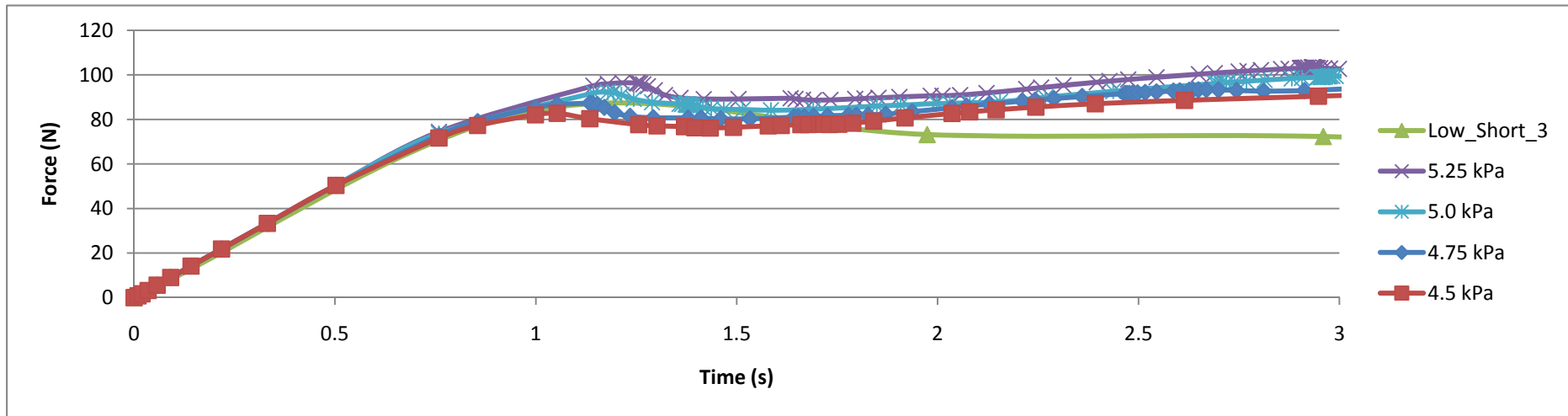
A20: Load-time curves in Test High_Long with different cohesion when $\beta = 25^\circ$



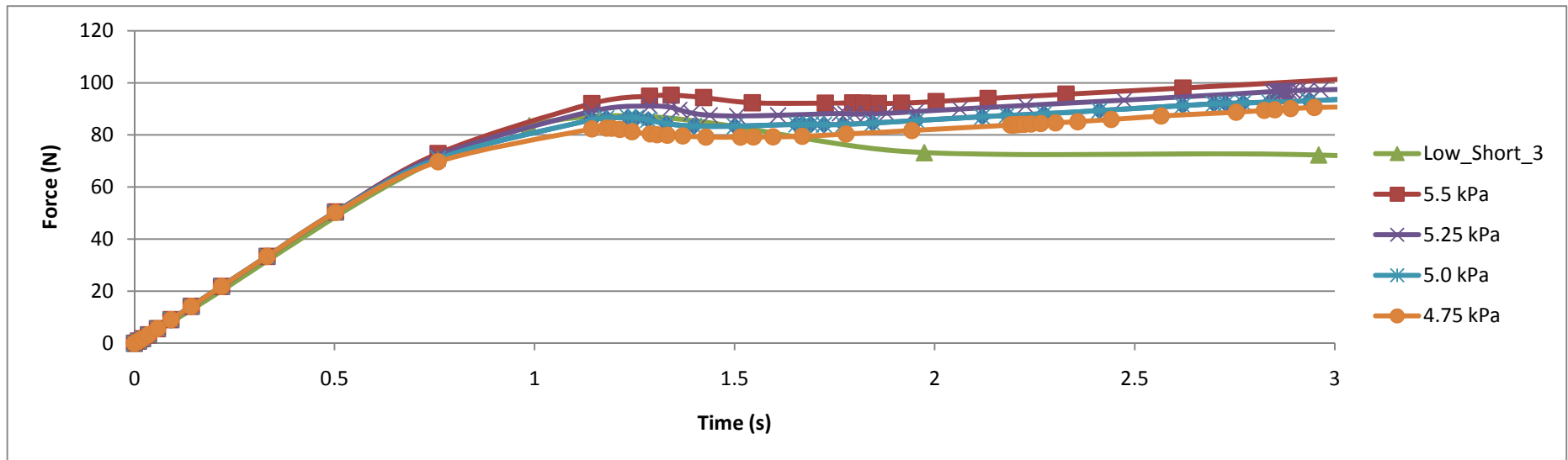
A21: Load-time curves in Test Low_Short with different cohesion when $\beta = 55^\circ$



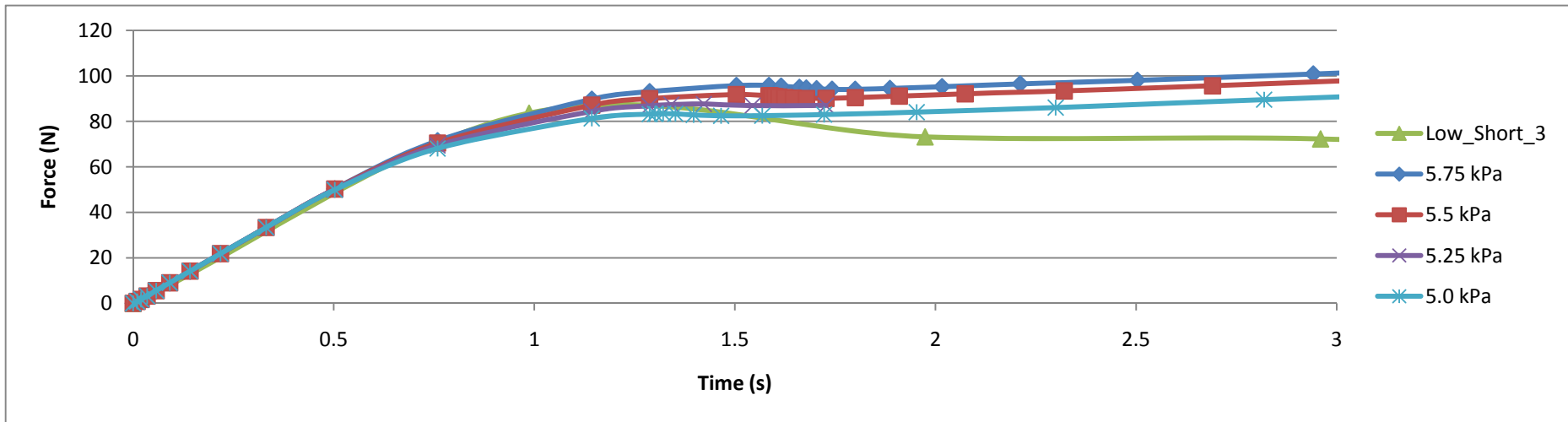
A22: Load-time curves in Test Low_Short with different cohesion when $\beta = 50^\circ$



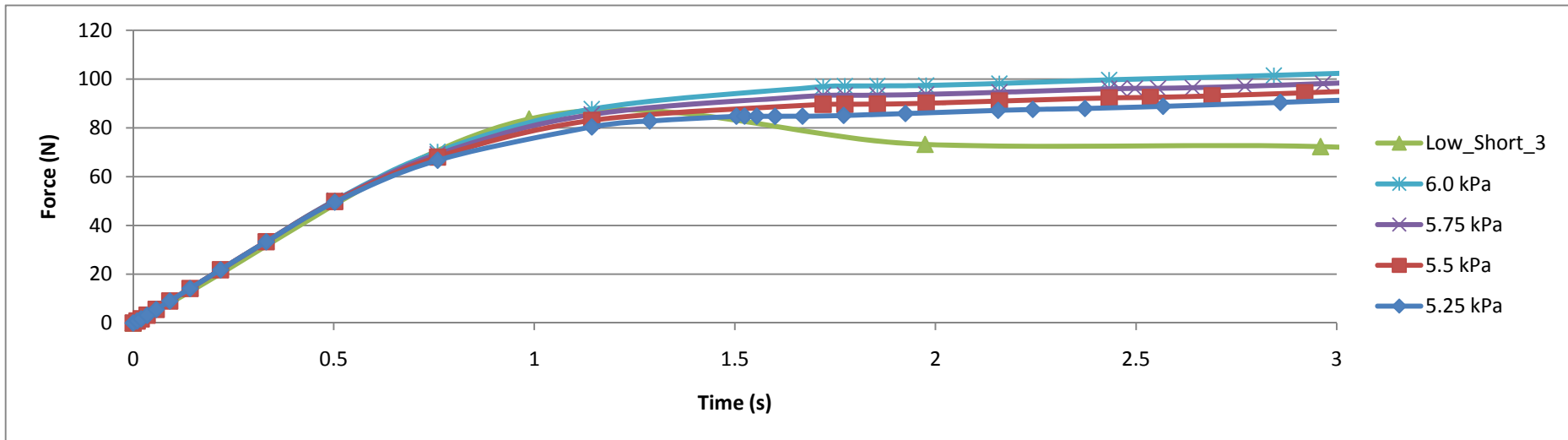
A23: Load-time curves in Test Low_Short with different cohesion when $\beta = 45^\circ$



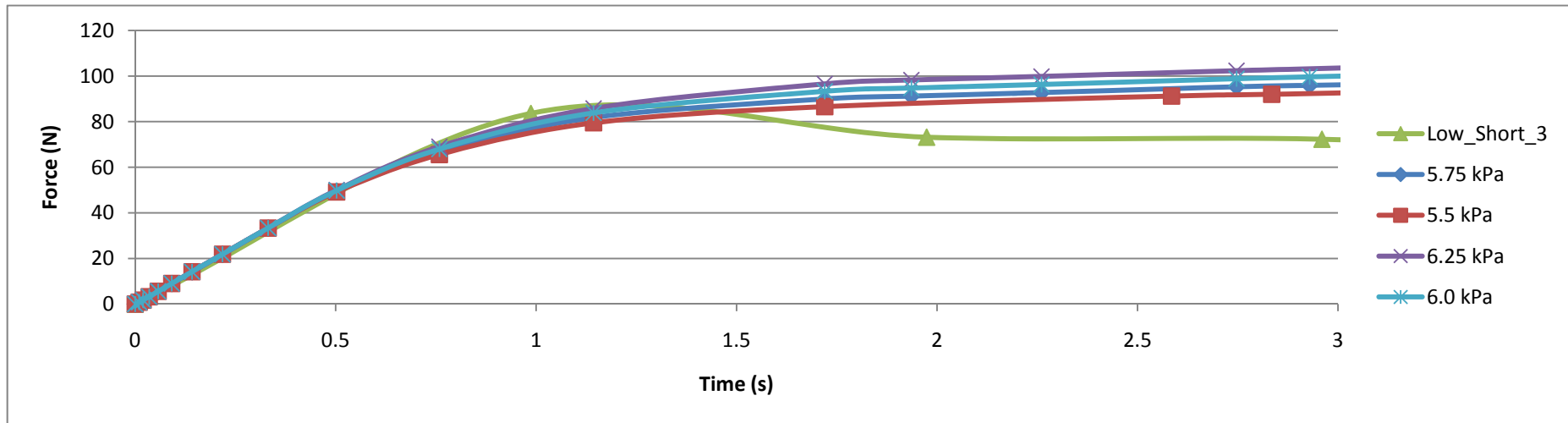
A24: Load-time curves in Test Low_Short with different cohesion when $\beta = 40^\circ$



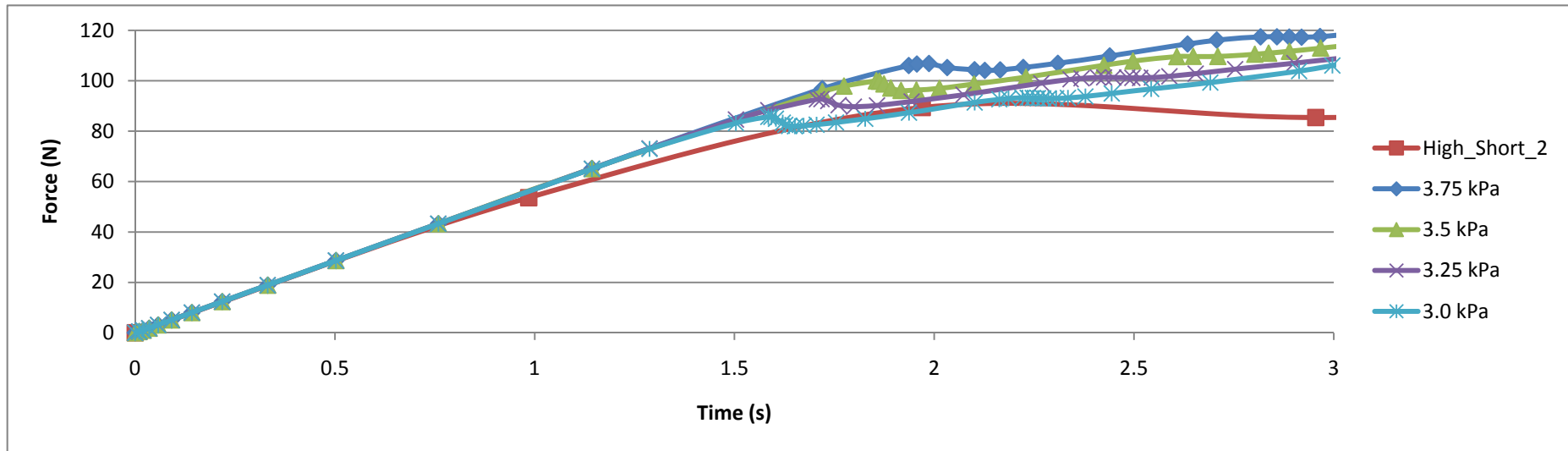
A25: Load-time curves in Test Low_Short with different cohesion when $\beta = 35^\circ$



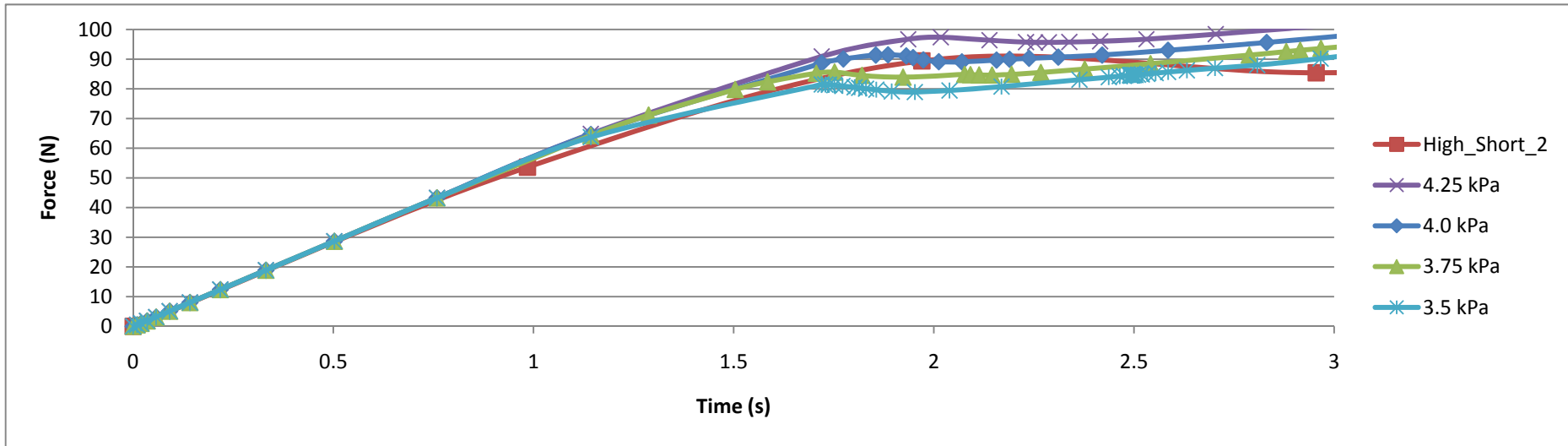
A26: Load-time curves in Test Low_Short with different cohesion when $\beta = 30^\circ$



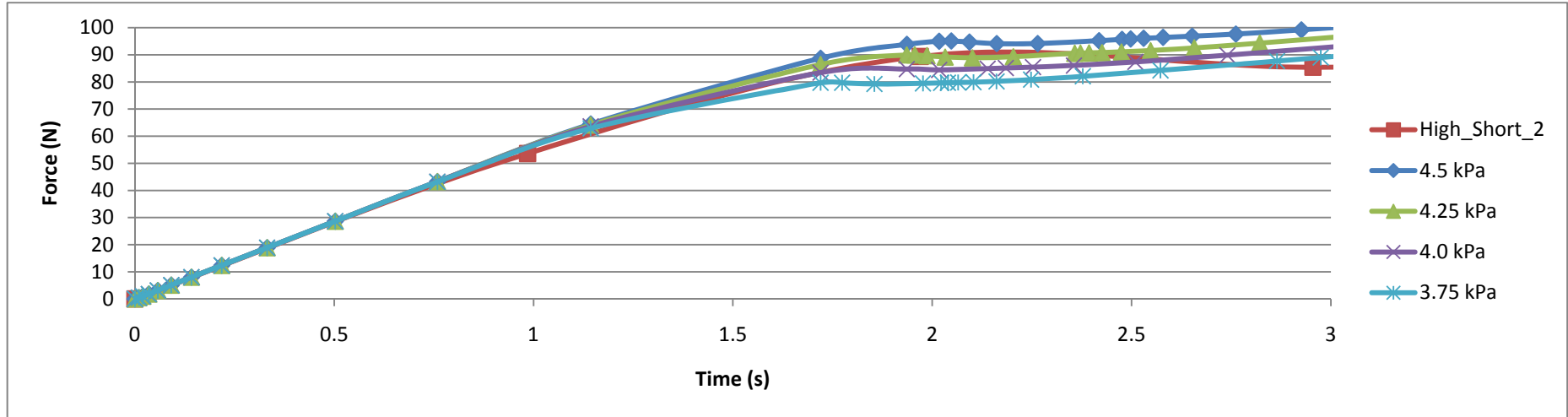
A27: Load-time curves in Test Low_Short with different cohesion when $\beta = 25^\circ$



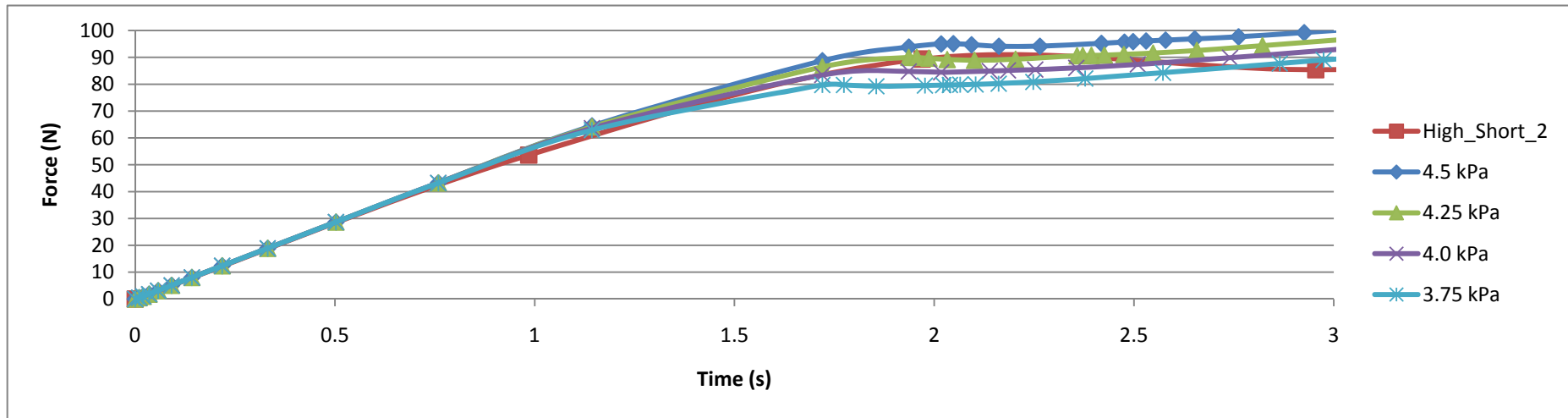
A28: Load-time curves in Test High_Short with different cohesion when $\beta = 55^\circ$



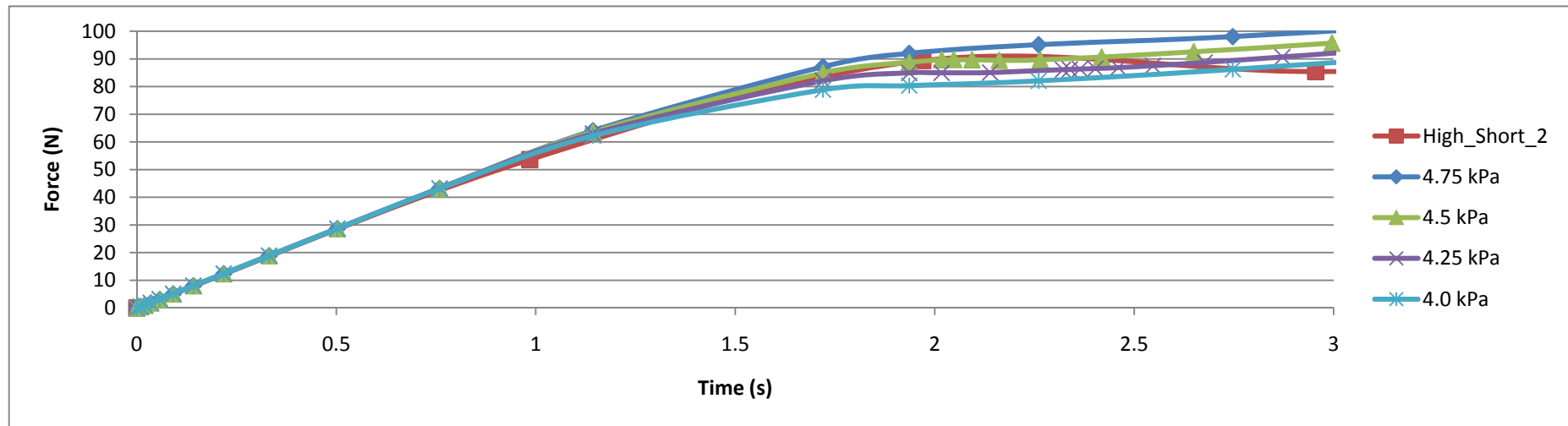
A29: Load-time curves in Test High_Short with different cohesion when $\beta = 50^\circ$



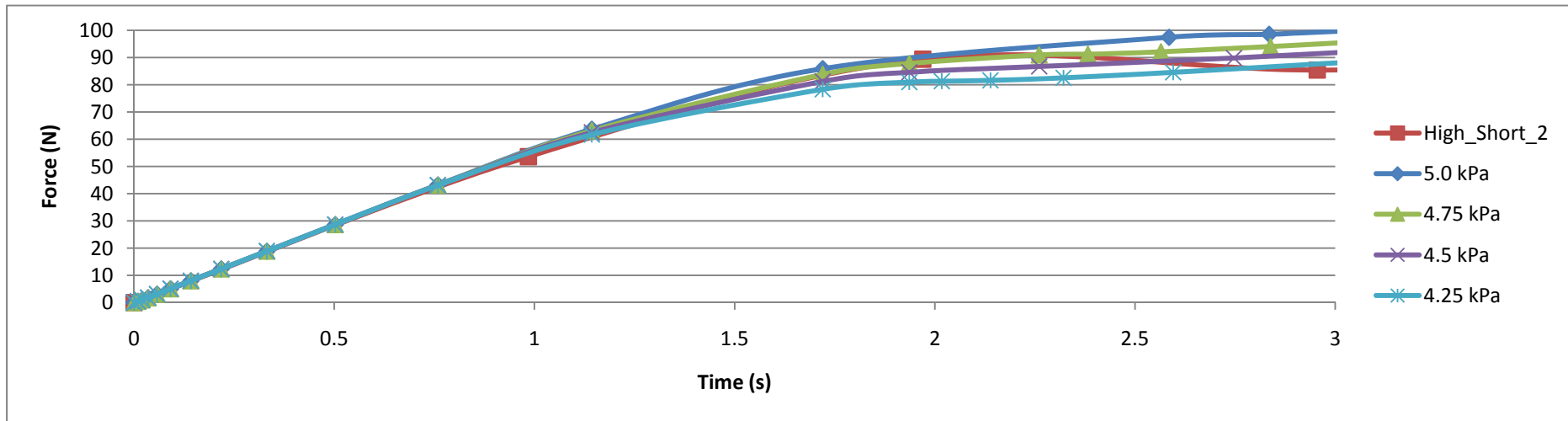
A30: Load-time curves in Test High_Short with different cohesion when $\beta = 45^\circ$



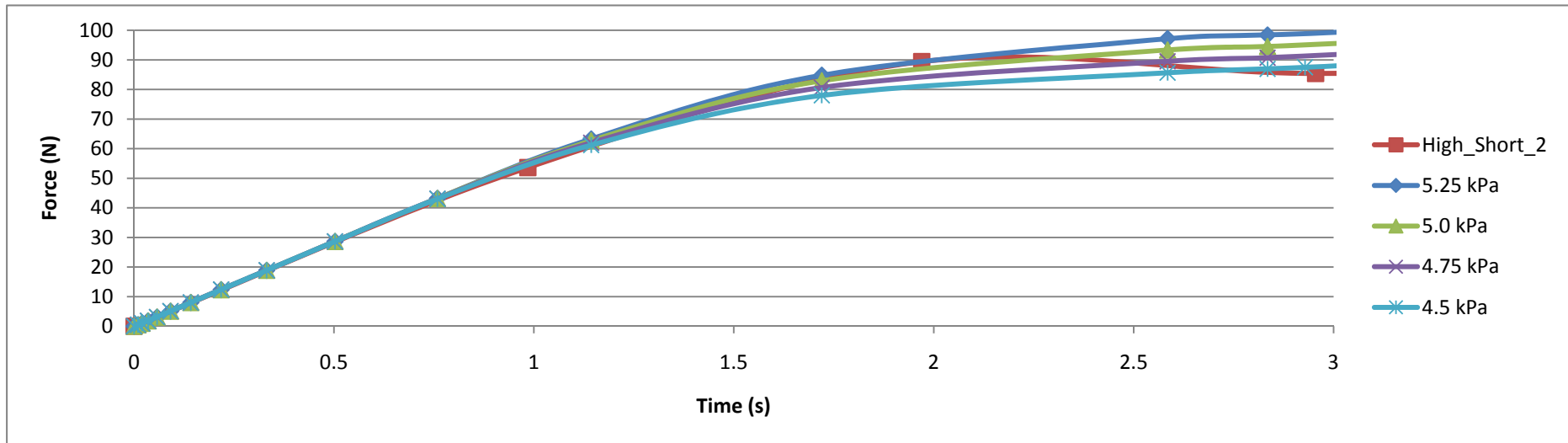
A31: Load-time curves in Test High_Short with different cohesion when $\beta = 40^\circ$



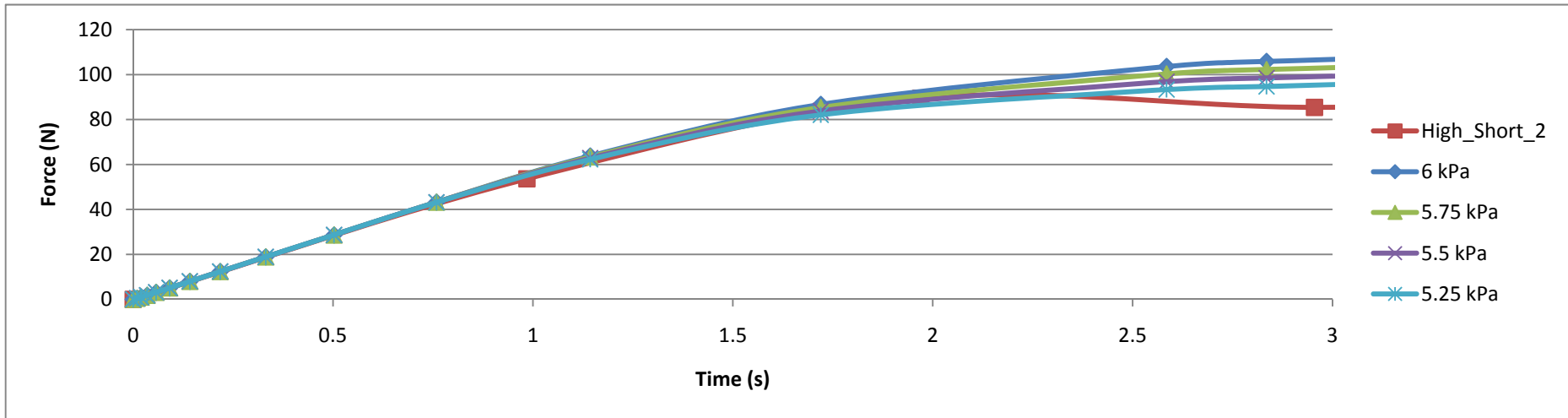
A32: Load-time curves in Test High_Short with different cohesion when $\beta = 35^\circ$



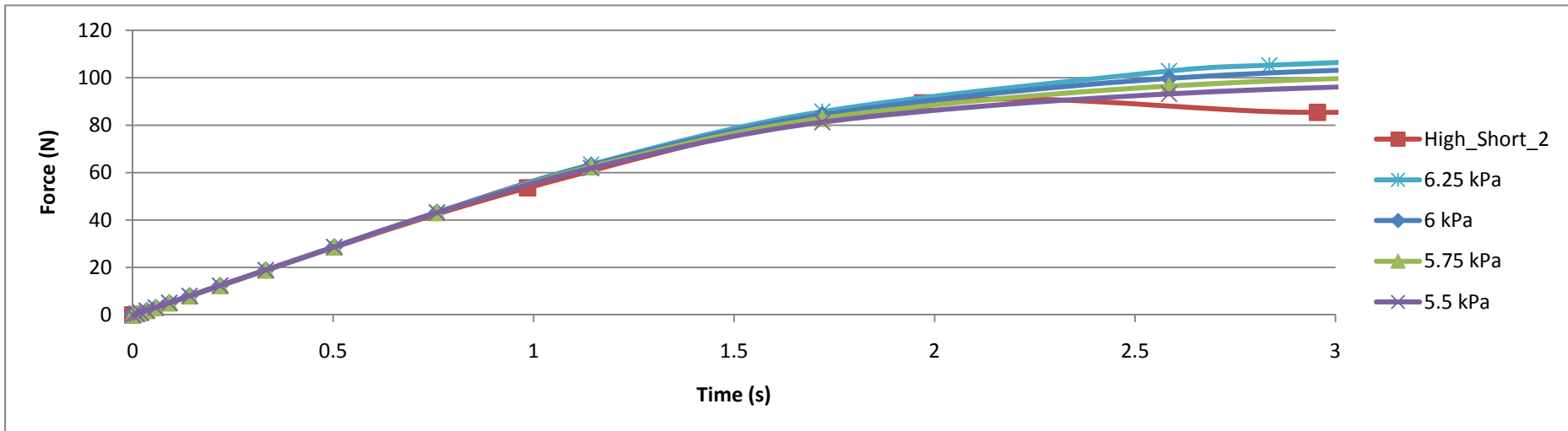
A33: Load-time curves in Test High_Short with different cohesion when $\beta = 30^\circ$



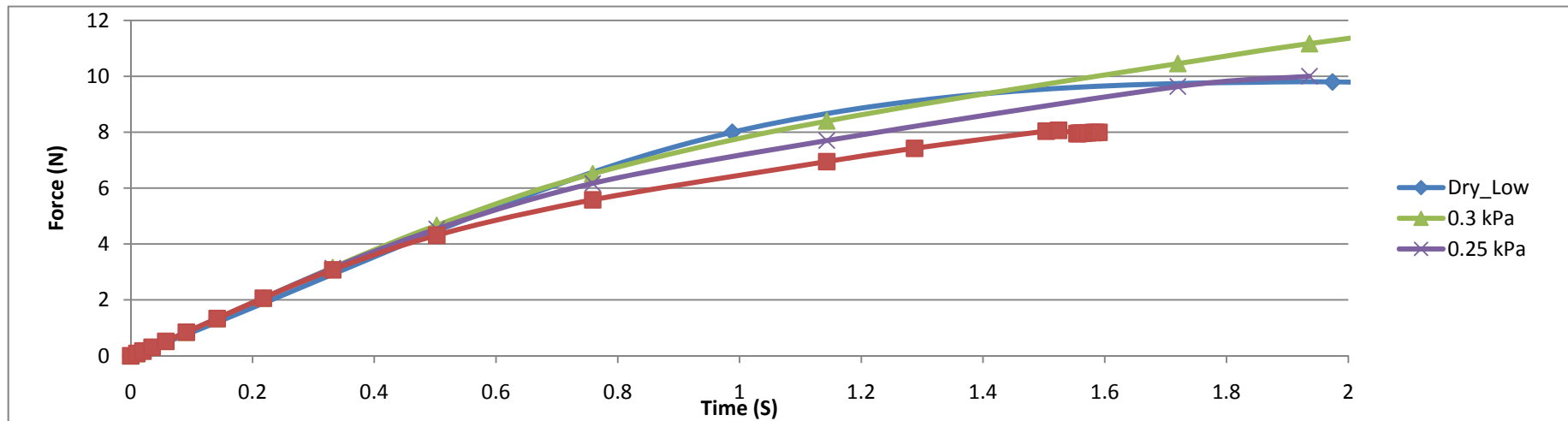
A34: Load-time curves in Test High_Short with different cohesion when $\beta = 25^\circ$



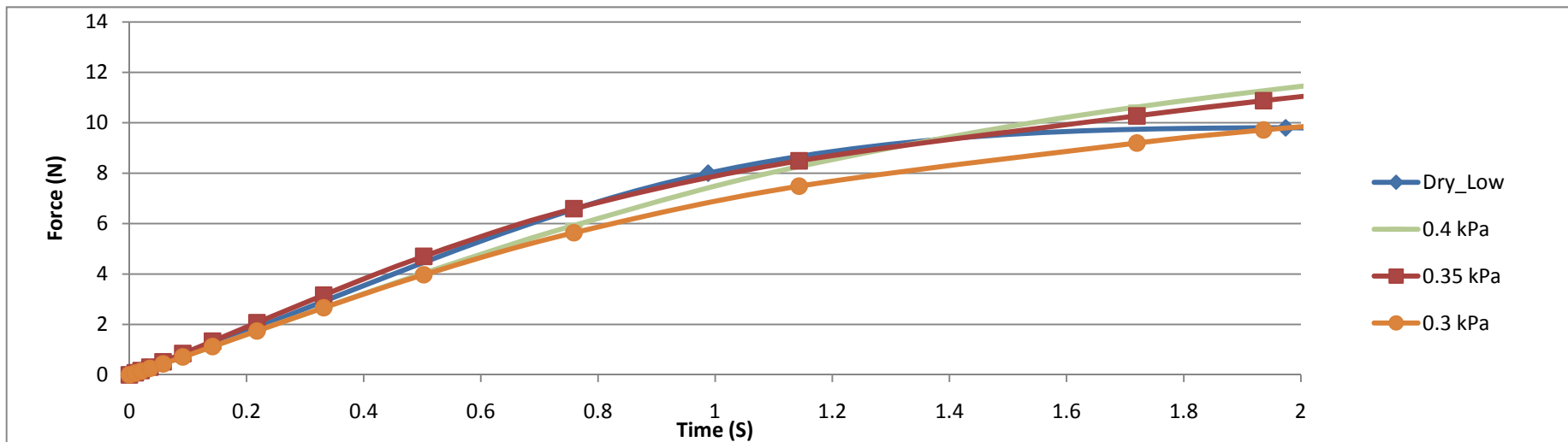
A35: Load-time curves in Test High_Short with different cohesion when $\beta = 20^\circ$



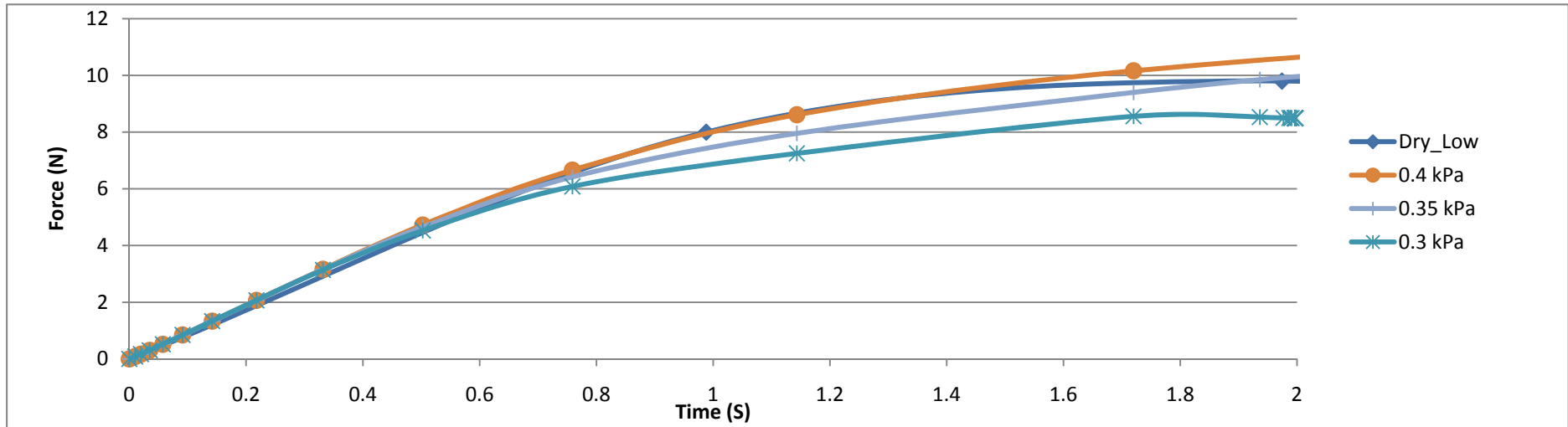
A36: Load-time curves in Test High_Short with different cohesion when $\beta = 15^\circ$



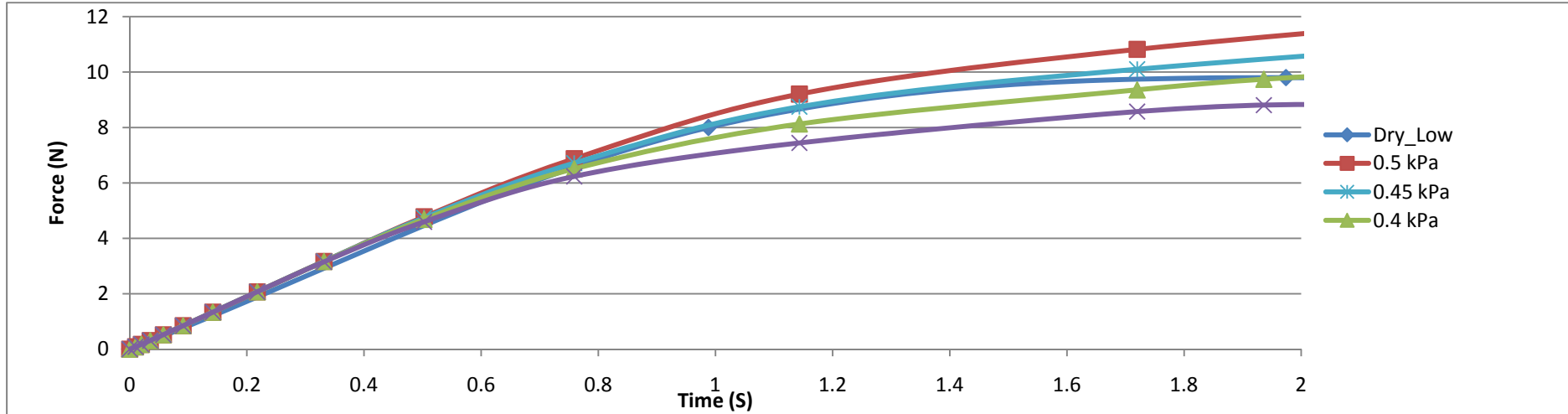
A37: Load-time curves in Test Dry_Low with different cohesion when $\beta = 30^\circ$



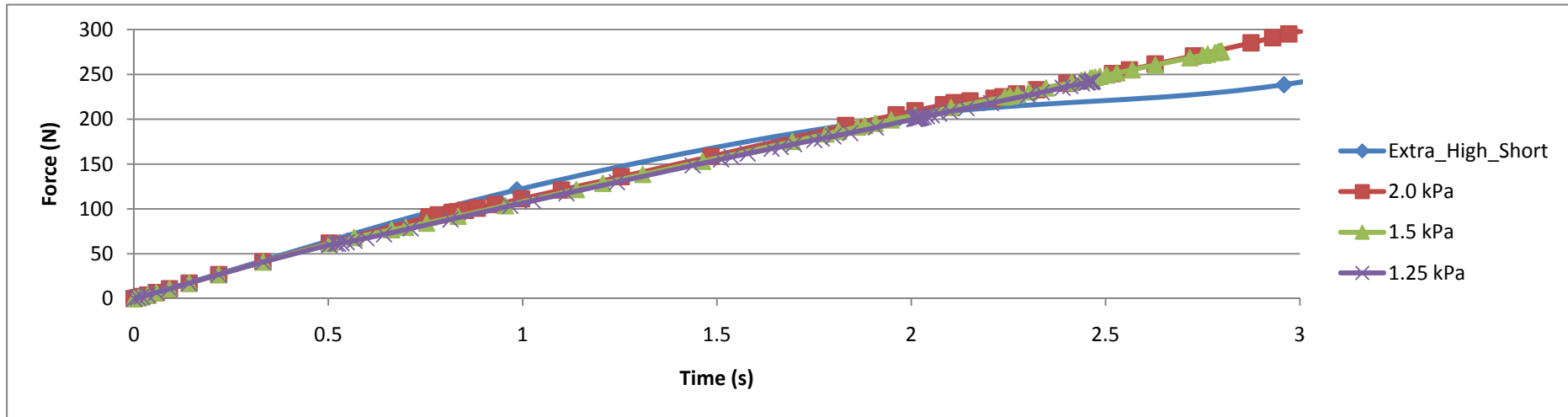
A38: Load-time curves in Test Dry_Low with different cohesion when $\beta = 25^\circ$



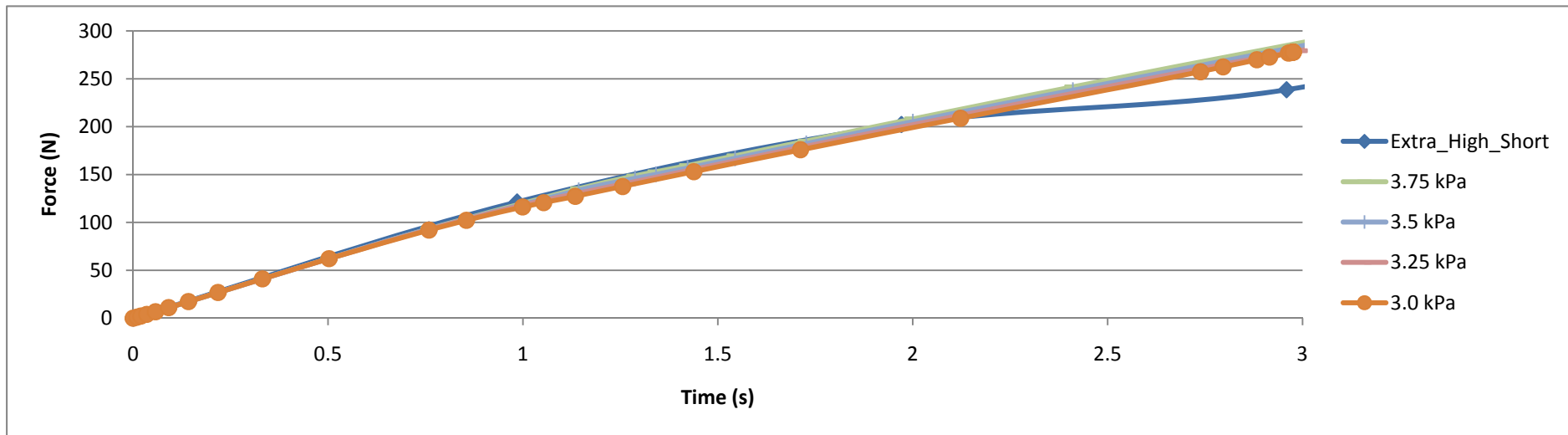
A39: Load-time curves in Test Dry_Low with different cohesion when $\beta = 20^\circ$



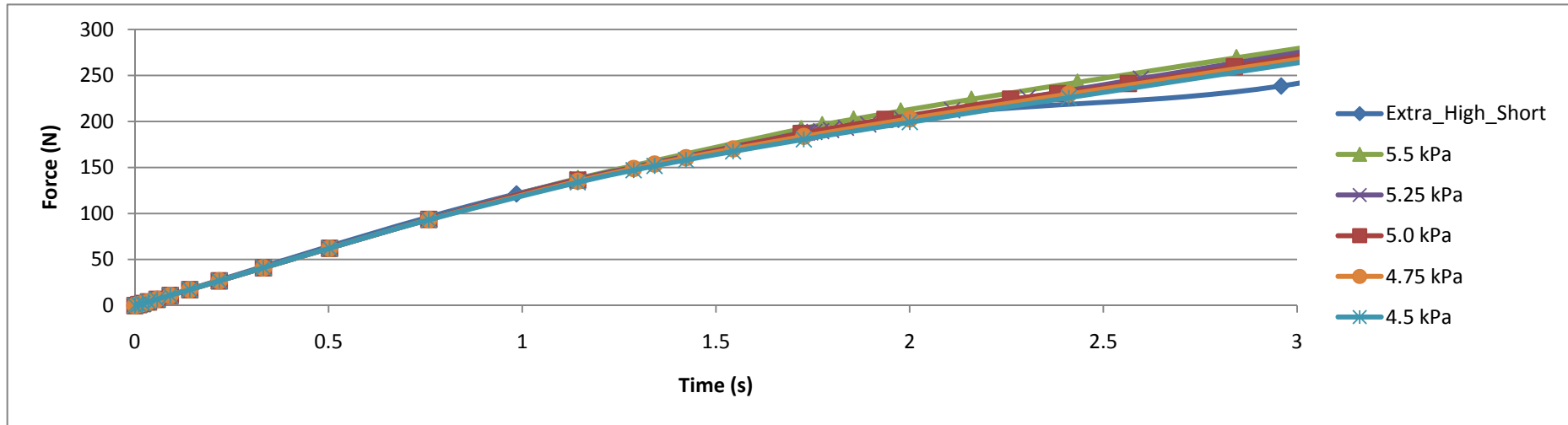
A40: Load-time curves in Test Dry_Low with different cohesion when $\beta = 15^\circ$



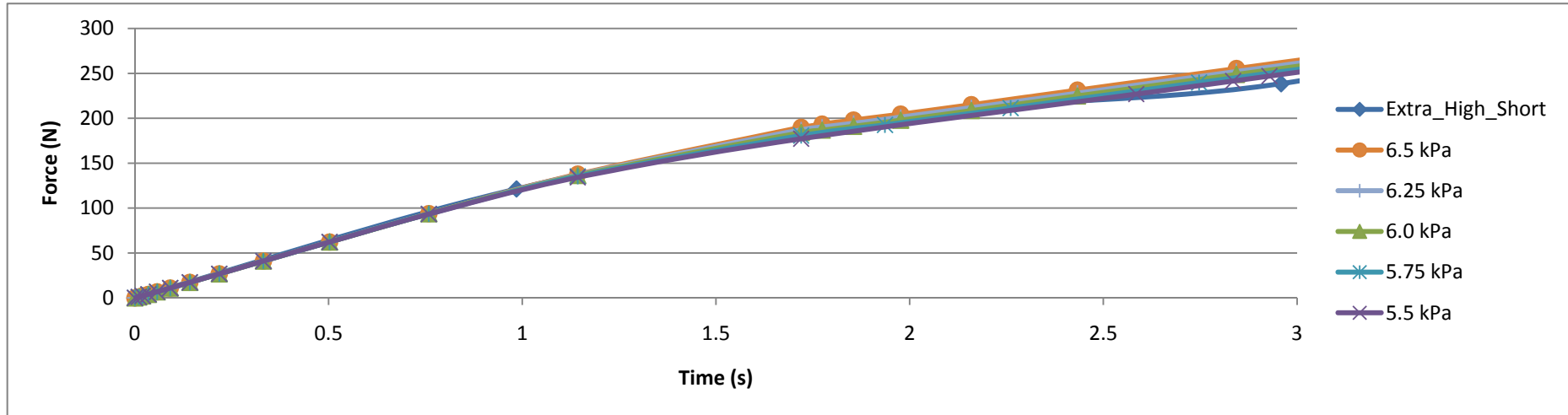
A41: Load-time curves in Test Extra_High_Short with different cohesion when $\beta = 55^\circ$



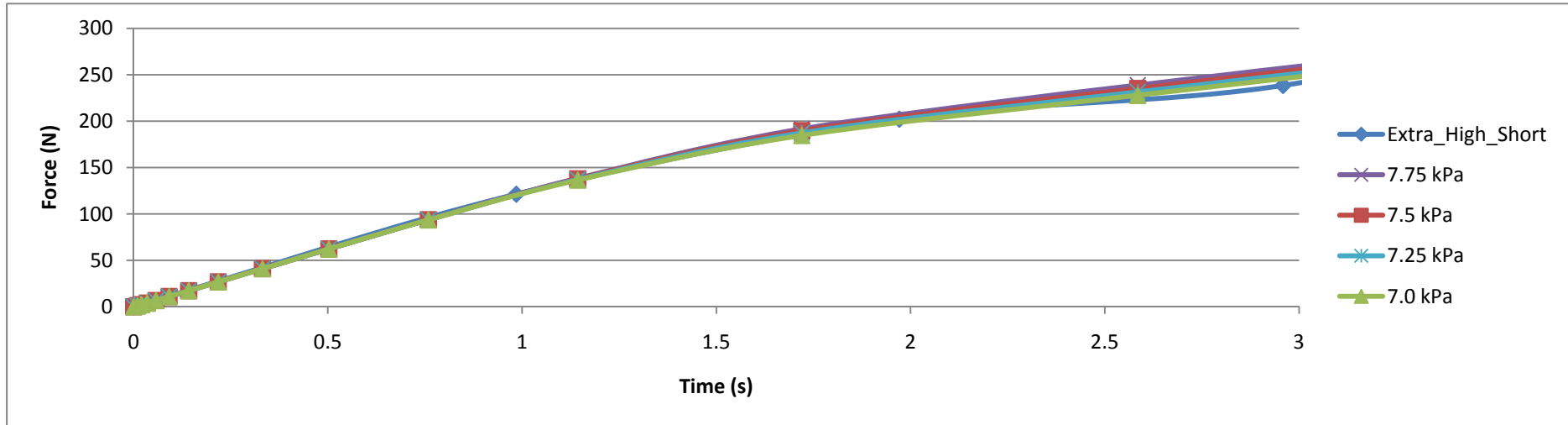
A42: Load-time curves in Test Extra_High_Short with different cohesion when $\beta = 50^\circ$



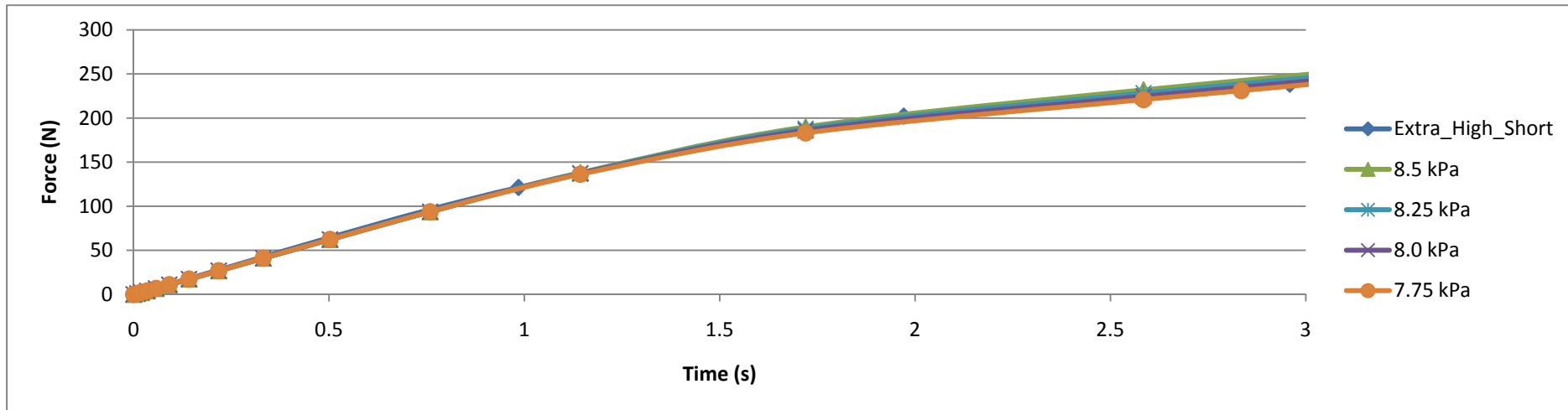
A43: Load-time curves in Test Extra_High_Short with different cohesion when $\beta = 45^\circ$



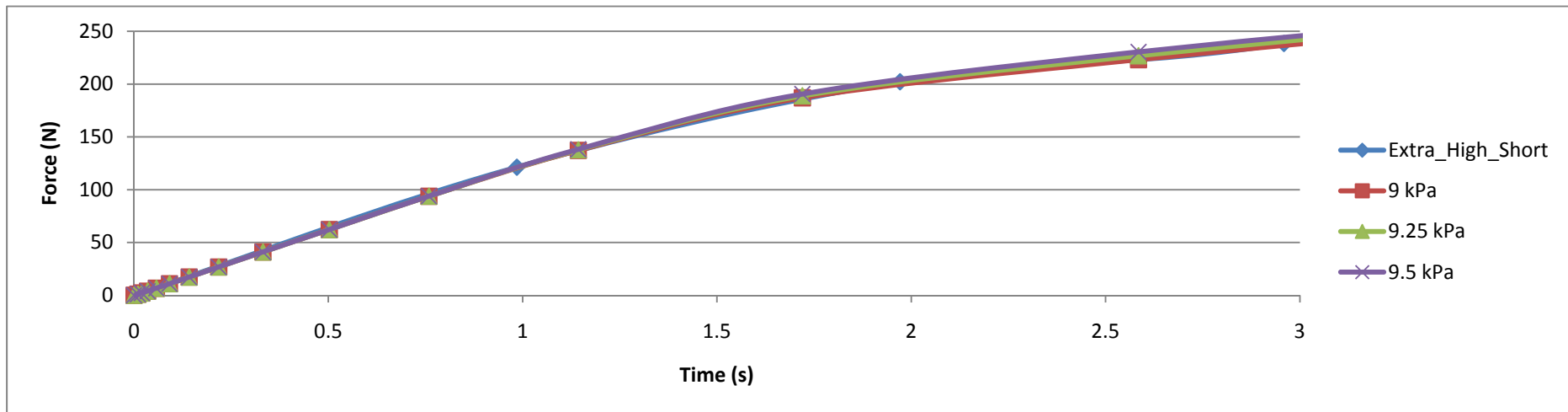
A44: Load-time curves in Test Extra_High_Short with different cohesion when $\beta = 40^\circ$



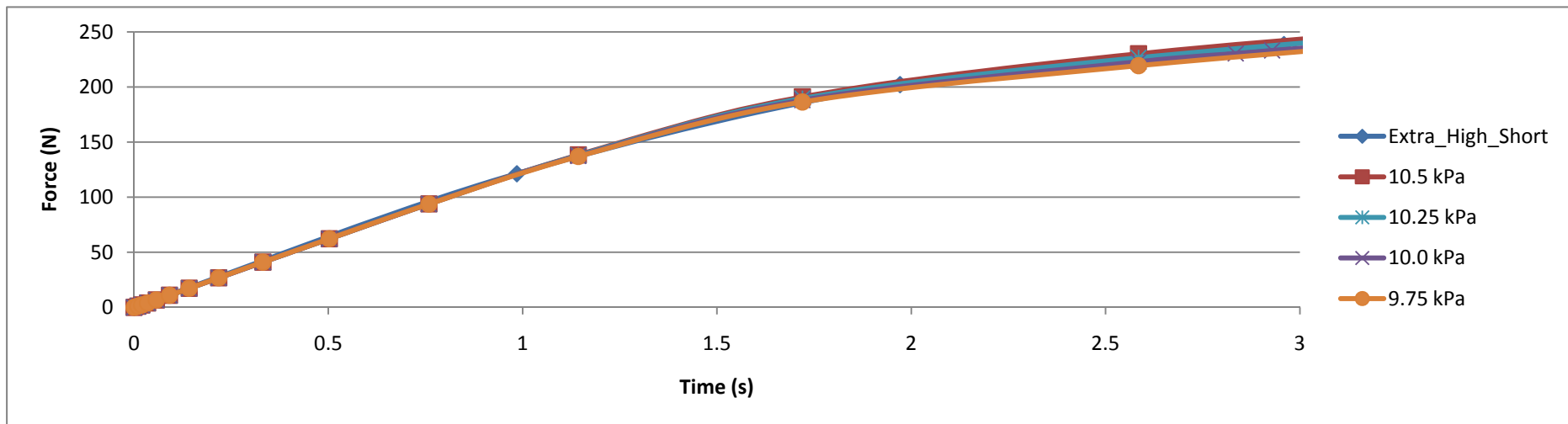
A45: Load-time curves in Test Extra_High_Short with different cohesion when $\beta = 35^\circ$



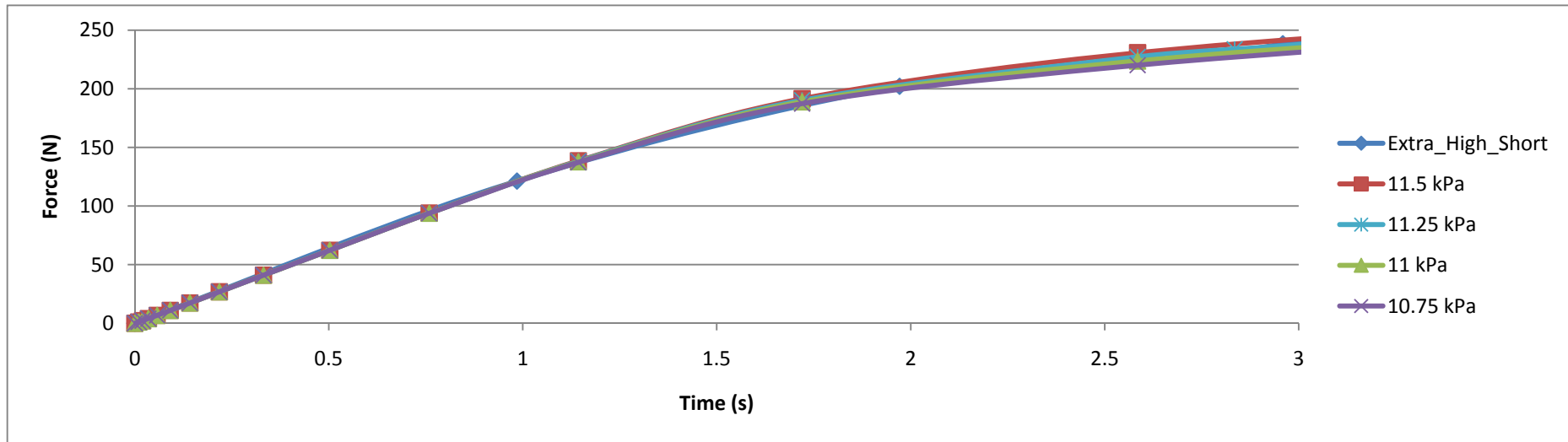
A46: Load-time curves in Test Extra_High_Short with different cohesion when $\beta = 30^\circ$



A47: Load-time curves in Test Extra_High_Short with different cohesion when $\beta = 25^\circ$



A48: Load-time curves in Test Extra_High_Short with different cohesion when $\beta = 20^\circ$

A49: Load-time curves in Test Extra_High_Short with different cohesion when $\beta = 15^\circ$

